UNIVERSIDAD AUTÓNOMA DE SAN LUÍS POTOSÍ

Doctorado Institucional en Ingeniería y Ciencia de Materiales

STUDY ON HYDROLYTIC EVOLUTION AND MULTI-TARGETED REGULATION MECHANISM OF THE EDGES OF MOLYBDENITE FINES

TESIS

QUE PARA OBTENER EL GRADO DE

DOCTORA EN INGENIERÍA Y CIENCIA DE MATERIALES

PRESENTA

Jie Wu

DIRECTORA

Dra. Mildred Quintana Ruiz

PATROCINADO POR CONACyT Beca número 813204

San Luis Potosí, S.L.P. Abril 2026

UNIVERSIDAD AUTÓNOMA DE SAN LUÍS POTOSÍ

Doctorado Institucional en Ingeniería y Ciencia de Materiales

STUDY ON HYDROLYTIC EVOLUTION AND MULTI-TARGETED REGULATION MECHANISM OF THE EDGES OF MOLYBDENITE FINES

TESIS

QUE PARA OBTENER EL GRADO DE

DOCTORA EN INGENIERÍA Y CIENCIA DE MATERIALES

PRESENTA

Jie Wu

DIRECTORA

Dra. Mildred Quintana Ruiz

Sinodales

Dra. Mildred Quintana Ruiz _____

Dr. Shaoxian Song _____

Dra. Aurora Robledo Cabrera _____

Dr. Hiram Joazet Ojeda Galván _____

Dra. Socorro Oros Ruiz _____

Dra. Selene Concepción Acosta Morales _____

San Luis Potosí, S.L.P. Abril 2026

Acknowledgment

Time has passed swiftly, and my period of study has now reached its conclusion. This thesis stands as the culmination of a rigorous and meaningful academic endeavor, which would not have been possible without the steadfast guidance of my supervisors and the invaluable support of my colleagues.

I would like to express my sincere gratitude to all the people who have helped me throughout my PhD studies. First of all, I am deeply grateful to Dra Mildred Quintana Ruiz, Dr. Bingqiao Yang, and Dr Shaoxian Song. Their patient guidance has been invaluable from the initial topic selection and experimental research to the analysis of specific phenomena and the final writing of this thesis. I still remember when I wrote my first paper, my supervisors helped me revise the grammar and structure of the paper from beginning to end, and patiently explained writing methods and skills to me. Under their careful guidance and encouragement, I was able to successfully finish my doctoral study. Dra Mildred Quintana Ruiz, Dr. Bingqiao Yang, and Dr Shaoxian Song Hu's diligence and persistent pursuit of scientific truth, tireless efforts to solve scientific problems, rigorous and serious attitude towards scientific research and gentle personality charm have benefited me a lot.

During the study in Institucional en Ingenieria y de Ciencia de Materiales de la Universidad Autonoma de San Luis Potosi, I was thankful for the sincere advice of the committee professors Dr. Alejandro López Valdivieso, Dra. Aurora Robledo Cabrera, Dr. Hiram Joazet Ojeda Galván, and Dra. Socorro Oros Ruiz on my seminal report each semester. Their excellent suggestions significantly improved my experiment and analysis. I would like to thank Ubaldo, Maricela, and Eva. They always helped me enthusiastically in preparing the documents I needed from enrollment to graduation. Meanwhile, thanks to Dra. Selene Concepción Acosta Morales and Dra. Jessica Viridiana García Meza, I was interested in your lessons and learned a lot. Furthermore, I want to express my gratitude to Dra. Feifei Jia, Dra. Xian Zhang, Dr. Peng Chen, Dra. Jianbo Li and Dr. Hao Yi. Thank you for your help, concern and encouragement. I also appreciated all the friends at UASLP, and all the friends at Wuhan University of Technology and Wuhan Institute of Technology, who have been very patient in helping me solve many problems. Especially, I really appreciated Dr. Xiang Tian's support and help during my master's to doctoral study.

Finally, a special thanks to my family. Thanks to your love and understanding, I was able to complete my studies successfully. Without your support, I would not be able to choose what I want to do as freely as I do today. In the future, I will continue to study hard, enrich myself in all aspects, and live up to your love and support.

This work was supported by the scholarship from Consejo Nacional de Humanidades Ciencias y Tecnolog á (CONAHCYT) of Mexico (No. 813204).

Abstract

Efficient flotation recovery of molybdenite fines (–20 μm) remains a significant global challenge. Molybdenite is an anisotropic mineral with two distinct surfaces: hydrophobic faces and hydrophilic edges. As the particle size decreases, the proportion of molybdenite edges increases markedly, leading to the reduced hydrophobicity and poor floatability. Consequently, the natural floatability of molybdenite fines diminishes sharply due to the high edge/face ratio. Currently, conventional collectors such as hydrocarbon oils are ineffective for recovering molybdenite fines because these oils primarily adsorb on molybdenite faces rather than the dominant edges, leading to substantial losses of molybdenite resources. This work aims to develop novel, highly efficient, and environmentally friendly collectors that specifically target the regulation of edge hydrophobicity, which is crucial for improving the flotation efficiency of molybdenite fines.

In this study, the flotation performance of molybdenite fines using several collectors, including the traditional sulfide mineral collector sodium isobutyl xanthate (SIBX) and three alternative collectors N-(N-butyl) thiophosphoric triamide (NBPT), potassium cetyl phosphate (PCP), and sodium 2-mercaptobenzothiazole (MBT) were systematically investigated. The interaction mechanisms between these collectors and molybdenite surfaces were investigated using scanning electron microscopy (SEM), atomic force microscopy (AFM), X-ray photoelectron spectroscopy (XPS), and density functional theory (DFT) calculations. Since molybdenite surfaces are susceptible to oxidation under natural conditions, particularly at edge sites, the influence of surface oxidation on the flotation behavior of molybdenite fines was further examined. In addition, dodecylamine (DDA) was evaluated as a collector for both unoxidized and oxidized molybdenite fines to assess its effectiveness in improving flotation performance.

The results showed that NBPT, PCP, and MBT significantly enhanced the flotation of molybdenite fines, achieving floatabilities of approximately 90% due to their preferential chemical adsorption on edge sites, which increased edge hydrophobicity. Furthermore, DDA exhibited superior performance compared with kerosene for both unoxidized and oxidized molybdenite fines. Even after oxidation, the floatability increased to about 90% at a DDA dosage of 100 mg/L, whereas kerosene achieved only 33.62% at 400 mg/L. These findings indicate that regulating the hydrophobicity of molybdenite edges is crucial for efficient flotation of molybdenite fines and provides a promising strategy for improving their recovery.

Keywords: Molybdenite fines; Flotation; Collectors; Face and edge; Oxidation

Resumen

La recuperación eficiente por flotación de finos de molibdenita (−20 μm) sigue siendo un desafío significativo a nivel mundial. La molibdenita es un mineral anisotrópico que presenta dos superficies distintas: caras hidrofóbicas y bordes hidrofílicos. A medida que disminuye el tamaño de partícula, la proporción de bordes de molibdenita aumenta considerablemente, lo que conduce a una reducción de la hidrofobicidad y a una baja flotabilidad. En particular, la flotabilidad natural de los finos de molibdenita disminuye notablemente debido a la alta relación borde/cara. Actualmente, los colectores más comúnmente utilizados, como los aceites hidrocarbonados, no pueden recolectar eficazmente los finos de molibdenita porque estos aceites se adsorben principalmente en las caras de la molibdenita en lugar de en los bordes dominantes, lo que provoca una gran pérdida de recursos de molibdenita. Este trabajo tiene como objetivo desarrollar colectores novedosos, altamente eficientes y ambientalmente amigables que se orienten específicamente a la regulación de la hidrofobicidad de los bordes, lo cual es crucial para mejorar la eficiencia de flotación de los finos de molibdenita.

En este trabajo, se investigó sistemáticamente el desempeño de flotación de los finos de molibdenita utilizando varios colectores, incluido el colector tradicional para minerales sulfurados xantato de isobutilo de sodio (SIBX) y tres colectores alternativos: triamida tiodifosfórica N-(N-butil) (NBPT), fosfato de cetilo de potasio (PCP) y 2-mercaptobenzotiazolato de sodio (MBT). Los mecanismos de interacción entre estos colectores y las superficies de molibdenita se exploraron mediante microscopía electrónica de barrido (SEM), microscopía de fuerza atómica (AFM), espectroscopía de fotoelectrones de rayos X (XPS) y cálculos de teoría del funcional de la densidad (DFT). Considerando que las superficies de molibdenita son susceptibles a la oxidación en condiciones naturales, particularmente en los sitios de borde, también se examinó la influencia de la oxidación superficial en el comportamiento de flotación de los finos de molibdenita. Además, se evaluó la dodecilamina (DDA) como colector para finos de molibdenita tanto no oxidados como oxidados con el fin de analizar su eficacia para mejorar el desempeño de flotación.

Los resultados demostraron que NBPT, PCP y MBT mejoraron significativamente la flotación de los finos de molibdenita, alcanzando flotabilidades cercanas al 90 %, debido a su adsorción química preferencial en los sitios de borde, lo que incrementa la hidrofobicidad de estos. Además, la DDA mostró un desempeño superior en comparación con el queroseno tanto para finos de molibdenita no oxidados como oxidados. Incluso después de la oxidación, la flotabilidad aumentó hasta aproximadamente el 90 % con una dosificación de DDA de 100 mg/L, mientras que el queroseno solo alcanzó el 33.62 % a una dosificación de 400 mg/L.

Estos resultados indican que la regulación de la hidrofobicidad de los bordes de la molibdenita es crucial para la flotación eficiente de los finos de molibdenita y proporcionan estrategias prometedoras para mejorar su recuperación.

Palabras clave: Finos de molibdenita; Fotación; Colector; Caras y bordes; Oxidación.

Contents

List of Figures

List of Tables

Chapter I. Introduction

1.1 Justification

With the continuous development and consumption of molybdenum (Mo) resources, the high-grade and easy-processed molybdenite (MoS_2) is decreasing sharply. Therefore, it is necessary to recover fine-disseminated molybdenite to meet the market demands [1]. Flotation is the most important method to collect molybdenite. To effectively recover this type of ore, fine-grinding is essential before flotation. Nevertheless, fine-grinding will produce numerous fine particles. Many researchers have reported that molybdenite fines cannot be efficiently collected by flotation [2, 3].

The floatability of molybdenite fines depends on the edge/face ratio [4]. Molybdenite is a typical anisotropic mineral that exhibits two types of surfaces, namely face and edge. The face is formed by the rupture of van der Waals force, while the edge is generated by the break of Mo–S covalent bond [5]. The crystalline structure of molybdenite is shown in Fig. 1.1. Molybdenite faces exhibit high inertness and strong hydrophobicity, whereas molybdenite edges display high chemical activity and strong hydrophilicity [6]. As the particle size of molybdenite decreases, the edge/face ratio substantially increases [7]. Molybdenite fines exhibit strong hydrophilicity and poor floatability due to their high edge/face ratio [8].

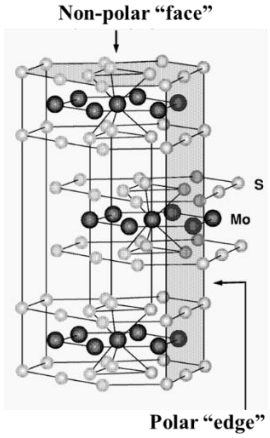

Fig. 1.1 The crystalline structure of molybdenite

Agglomeration flotation and nano-bubble flotation are the primary approaches used to improve the flotation of molybdenite fines [9, 10]. Both methods concentrate on regulating the hydrophilicity of molybdenite faces or strengthening the interaction between faces and bubbles during the flotation process. However, the adverse effects of edges' properties on the

flotation of molybdenite fines are overlooked [11, 12]. Interaction forces between particles or between particles and bubbles (including van der Waals force, hydrophobic force, and electrostatic interaction) are crucial factors in agglomeration flotation and nano-bubble flotation [13]. However, the edges dominate on molybdenite fines. In addition, the edges have strong hydrophilicity and a lot of negative electrons, whose strong hydration force and electrostatic repulsion force will greatly offset the hydrophobic force of the faces, thus hindering the collision and adhesion between molybdenite particles or between particles and bubbles and then influencing agglomeration flotation and nano-bubble flotation of molybdenite fines [14, 15].

Notably, the edge properties have a great impact on the flotation of molybdenite fines. At present, hydrocarbon oils have been widely used as collectors to improve the flotation efficiency of molybdenite [16]. However, these oil collectors are preferentially adsorbed on molybdenite face through van deer Waals force and hydrophobic force [17], which are hard to interact with molybdenite edge. As molybdenite particle size reduces, the proportion of edges increases sharply, thus oil collectors cannot efficiently collect molybdenite fines [18]. Furthermore, surface oxidation is a critical factor influencing the natural floatability of molybdenite [19]. Molybdenite fines are more susceptible to oxidation because of the dominant edges, which are more reactive than faces [4], further decreasing the hydrophobicity of molybdenite fines.

To improve the flotation performance of molybdenite fines, it is crucial to regulate the hydrophobicity of the edges. However, previous studies mainly concentrated on the anisotropic surface properties and adsorption differences on molybdenite faces and edges. Few studies investigate the flotation of molybdenite fines through the targeted regulation of molybdenite edge. Therefore, a promising approach has been proposed: developing novel collectors that target molybdenite edges and render them hydrophobic. Targeted regulation of edge properties not only enhances its hydrophobicity but also promotes the interaction between edge and bubbles, thus significantly improving the flotation efficiency of molybdenite fines.

1.2 Objectives

1.2.1 General objective

To address the challenges in the flotation of molybdenite fines, it is essential to develop new technologies that regulate the properties of molybdenite edges. This approach will provide both a scientific basis and technical support for the efficient recovery of molybdenite fines.

1.2.2 Goals

In this work, we systematically investigated the hydrolytic evolution and multi-targeted regulation mechanism of the edges of molybdenite fines. Several collectors with different functional groups, including SIBX, NBPT, PCP, MBT, and DDA, were employed to regulate the hydrophobicity of molybdenite edges and enhance flotation performance. Combined flotation tests, advanced characterizations, and theoretical calculations were used to elucidate the adsorption mechanisms of these collectors on molybdenite faces and edges. This work establishes a framework for regulating the interfacial properties of molybdenite edges and provides new insights into the design of efficient collectors for the flotation recovery of molybdenite fines.

References:

[1] S. Song, X. Zhang, B. Yang, A. Lopez-Mendoza, Flotation of molybdenite fines as hydrophobic agglomerates, Sep. Purif. Technol. 98 (2012) 451–455.

[2] J. Fu, K. Chen, H. Wang, C. Guo, W. Liang, Recovering molybdenite from ultrafine waste tailings by oil agglomerate flotation, Miner. Eng. 39 (2012) 133–139.

[3] S. Castro, A. Lopez-valdivieso, J.S. Laskowski, Review of the fl otation of molybdenite . Part I : Surface properties and fl oatability, Int. J. Miner. Process. 148 (2016) 48–58.

[4] J.R. Lince, P.P. Frantz, Anisotropic oxidation of MoS2 crystallites studied by angle-resolved X-ray photoelectron spectroscopy, Tribol. Lett. 9 (2001) 211–218.

[5] S. Kelebek, Critical surface tension of wetting and of floatability of molybdenite and sulfur, J. Colloid Interface Sci. 124 (1988) 504–514.

[6] M. Zanin, I. Ametov, S. Grano, L. Zhou, W. Skinner, A study of mechanisms affecting molybdenite recovery in a bulk copper/molybdenum flotation circuit, Int. J. Miner. Process. 93 (2009) 256–266.

[7] J. Wu, J. Feng, B. Yang, R. Martin, S. Song, M. Quintana, F. Jia, X. Tian, The anisotropic adsorption of potassium cetyl phosphate on molybdenite surface and its implication for improving the flotation of molybdenite fines, J. Mol. Liq. 378 (2023) 121616.

[8] B. Yang, J. Wu, B. Deng, H. Shao, S. Song, M. Quintana, Improving the Flotation of Unoxidized and Oxidized Molybdenite Fines Using Dodecylamine as a Collector: Flotation Tests and Interaction Mechanism, Minerals. 14 (2024) 468.

[9] B. Yang, S. Song, A. Lopez-Valdivieso, Kinetics of hydrophobic agglomeration of molybdenite fines in aqueous suspensions, Physicochem. Probl. Miner. Process. 51 (2015) 181–189.

[10] X. Wang, S. Yuan, J. Liu, Y. Zhu, Y. Han, Nanobubble-enhanced flotation of ultrafine molybdenite and the associated mechanism, J. Mol. Liq. 346 (2022) 118312.

[11] A. Alvarez, L. Gutierrez, J.S. Laskowski, Use of polyethylene oxide to improve flotation of fine molybdenite, Miner. Eng. 127 (2018) 232–237.

[12] B. Yang, S. Song, A. Lopez-Valdivieso, Morphology of hydrophobic agglomerates of molybdenite fines in aqueous suspensions, Sep. Sci. Technol. 50 (2015) 1560–1564.

[13] L. Tian, M. Fan, P. Fan, H. Yang, Research progress on compound force field separation equipment of fine particles, Sep. Sci. Technol. (2024) 1–31.

[14] Z. Lu, Z. Lu, S. Peng, X. Zhang, Q. Liu, Microwetting of pH-Sensitive Surface and Anisotropic MoS2 Surfaces Revealed by Femtoliter Sessile Droplets, Langmuir. 32 (2016) 11273–11279.

[15] T. J.Ornelas, O. I.Madrid, B. J.L.Reyes, L. A.A.Sanchez, P. D.Valdez, V. A.Lopez, Surface properties and floatability of molybdenite, in: Proceeding 2006 China-Mexico Work. Miner. Part. Technol., San Luis Potosi, 2006.

[16] W. Ge, J. Liu, H. Ren, Y. Zhu, W. Han, Y. Han, Enhanced mixed flotation of copper–molybdenum ore using dodecyl dimethyl betaine-emulsified kerosene as environmentally friendly collector, J. Clean. Prod. 447 (2024) 141576.

[17] R.C. Santana, J.A. Ribeiro, M.A. Santos, A.S. Reis, C.H. Ata ́de, M.A.S. Barrozo, Flotation of fine apatitic ore using microbubbles, Sep. Purif. Technol. 98 (2012) 402–409.

[18] Z. Wei, Y. Li, L. Huang, New insight into the anisotropic property and wettability of molybdenite: A DFT study, Miner. Eng. 170 (2021) 107058.

[19] W. Pan, S. Li, Y. Zhu, L. Gao, Z. Ma, Y. Cao, S. Du, Hydration mechanism of molybdenite affected by surface oxidation: New insights from DFT and MD simulations, Colloids Surfaces A Physicochem. Eng. Asp. 698 (2024) 134599.

Chapter II. Literature Review

2.1. Introduction

Molybdenum (Mo) is a rare and strategic metal, which has many advantages such as high strength and a melting point, excellent corrosion and abrasion resistance, low coefficient of linear expansion and high modulus of elasticity [1]. With the development of science and technology, the industrial demand for molybdenum is increasing. At present, molybdenum has become an indispensable and irreplaceable strategic resource in the national economy, with widespread applications across various sectors including the iron and steel industry, the chemicals and textile industries, agriculture, and aerospace and military applications [2–4]: (1) In iron and steel industry: molybdenum is predominantly utilized in the iron and steel industry, where it accounts for approximately 75% of total molybdenum consumption [2]. Within this sector, 34% is used in stainless and heat-resistant steels, 29% in alloy steels, and 12% in other steel products. Molybdenum is added to steel products as an additive, which allows steel products to exhibit a uniform microcrystalline structure and improves their hardness, toughness and creep resistance; (2) In chemicals and textiles: due to its high stability in various reaction media, molybdenum and its alloys are widely used as corrosion-resistant materials in the chemical industry, petroleum refining, glass production and other industrial applications. Approximately 25% of molybdenum is employed in the catalyst industries and other chemical applications. For example, molybdenum compounds are used in manufacturing valves and heat exchangers, and molybdenum blue, a compound derived from molybdate, is used as a dye for silk, wool, and cotton fabrics; (3) In agriculture: ammonium molybdate serves as a raw material for fertilizer production. Trace amounts of molybdenum can promote the growth of certain plants, particularly legumes; (4) In aerospace and military applications: molybdenum is used in the production of rocket and missile components such as nozzles, ramjet nozzles and combustion chambers. Since spacecraft can experience surface temperatures of 1482–1646 ℃ during launch and reentry, molybdenum, due to its high-temperature resistance, is typically employed for nozzles, wings, flame baffles, guide blades, and other critical components.

Molybdenum is relatively scarce on in the Earth’s crust, comprising only 0.001% of the Earth’s crust by weight. According to data from the United States Geological Survey, global molybdenum resources are predominantly concentrated in North and South America, Asia (particularly China) and the CIS countries, with Eastern Europe following. In contrast, Africa, Oceania and most Asian countries have limited molybdenum resources. Specifically, the primary global molybdenum reserves are distributed in China, Peru, the United States, Chile,

Russia and Mexico. With the rapid development of science and technology, the demand for molybdenum is on the rise. According to the latest data from the International Molybdenum Association (IMOA), global molybdenum production in 2022 was 262,100 tons, 1% less than in 2021. However, global molybdenum consumption reached 286,400 tons, an increase of about 3% compared to the previous year. Notably, molybdenum plays an important role in industrial and technological development.

Molybdenum does not occur as a free metal in nature and is exclusively found in complex ores with other metals in the form of compounds. Currently, only 24 types of minerals of molybdenum-containing minerals are known. These minerals are primarily divided into two categories, molybdenum sulfide (molybdenite) minerals and molybdenum oxide ores. Among them, molybdenite is the most significant and widely utilized [5]. Molybdenite (MoS_2) serves as the principal source for molybdenum extraction, contributing 99% of global molybdenum production. In addition to forming a single deposit, molybdenite also commonly coexists with other sulfide minerals to form polymetallic deposits, such as porphyry Cu–Mo ores. Porphyry Cu–Mo ores are the primary resources for the extraction of both copper and molybdenum, accounting for 75% of global copper production and 50% of global molybdenum production [6, 7]. In porphyry Cu–Mo ores, copper and molybdenum mainly occur in the forms of chalcopyrite and molybdenite, respectively [8]. However, porphyry Cu–Mo ores present challenges including low raw ore grade, fine embedded particle size, low recovery and high production cost [2].

Based on the excellent natural floatability of molybdenite, it is generally accepted that froth flotation is the most effective method for the recovery of molybdenite [9]. During flotation, molybdenite recovery is affected by many factors. For example, particle size, mineral type and mineral liberation are found to have a significant influence on molybdenite recovery and concentrate grade [1, 9]. Furthermore, process-related parameters such as feed solids concentration, pH, collectors and depressants also affect molybdenite flotation performance [10, 11]. Other factors including the concentration of organic and inorganic ions in water, pulp potential and flotation gas utilization should be carefully considered and adjusted to achieve optimal molybdenite recovery [12, 13].

The selection of collectors with strong collecting ability and high selectivity is a critical factor in molybdenite flotation. Currently, hydrocarbon oils such as kerosene are commonly used as molybdenite collectors. However, due to declining market demand, kerosene has been removed from the production catalog in some countries, leading to its discontinuation by large refineries. In addition, the stable composition of kerosene is increasingly difficult to maintain, which leads to a negative impacct on molybdenum production [14]. Consequently, it is urgent to seek kerosene substitutes. Meanwhile, with the continuous development and

consumption of molybdenum resources, high-grade and easily processed molybdenite deposits are becoming scarcer. Consequently, the utilization of finely-disseminated and refractory molybdenite attracts increasing attention [15]. However, these refractory molybdenite ores require fine grinding to liberate them from other minerals, which causes a large amount of fine particles (–20 μm).

Previous research has indicated that the floatability of molybdenite fines drops sharply, resulting in the loss of valuable molybdenite resources. At present, the efficient recovery of molybdenite fines remains a challenging task globally. Improving the flotation performance of molybdenite fines is crucial not only for the effective recovery of molybdenum resources but also for reducing the overall cost of mineral processing. This review provides a comprehensive overview the current status of the recovery of molybdenite fines. It summarizes the crystalline structure of molybdenite and evaluates its inherent floatability. It compares the hydrophobicity of molybdenite face and edge, suggesting that the hydrophilic edge contributes to the reduced floatability of molybdenite fines. The review analyzes the influence factors of particle size, surface oxidation and collectors on the flotation of molybdenite fines, with a particular emphasis on hydrocarbon oils and thiol collectors. However, these collectors possess limitations that hinder significant improvements in the flotation of molybdenite fines. In addition, the review analyzes two methods, namely agglomeration flotation and nano-bubble flotation, recently used to improve the flotation of molybdenite fines. Finally, the review summarizes current studies of molybdenite anisotropy and points out the difference between molybdenite face and edge. This review provides a better understanding of molybdenite properties and valuable insights for future molybdenite flotation.

2.2. Crystalline structure and natural floatability of molybdenite

The crystalline structure of molybdenite was first elucidated by Dikinson and Pauling [16]. Molybdenite crystallizes in the hexagonal system as the common 2H polytype and in the trigonal system as the 3R polytype (less frequent). Molybdenite (2H) exhibits a hexagonal layered structure with a complete basal cleavage, consisting of layers of trigonal prismatic coordination polyhedra, where each Mo atom is surrounded by a trigonal prism of sulfur (S) atoms. The S atoms form the upper and lower surfaces with the smaller Mo atoms sandwiched between these layers. The sulfur–sulfur distances are 2.98 Å, while the distance between layers is 3.95 Å [17].

A mineral with anisotropic surface properties is characterized by different surface properties on different sides of the crystal. This is the case of the sheet structure of inherently hydrophobic minerals, such as molybdenite, talc, graphite, etc [18]. Commonly, minerals

with anisotropy do not have to be hydrophobic, as in the case of clay, which is well recognized to have two types of hydrophilic surfaces, faces and edges [19]. Molybdenite exhibits two kinds of surfaces, namely non-polar faces and polar edges. The non-polar faces are formed by the rupture of van der Waals forces, while the polar edges are generated by the rupture of the covalent Mo–S bonds [20]. Therefore, the faces are hydrophobic while the edges are hydrophilic. Notably, the hydrophobic faces are responsible for the natural floatability of molybdenite.

2.3. Influencing factors of molybdenite flotation

2.3.1 Particle size

Although the effect of particle size on flotation performance has been widely studied to date [21], many important physicochemical factors related to particle size have been identified, the net effect of these factors is difficult to predict. For instance, in particle-bubble interactions, particle size is known to play a key role in the probability of particles colliding with bubbles, the attachment of particles to bubbles after collision, as well as their retention in the pulp phase [22, 23]. Fine particles typically show slow recovery rates owing to a decrease in particle-bubble collisions. Furthermore, fine particles tend to have large specific surface areas, which can result in excessive adsorption of reagents and other effects associated with chemically active particles. These factors can have a considerable impact on grades and recovery [24].

Notably, particle size significantly impacts molybdenite flotation. As shown in Fig. 2.1, an optimal particle size (38–75 μm) can achieve satisfactory recovery of molybdenite [1]. Nevertheless, molybdenite recovery decreases significantly at both coarse and fine particle sizes. The poor floatability of coarse molybdenite particles is attributed to the disruption of bubble-particle aggregates in turbulent zones and a decrease in the buoyancy of bubble-particle aggregates [25]. Molybdenite flotation is significantly influenced by the face/edge ratio, which varies with particle size. For molybdenite fines, the face/edge ratio declines, hydrophilic edge become dominant, hydrophobicity decreases, and thus floatability drops significantly [26]. Additionally, froth flotation responds poorly to molybdenite fines mainly because fine particles with low mass have a low probability of collision and adhesion with air bubbles [27], leading to a low flotation rate. Consequently, the flotation efficiency of molybdenite fines drops significantly. To efficiently collect molybdenite fines, employing collectors with strong collecting ability is necessary.

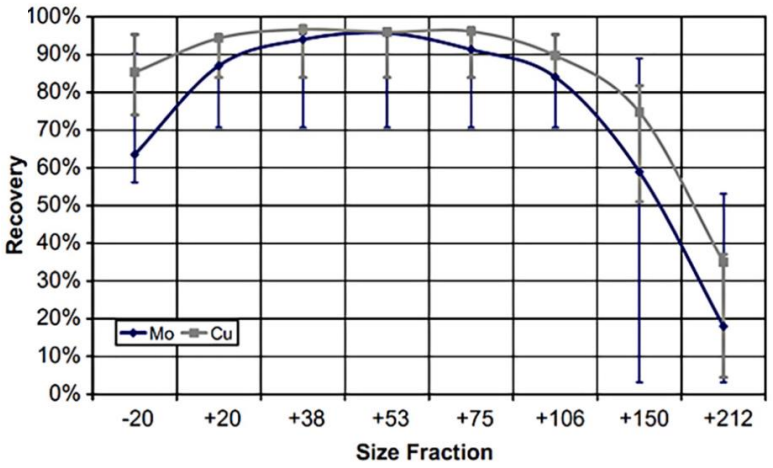

Fig. 2.1 Average size by size recovery of Mo and Cu for the 18 months from April 2005 until October 2006 of Bingham Canyon mine.

2.3.2 Surface oxidation

Because covalent bonds are broken to produce edge surfaces, these surfaces are considerably more reactive than face surfaces. When molybdenite is oxidized, the reaction occurs primarily at the edge surfaces, and secondarily at defect sites in face regions [28]. Therefore, Molybdenite fines are more easily oxidized due to the dominant edges. Chander and Fuerstenau reported that the floatability of molybdenite (without collectors) was strongly affected by surface oxidation, primarily because of the effect of the oxidation products on electrical and hydration phenomena. Oxidation species (e.g., $HMoO_4^-$ and MoO_4^{2-}) determine the electric charge at edges, thereby rendering them hydrophilic [29]. In addition, they found that the contact angle of roasted molybdenite decreased from 80 ° to 30 ° with increasing temperature. Therefore, surface oxidation is a crucial factor in the flotation of molybdenite fines.

2.3.3 Flotation collectors

2.3.3.1 Hydrocarbon oils

Hydrocarbon oils, such as kerosene, diesel oil, and transformer oil, are typical molybdenite collectors. Hydrocarbon oils differ in their effectiveness in enhancing the natural floatability of molybdenite. The collecting ability of hydrocarbon oils for molybdenite is closely related to their composition, chemical structure, chain length, viscosity and distillation range. For instance, Li et al. demonstrated that the viscosity, hydrophobicity and collecting ability increased as the carbon chain length of hydrocarbon oils increased, but their dispersion became worse [30]. Zhu et al. found that low-viscosity hydrocarbon oils could

achieve a high grade but low recovery in molybdenite flotation, whereas high-viscosity hydrocarbon oils exhibited the opposite flotation result due to their large molecules and strong collecting ability, which favored the adhesion of both fine and coarse molybdenite particles to the froth [31]. In addition, the distillation range of hydrocarbon oils also has an impact on molybdenite flotation efficiency. Smit et al pointed out that hydrocarbon oils with a distillation range below 180 ℃ showed poor collecting ability and flotation performance in molybdenite flotation. In contrast, when the distillation range exceeded 180 ℃, the collecting ability improved with increasing distillation range. However, the flotation rate decreased when the distillation ranges of hydrocarbon oils surpassed 310 ℃ [32]. Furthermore, researchers have investigated the interaction mechanism between hydrocarbon oils and molybdenite surfaces. It was found that hydrocarbon oils physically adsorb on molybdenite surfaces through van der Waals forces and hydrophobic interactions due to their low chemical activity and inability to ionize in aqueous solutions [26].

Kerosene is the most commonly used collector in molybdenite flotation for enhancing the hydrophobicity of molybdenite surfaces [33]. However, its flotation efficiency is limited. As a non-polar hydrocarbon oil, kerosene is barely soluble in water and exists only as oil droplets when submerged. The dispersion of these oil droplets in aqueous solutions is restricted, leading them to coalesce rather than approach the molybdenite surface [34]. Hence, the flotation performance of molybdenite deteriorates sharply, resulting in increased kerosene consumption, which imposes a substantial economic burden and raises environmental concerns [35]. Emulsification is considered an effective method to improve the dispersion of kerosene in water [36]. Emulsifying kerosene breaks larger droplets into smaller ones, increasing the specific surface area of the kerosene droplets. This method enhances the dispersion of kerosene and then facilitates more effective collision, adhesion, and spreading of the droplets on molybdenite particles, thereby improving their hydrophobicity [37]. Replacing pristine kerosene with emulsified kerosene can accelerate the diffusion of hydrocarbon oil in the slurry, enhance its adsorption on molybdenite surfaces, reduce the dosage of reagents, and increase the flotation rate [38]. Consequently, emulsified kerosene should be introduced in the flotation of molybdenite as a collector.

2.3.3.2 Emulsification of hydrocarbon oil

Emulsification methods can be divided into mechanical emulsification and chemical emulsification. Mechanical emulsification primarily employs equipment such as homogenizers, mechanical stirrers and ultrasonic emulsifiers, etc., which directly emulsify water and kerosene. Nevertheless, emulsified kerosene produced through this method has poor stability and must be used immediately during the flotation process, thereby limiting its

applicability. On the other hand, chemical emulsification uses emulsifiers to modify kerosene, which is the main method for kerosene emulsification. Emulsifiers are surfactants with both hydrophilic and lipophilic groups. During the flotation process, these emulsifiers adsorb at the oil-water interface, with their polar groups extending into the aqueous phase while their non-polar groups extend into the oil phase. This interaction reduces the surface tension at the oil-water interface, thereby enhancing the dispersion of kerosene and stabilizing the oil-in-water (O/W) emulsion to prevent the coalescence of small oil droplets. The reduction in oil droplet size leads to a thinner oil film on mineral surfaces [39], which effiectively improves molybdenite flotation.

Over the past few decades, researchers have investigated the emulsification of kerosene to improve molybdenite flotation. For example, Masayoshi et al. reported that molybdenite recovery increased significantly from 88.3% to 95.3% after emulsifying kerosene with the emulsifier alkylphenol polyglycolethers [40]. Ge et al. observed that under the same reagent system, emulsified kerosene could increase molybdenite recovery by 7.2% compared with kerosene [41]. Ronzio pointed out that emulsified kerosene was more stably adsorbed on molybdenite surfaces, thus strengthening the adhesion between molybdenite particles and bubbles, resulting in a 2.1% increase in molybdenite floatability [42]. Emulsifier and emulsification technology can improve molybdenite flotation, but the improvement is limited. Furthermore, the adoption of new technologies often requires additional investment and has not been widely adopted in industry.

2.3.3.3 Magnetization of hydrocarbon oil

The objectives of magnetization and emulsification are similar: to increase the dispersion of hydrocarbon oil in the slurry. It is well known that improving the dispersion of hydrocarbon oils is crucial for increasing the flotation efficiency of molybdenite [43, 44]. Amrouche et al. demonstrated that the surface tension of hydrocarbon oil could be affected by a magnetic field [45]. For non-polar hydrocarbon oil, an increase in magnetic field intensity improves interfacial behavior, which reduces the oil-water interfacial behavior and enhances the dispersion of the hydrocarbon oil in water. Conversely, the surface tension decreases as the magnetic field increases, causing poor dispersion of hydrocarbon oil in water. Li et al pointed out that magnetized kerosene exhibited superior collecting ability compared to unmagnetized kerosene, thereby improving molybdenite recovery across various particle sizes [2]. Following magnetization treatment, the interaction force and viscosity of hydrocarbon oil molecules decrease, resulting in smaller oil droplets and thus enhancing the collecting ability of hydrocarbon oil.

2.3.3.4. Thiol collectors

With the continuous development of easily processed molybdenite ores, low-grade and complex associated molybdenite deposits have gradually become the primary source of molybdenum recovery by flotation [33]. However, these molybdenite ores are often distributed with fine particle sizes and coexist with other minerals. Hydrocarbon oil collectors have problems such as high dosage, restrictive operating conditions and poor collecting ability in the flotation of these ores. Therefore, thiol collectors (xanthates, dithiophosphates, dithiocarbamates, etc.) with strong collecting ability have been applied to molybdenite flotation [17].

Malhotra compared the impacts of thiol collectors and hydrocarbon oil collectors on molybdenite flotation and found that xanthate and mercaptan achieved the same collecting performance as hydrocarbon oil collectors [46]. Li et al. used butyl xanthate as a molybdenite collector. The results demonstrated that the recovery rate of molybdenite could exceed 90%, indicating that xanthate exhibits a strong collecting ability for molybdenite [47]. Zhong et al. suggested that the sulfur atom in potassium butyl xanthate is chemically adsorbed on the Mo atom of molybdenite edges, thus significantly improving molybdenite floatability [48].

Dodecyl mercaptan, a typical mercaptan collector, has been widely used in molybdenite flotation. Compared to hydrocarbon oil collectors, dodecyl mercaptan has advantages such as lower dosage and better collecting ability. Douglas reported that using dodecyl mercaptan as a molybdenite collector, molybdenite recovery could be increased by 5% to 40% compared to oil collectors, assuming similar concentrate grades [49].

The sulfhydryl within thiol collectors mainly interact with the molybdenum atom on molybdenite edges. It is known that the proportion of molybdenite edges is small in coarse particles, hence thiol collectors are usually used as auxiliary agents to hydrocarbon oil collectors. Castro and Mayta further revealed that molybdenite fines (6.8 μm) did not respond to an increase in xanthate dosage, while the flotation recovery and rate of coarse particles (51.7 μm) increased significantly. These results indicate that the effectiveness of xanthate as a collector increases with particle size due to its higher degree of inherent hydrophobicity associated with the larger faces/edges ratio [50]. In addition, the interaction mechanism of thiol collectors with other sulfide minerals is analogous to that with molybdenite, indicating that thiol collectors cannot selectively collect molybdenite. Moreover, thiol collectors possess unpleasant odors and certain toxicity, which may cause harm to human health and the environment.

2.4. Flotation method of molybdenite fines

2.4.1 Agglomeration flotation

To improve the flotation efficiency of molybdenite fines, many methods have been developed, one of which is agglomeration flotation [27]. The basic process of agglomeration flotation can be described as follows: when a small amount of oil is added to the agitated slurry, it serves as an adhesive for hydrophobic fine particles through capillary forces, resulting in the formation of larger aggregates composed of fine particles bound by the oil. These larger hydrophobic aggregates then replace individual fine particles to interact with air bubbles, whereas hydrophilic particles remain dispersed in the slurry [51]. Consequently, the agglomerated products can be separated from the slurry by a simple froth flotation operation, owing to the increased collision and attachment probabilities between the fine particles and bubbles [52].

At present, agglomeration flotation is not a novel technique in the mineral industry, which has been explored to improve the flotation and grade of coal fines [53], fine-sized gold and metal oxide minerals [54, 55]. Recently, studies have also focused on the hydrophobic agglomeration flotation of molybdenite fines [14]. Song et al. investigated the flotation of hydrophobic molybdenite agglomerates under intense mechanical conditioning with the addition of a small amount of kerosene. Their results revealed that agglomeration flotation was considerably more effective than conventional flotation for the collection of molybdenite fines [56]. Fu et al. used kerosene, diesel, transformer, and rapeseed oils as bridging reagents to recover molybdenite from ultrafine waste tailings by oil agglomerate flotation. In the industrial experiment, 95% of molybdenum was recovered at a satisfactory grade of 22.62% using transformer oil as the collector [57]. Lin et al. studied the flotation behavior of molybdenite fines with various neutral oils across different pH ranges. It was found that excellent aggregation of molybdenite particles and good floatability of molybdenite fines could be achieved in the presence of transformer oil over the wide pH range of 2–11 [26]. However, due to the high consumption of oily collectors and conditioning energy, agglomeration flotation by oil is not economical and has not been widely adopted in industry.

2.4.2 Nano-bubble flotation

Molybdenite fines in flotation often show an unsatisfactory recovery because of their low collision probability with flotation bubbles [58]. Recently, nano-bubble flotation has also been employed to increase the recovery of molybdenite fines. Nano-bubbles, which are bubbles smaller than 1 μm, can be produced by various methods such as hydrodynamic cavitation, ultrasonication, solvent exchange and temperature variations [59]. Fundamental

and experimental studies have shown that the bubble size significantly influences flotation performance, a smaller bubble size can improve the flotation recovery of fine particles [60]. Compared to conventional-sized bubbles, nano-bubbles attach more readily to particles due to their unique characteristics such as large specific surface area, lower ascending velocity in water and reduced rebound velocity from surfaces, greater contact angle on solid surfaces, among others [61]. Consequently, nano-bubble flotation has emerged as a promising approach for enhancing the flotation efficiency of fine particles [62]. For example, Wang et al. found that the attachment of nano-bubbles could efficiently enhance the recovery of molybdenite fines (–23 μm) by reducing the repulsive force between particles promoting particle aggregation, improving the hydrophobicity of mineral surfaces, further enhancing the bubble-particle collision and attachment, thereby increasing the flotation recovery [63]. Nevertheless, the limited availability of cost-effective nano-bubble generators and the need for further investigation into the stability of nano-bubbles pose challenges to their widespread application in large-scale commercial operations [64].

2.5. Anisotropy study of molybdenite

Molybdenite is not only the primary raw material for molybdenum production but also a crucial sulfide mineral. Due to its exceptional physical and chemical properties, molybdenite has been widely used in lubrication, catalysis, photovoltaics, batteries, nanoelectronics and optoelectronics. Molybdenite exhibits distinct anisotropy, resulting in two different surfaces. Molybdenite surface properties and application efficiency depend on its anisotropy, hence numerous studies have investigated molybdenite anisotropy.

Molybdenite faces are heterogeneous in nature and terraces and clusters of micro-crystals of molybdenite having nano-edges and nano-faces are observed on such faces. Lu et al. investigated the surface potentials of molybdenite faces and edges using an atomic force microscope. It was found that the point of zero charge (PZC) of molybdenite edges was around pH = 3, whereas the PZC of molybdenite faces was below pH = 3 [65]. Lu et al. revealed the micro-wettability of molybdenite faces and edges by analyzing the morphology of femtoliter interfacial droplets. They reported that the oil contact angle of molybdenite edges fluctuated between 48 ° and 90 °, while the oil contact angle of molybdenite faces was less than 1 °. Moreover, a strong hydrophobic force between the probe and molybdenite faces was detected, but no hydrophobic attraction was observed between the probe and molybdenite edges [66]. Feng et al. used atomic force microscopy to study the interaction forces between micrometer-sized dodecane droplets and molybdenite faces in various electrolyte solutions. The results showed that the competition between repulsive electric double layer (EDL) forces and attractive hydrophobic forces was directly responsible for

oil–molybdenite attachment behavior. High pH and low salinity (<24 mM NaCl) led to strong repulsive EDL forces, which stabilized the interaction and prevented the attachment of oil to molybdenite. In contrast, low pH and high salinity facilitated oil attachment to molybdenite through the reduction of EDL force, allowing attractive hydrophobic forces to dominate [67]. Li et al. reported that the surface energy of the face was 0.0426 J/m^2, while that of the edge was 0.1952 J/m^2 [68]. The surface energy of hydrocarbon oil is 0.03 J/m^2, which is close to that of molybdenite faces. Therefore, hydrocarbon oil is favorably adsorbed on the face rather than the edge, which explains why kerosene cannot effectively collect molybdenite fines with edge-dominated surfaces.

Beaussart et al., showed that the molecular weight of polymers determined the adsorbed amounts on molybdenite surfaces. Additionally, the content of hydrated water on the polymer surface was closely related to the properties of substituted functional groups within polymer molecules. Bubble-surface collisions further indicated that polymers affected thin film rupture and dewetting rate differently, which correlated with differences in the adsorbed layer morphology. They established a relationship between the thickness of the polymer adsorption layer, the rupture rate of the hydrated film and molybdenite recovery [69]. Kor et al. investigated the adsorption of carboxymethylcellulose on molybdenite surfaces. Their results showed that a higher degree of carboxyl substitution in the adsorbing polymer resulted in thinner adsorbed layers with a worse inhibition effect [70]. Xie et al. used atomic force microscopy to directly measure the interaction forces between an air bubble and molybdenite surface before and after polymer (i.e., guar gum) adsorption. It was found that bubbles were unable to adhere molybdenite surface after treatment with polymer solution, mainly because the adsorption of polymer on molybdenite surfaces reduced the hydrophobic force between molybdenite and bubbles. Moreover, the adsorption of polymer might introduce spatial repulsion forces as polymer concentration increases [71].

2.6. Research gap

Molybdenum plays a critical role in the metallurgical and chemical industries. Molybdenite is the principal resource for molybdenum extraction and can also be collected as a byproduct from porphyry Cu–Mo ores. Froth flotation is a highly effective approach for separating molybdenite from chalcopyrite, which has been probed extensively. Previous studies have demonstrated that molybdenite is an anisotropic mineral with hydrophobic faces and hydrophilic edges. Surface potential, contact angle and surface energy can be employed to interpret different reactions on molybdenite surfaces.

Particle size is a key factor in molybdenite flotation. Particles that are too fine can decrease molybdenite floatability. Surface oxidation also has a great impact on molybdenite

flotation. Molybdenite floatability decreases because hydrophilic edges are oxidized, rendering the hydrophobicity further reduced. In addition, collectors play an important role in molybdenite flotation. As high-grade molybdenite deposits diminish, low-grade and fine-disseminated molybdenite ores are gradually explored to satisfy market demands. These ores need fine grinding before flotation, which causes a lot of fine particles. Due to the above-mentioned reasons, traditional collectors cannot effectively recover molybdenite fines. Although researchers have developed some approaches (eg. agglomeration flotation and nano-bubble flotation) to improve the flotation of molybdenite fines, these methods have not been widely adopted due to their high investment costs. Therefore, seeking new methods to improve the floatability of molybdenite fines is extremely essential.

Hydrophilic edges dominate on molybdenite, which greatly decreases the hydrophobicity of molybdenite fines, resulting in poor flotation performance. Notably, exploring novel collectors that are efficient and targeted at molybdenite edges is a promising method for recovering molybdenite fines. These collectors can selectively adsorb on molybdenite edges, thereby enhancing their hydrophobicity and improving the floatability of molybdenite fines. At present, the research on molybdenite mainly focuses on its anisotropy, polymer adsorption, agglomeration flotation, seawater flotation and so on. Nevertheless, there has been limited investigation into targeted regulation of edge interface properties in the flotation of molybdenite fines. This research can not only enhance the flotation efficiency of molybdenite fines but also provide theoretical guidance for regulating edge interface properties.

Reference

[1] B. Triffett, C. Veloo, B.J.I. Adair, D. Bradshaw, An investigation of the factors affecting the recovery of molybdenite in the Kennecott Utah Copper bulk flotation circuit, Miner. Eng. 21 (2008) 832–840.

[2] H. Li, W. Xiao, J. Jin, Y. Han, Influence mechanism of magnetized modified kerosene on flotation behavior of molybdenite, Minerals. 12 (2021) 2.

[3] O.Y. Plotinskaya, V. V Shilovskikh, J. Najorka, E. V Kovalchuk, R. Seltmann, J. Spratt, Grain-scale distribution of molybdenite polytypes versus rhenium contents: μXRD and EBSD data, Mineral. Mag. 83 (2019) 639–644.

[4] X. Chen, X. Liu, Z. Zhao, M. Hao, Research of the dissolving capacity of molybdenite in the white matte, Int. J. Refract. Met. Hard Mater. 52 (2015) 1–5.

[5] J.X. Kang, X.K. Li, Thoughts on the development of molybdenum beneficiation technology, in: IOP Conf. Ser. Earth Environ. Sci., IOP Publishing, 2021: p. 12001.

[6] B. Yang, H. Yan, M. Zeng, P. Huang, F. Jia, A. Teng, A novel copper depressant for selective flotation of chalcopyrite and molybdenite, Miner. Eng. 151 (2020) 106309.

[7] G. Liu, Y. Lu, H. Zhong, Z. Cao, Z. Xu, A novel approach for preferential flotation recovery of molybdenite from a porphyry copper–molybdenum ore, Miner. Eng. 36 (2012) 37–44.

[8] J.S. Laskowski, S. Castro, O. Ramos, Effect of seawater main components on frothability in the flotation of Cu-Mo sulfide ore, Physicochem. Probl. Miner. Process. 50 (2014) 17–29.

[9] S. Raghavan, L.L. Hsu, Factors affecting the flotation recovery of molybdenite from porphyry copper ores, Int. J. Miner. Process. 12 (1984) 145–162.

[10] A.R. Gerson, R.S.C. Smart, J. Li, N. Kawashima, D. Weedon, B. Triffett, D. Bradshaw, Diagnosis of the surface chemical influences on flotation performance: Copper sulfides and molybdenite, Int. J. Miner. Process. 106 (2012) 16–30.

[11] M. Zanin, I. Ametov, S. Grano, L. Zhou, W. Skinner, A study of mechanisms affecting molybdenite recovery in a bulk copper/molybdenum flotation circuit, Int. J. Miner. Process. 93 (2009) 256–266.

[12] S.R. Rao, J.A. Finch, A review of water re-use in flotation, Miner. Eng. 2 (1989) 65–85.

[13] W. Liu, C.J. Moran, S. Vink, A review of the effect of water quality on flotation, Miner. Eng. 53 (2013) 91–100.

[14] T. He, H. Wan, N. Song, L. Guo, The influence of composition of nonpolar oil on flotation of molybdenite, Miner. Eng. 24 (2011) 1513–1516.

[15] J. Wu, J. Feng, B. Yang, R. Martin, S. Song, M. Quintana, F. Jia, X. Tian, The anisotropic adsorption of potassium cetyl phosphate on molybdenite surface and its implication for improving the flotation of molybdenite fines, J. Mol. Liq. 378 (2023) 121616.

[16] R.G. Dickinson, L. Pauling, The crystal structure of molybdenite, J. Am. Chem. Soc. 45 (1923) 1466–1471.

[17] S. Castro, A. Lopez-valdivieso, J.S. Laskowski, Review of the fl otation of molybdenite . Part I : Surface properties and fl oatability, Int. J. Miner. Process. 148 (2016) 48–58.

[18] S. Chander, W.I.E. JM, F. DW, On the native floatability and surface properties of naturally hydrophobic solids, in: AIChE Symp. Ser., 1975.

[19] S.B. Johnson, G. V Franks, P.J. Scales, D. V Boger, T.W. Healy, Surface chemistry–rheology relationships in concentrated mineral suspensions, Int. J. Miner. Process. 58 (2000) 267–304.

[20] J. Wu, B. Yang, S. Song, Q. Mildred, F. Jia, X. Tian, The efficient recovery of molybdenite fines using a novel collector: Flotation performances, adsorption mechanism and DFT calculation, Miner. Eng. 107848 (2022).

[21] W.J. Trahar, The selective flotation of galena from sphalerite with special reference to the effects of particle size, Int. J. Miner. Process. 3 (1976) 151–166.

[22] H.R. Spedden, W.S. Hannan, Attachment of mineral particles to air bubbles in flotation, Trans. Am. Inst. Min. Metall. Eng. 183 (1949) 208–213.

[23] P.F. Whelan, D.J. Brown, Particle-bubble attachment in froth flotation, Trans. Inst. Min. Metall. 65 (1956) 181–192.

[24] D. Feng, C. Aldrich, Effect of particle size on flotation performance of complex sulphide ores, Miner. Eng. 12 (1999) 721–731.

[25] H. Soto, G. Barbery, Flotation of coarse particles in a counter-current column cell, Mining, Metall. Explor. 8 (1991) 16–21.

[26] Q. quan Lin, G. hua Gu, H. Wang, Y. cai Liu, J. gang Fu, C. qing Wang, Flotation mechanisms of molybdenite fines by neutral oils, Int. J. Miner. Metall. Mater. 25 (2018) 1–10.

[27] S. Li, X. Ma, J. Wang, Y. Xing, X. Gui, Y. Cao, Effect of polyethylene oxide on flotation of molybdenite fines, Miner. Eng. 146 (2020) 106146.

[28] J.R. Lince, P.P. Frantz, Anisotropic oxidation of MoS2 crystallites studied by angle-resolved X-ray photoelectron spectroscopy, Tribol. Lett. 9 (2001) 211–218.

[29] S.Chander, W.Fuerstenau, On the natural floatability of molybdenite, Trans. SME/AIME. 252 (1972) 62–69.

[30] B. Li, Z. Guo, M. Du, D. Han, J. Han, L. Zheng, C. Yang, Research Status and Outlook of Mechanism, Characterization, Performance Evaluation, and Type of Pour Point Depressants in Waxy Crude Oil: A Review, Energy & Fuels. 38 (2024) 7480–7509.

[31] Y. Zhu, Molybdenite flotation reagent, Met. Ore Dress. Abroad. (1998) 7–11.

[32] F.J. Smit, A.K. Bhasin, Relationship of petroleum hydrocarbon characteristics and molybdenite flotation, Int. J. Miner. Process. 15 (1985) 19–40.

[33] B. Yang, J. Wu, B. Deng, H. Shao, S. Song, M. Quintana, Improving the Flotation of Unoxidized and Oxidized Molybdenite Fines Using Dodecylamine as a Collector: Flotation Tests and Interaction Mechanism, Minerals. 14 (2024) 468.

[34] Y. Qiu, Z. Mao, K. Sun, L. Zhang, L. Yang, Y. Qian, T. Lei, Cost-efficient clean flotation of amorphous graphite using water-in-oil kerosene emulsion as a novel collector, Adv. Powder Technol. 33 (2022) 103770.

[35] M. Jin, G. Xie, W. Xia, Y. Peng, Flotation optimization of ultrafine microcrystalline graphite using a box-behnken design, Int. J. Coal Prep. Util. 38 (2018) 281–289.

[36] L. Li, X. Lu, J. Qiu, D. Liu, Effect of microemulsified collector on froth flotation of coal, J. South. African Inst. Min. Metall. 113 (2013) 877–880.

[37] J. Rubio, F. Capponi, R.T. Rodrigues, E. Matiolo, Enhanced flotation of sulfide fines using the emulsified oil extender technique, Int. J. Miner. Process. 84 (2007) 41–50.

[38] X. Weiwei, H. Kaiwu, W. Donghui, Z. Yuran, L. Xiu, Study on flotation properties of emulsified diesel oil, Energy Procedia. 14 (2012) 750–755.

[39] M. Porras, C. Solans, C. Gonz á lez, J.M. Guti é rrez, Properties of water-in-oil (W/O) nano-emulsions prepared by a low-energy emulsification method, Colloids Surfaces A Physicochem. Eng. Asp. 324 (2008) 181–188.

[40] M. WADA, H. MAJIMA, S. ToDA, Studies on the flotation of molybdenite. II: some experiments on the kerosene flotation, (1963) 96–104.

[41] W. Ge, J. Liu, H. Ren, Y. Zhu, W. Han, Y. Han, Enhanced mixed flotation of copper–molybdenum ore using dodecyl dimethyl betaine-emulsified kerosene as environmentally friendly collector, J. Clean. Prod. 447 (2024) 141576.

[42] R.A. Ronzio, The role of surfactants in the flotation of molybdenite at climax, (1970) 504–512.

[43] T.W. Healy, D.W. Fuerstenau, The isoelectric point/point-of zero-charge of interfaces formed by aqueous solutions and nonpolar solids, liquids, and gases, J. Colloid Interface Sci. 309 (2007) 183–188.

[44] Y. Gao, L. Pan, Understanding the mechanism of froth flotation of molybdenite using oily collectors from a perspective of thinning and rupture of thin liquid film, Miner. Eng. 163 (2021) 106805.

[45] F. Amrouche, S.R. Gomari, M. Islam, X. Donglai, New insights into the application of a magnetic field to enhance oil recovery from oil-wet carbonate reservoirs, Energy & Fuels. 33 (2019) 10602–10610.

[46] D. Malhotra, Evaluation of flotation capture agents for molybdenite flotation, in: SME-AIME Annu. Meet., 1985: pp. 24–28.

[47] C. Li, G. Zhang, L. Xun, H. Liu, Q. Shi, Flotation separation of molybdenite from talc using a new inhibitor Artemisia sphaerocephala Krasch gum, Miner. Eng. 174 (2021) 107227.

[48] C. Zhong, H. Wang, L. Zhang, M. Guo, B. Feng, Flotation separation of molybdenite and talc by xanthan gum, Powder Technol. 388 (2021) 158–165.

[49] D.R. Shaw, An excellent sulphide ore capture agent: dodecyl mercaptan, Miner. Eng. 33 (1981) 686–692.

[50] S.H. Castro, E. Mayta, A kinetics approach to the effect of particle size on the flotation of molibdenite. A. Sutulov Memorial Volume. Vol II, in: IV Meet. South. Hemisph. Miner. Technol. III Lat. Am. Congr. Froth Flot. Castro, S., Alvarez, J.(Eds.). Concepción, Chile, 1994: pp. 331–344.

[51] J. Choi, E. Lee, S.Q. Choi, S. Lee, Y. Han, H. Kim, Arsenic removal from contaminated soils for recycling via oil agglomerate flotation, Chem. Eng. J. 285 (2016) 207–217.

[52] Q.Q. Lin, G.H. Gu, H. Wang, C.Q. Wang, Y.C. Liu, J.G. Fu, R.F. Zhu, An effective approach for improving flotation recovery of molybdenite fines from a finely-disseminated molybdenum ore, J. Cent. South Univ. 25 (2018) 1326–1339.

[53] N. Gence, Coal recovery from bituminous coal by aggloflotation with petroleum oils, Fuel. 85 (2006) 1138–1142.

[54] S. Sen, A. Seyrankaya, Y. Cilingir, Coal–oil assisted flotation for the gold recovery, Miner. Eng. 18 (2005) 1086–1092.

[55] S. Duzyol, A. Ozkan, Effect of contact angle, surface tension and zeta potential on oil agglomeration of celestite, Miner. Eng. 65 (2014) 74–78.

[56] S. Song, X. Zhang, B. Yang, A. Lopez-Mendoza, Flotation of molybdenite fines as hydrophobic agglomerates, Sep. Purif. Technol. 98 (2012) 451–455.

[57] F. Jiangang, C. Kaida, W. Hui, G. Chao, L. Wei, Recovering molybdenite from ultrafine waste tailings by oil agglomerate flotation, Miner. Eng. 39 (2012) 133–139.

[58] T. Miettinen, J. Ralston, D. Fornasiero, The limits of fine particle flotation, Miner. Eng. 23 (2010) 420–437.

[59] S. Nazari, S.Z. Shafaei, M. Gharabaghi, R. Ahmadi, B. Shahbazi, Effect of frother type and operational parameters on nano bubble flotation of quartz coarse particles, J. Min. Environ. 9 (2018) 539–546.

[60] S. Nazari, A. Hassanzadeh, The effect of reagent type on generating bulk sub-micron (nano) bubbles and flotation kinetics of coarse-sized quartz particles, Powder Technol. 374 (2020) 160–171.

[61] A. Azevedo, R. Etchepare, S. Calgaroto, J. Rubio, Aqueous dispersions of nanobubbles: Generation, properties and features, Miner. Eng. 94 (2016) 29–37.

[62] C. Li, H. Zhang, A review of bulk nanobubbles and their roles in flotation of fine particles, Powder Technol. 395 (2022) 618–633.

[63] X. Wang, S. Yuan, J. Liu, Y. Zhu, Y. Han, Nanobubble-enhanced flotation of ultrafine molybdenite and the associated mechanism, J. Mol. Liq. 346 (2022) 118312.

[64] D. Tao, Recent advances in fundamentals and applications of nanobubble enhanced froth flotation: A review, Miner. Eng. 183 (2022) 107554.

[65] Z. Lu, Q. Liu, Z. Xu, H. Zeng, Probing Anisotropic Surface Properties of Molybdenite by Direct Force Measurements, Langmuir. 31 (2015) 11409–11418.

[66] Z. Lu, Z. Lu, S. Peng, X. Zhang, Q. Liu, Microwetting of pH-Sensitive Surface and Anisotropic MoS2 Surfaces Revealed by Femtoliter Sessile Droplets, Langmuir. 32 (2016) 11273–11279.

[67] L. Feng, R. Manica, J.S. Grundy, Q. Liu, Unraveling interaction mechanisms between molybdenite and a dodecane oil droplet using atomic force microscopy, Langmuir. 35 (2019) 6024–6031.

[68] H. Li, T. He, H. Wan, Y. Han, Y. Guo, J. Jin, Insights into Selection of the Auxiliary Collector and Its Applicability Analysis for Improving Molybdenite Flotation, Minerals. 11 (2021) 528.

[69] A. Beaussart, L. Parkinson, A. Mierczynska-Vasilev, D.A. Beattie, Adsorption of modified dextrins on molybdenite: AFM imaging, contact angle, and flotation studies, J. Colloid Interface Sci. 368 (2012) 608–615.

[70] M. Kor, P.M. Korczyk, J. Addai-Mensah, M. Krasowska, D.A. Beattie, Carboxymethylcellulose adsorption on molybdenite: the effect of electrolyte composition on adsorption, bubble–surface collisions, and flotation, Langmuir. 30 (2014) 11975–11984.

[71] L. Xie, J. Wang, D. Yuan, C. Shi, X. Cui, H. Zhang, Q. Liu, Q. Liu, H. Zeng, Interaction mechanisms between air bubble and molybdenite surface: impact of solution salinity and polymer adsorption, Langmuir. 33 (2017) 2353–2361.

Chapter III. Anisotropic adsorption of xanthate species on molybdenite faces and edges and its implication on the flotation of molybdenite fines

3.1 Introduction

Molybdenite (MoS_2) is a significant natural resource for molybdenum extraction, which is broadly applied in agriculture, metallurgy, catalysis and optoelectronics fields because of its distinguished lubricity, catalytic activity, thermal stability and photoelectric properties [1]. Typically, molybdenite is mainly concentrated in Cu–Mo porphyry ores, where molybdenite and chalcopyrite ($CuFeS_2$) coexist closely. To efficiently separate molybdenite and chalcopyrite, a two-stage flowsheet is commonly employed for flotation separation [2, 3]. In the first stage, non-polar oil and a thiol-type collector are commonly used to achieve the maximum recovery of molybdenite and chalcopyrite simultaneously. In the second stage, molybdenite and chalcopyrite are selectively floated using chalcopyrite or molybdenite depressants. Xanthate is the primary thiol-type collector, which has been broadly applied in the flotation of sulfides because of its strong collecting ability and good availability. Thus, the use of xanthate in the bulk flotation of Cu–Mo sulfides is generally inevitable [4, 5]. However, little attention has been paid to investigating the influence of xanthate on the flotation of molybdenite particles, not to mention the interaction mechanism of xanthate species on anisotropic molybdenite surface. Thus, it is significant to clarify the interaction mechanism of xanthate species on anisotropic molybdenite surface and to unveil its implication on the flotation of molybdenite fines.

As a laminar mineral with apparent anisotropy, molybdenite consists of two types of surfaces: polar edges and non-polar faces. The inherently hydrophobic faces are attributed to the disruption of the van der Waals force between S–Mo–S layers, while the relatively hydrophilic edges are derived from the cleavage of S–Mo covalent bonds [6]. The face/edge ratio can significantly affect molybdenite hydrophobicity, thus influencing its flotation performance. In addition, the anisotropic properties of molybdenite cause faces and edges to exhibit distinctly different characteristics. For example, edges had a lower open circuit potential and higher point of zero charge than faces [7, 8]. The critical wetting surface tension of edges (72.5 mN/m) was about 2.5-fold that of faces (29 mN/m) [9]. The surface free energy of edges (0.1952 J/m^2) was approximately five times higher than faces (0.0426 J/m^2) [10]. These apparent distinctions of faces and edges may significantly affect their response to flotation reagents. Therefore, it is imperative to unveil the interaction mechanism of xanthate

on molybdenite faces and edges, and to elucidate its impact on the flotation of molybdenite fines [11].

Over the past decades, some investigations have studied the interaction mechanism between xanthate and molybdenite surfaces. For instance, Allision et al. detected the formation of dixanthogen as well as an unidentified product on the molybdenite surface with various alkyl xanthates using a spectrophotometric technique [12]. However, Afenya et al. found that only dixanthogen adsorbed on molybdenite faces after the introduction of xanthate [13, 14]. On the other hand, Russian researchers reported xanthate adsorbed on molybdenite, but no insoluble metal xanthate was observed [13]. Nevertheless, Zhang et al. summarized that both metal xanthate and dixanthogen existed on molybdenite surfaces using an Infrared Spectrometer [15]. Despite previous investigations proposing the possible xanthate products formed on molybdenite surfaces, no convincing conclusion has been drawn. In fact, these results are even contradictory. The anisotropy of molybdenite may be responsible for these inconsistent conclusions. Nevertheless, the investigation concerns about the interaction of xanthate species with faces and edges is rare.

In this work, sodium isobutyl xanthate (SIBX) was employed to clarify the interaction of xanthate with faces and edges. Flotation behaviors and adsorption mechanisms were explored via micro-flotation tests, contact angle, adsorption capacity, FTIR, electrochemical tests, AFM, XPS and DFT calculations. This work aimed to unveil the interaction mechanism of xanthate species with molybdenite faces and edges, thus clarifying its impact on the flotation of molybdenite fines.

3.2 Experimental

3.2.1 Materials

Pure molybdenite was obtained from Wuzhou City, China. The minerals were selected by hand, ground and sieved to obtain −20 μm particles for flotation and chemical analysis. X-ray diffraction (XRD) pattern showed that all the peaks observed belonged to molybdenite (Fig. 3.1). In addition, the chemical assaying revealed that molybdenite samples had a high level of purity (97%).

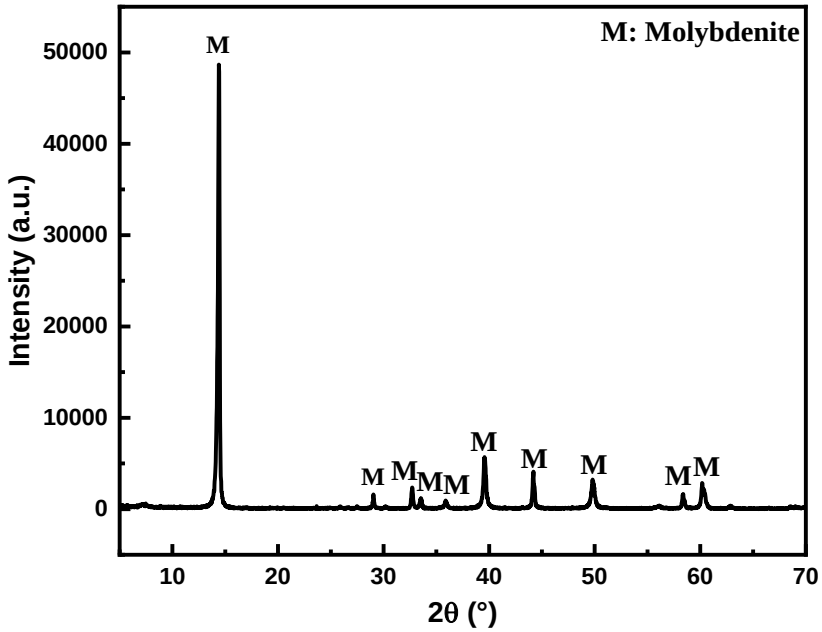

Fig. 3.1 The XRD pattern of pure molybdenite ores.

All chemical reagents utilized in this work were purchased from Aladdin, China. SIBX, methyl isobutyl carbinol (MIBC), HCl and NaOH served as the collector, frother and pH regulators. Deionized water was utilized throughout all tests.

3.2.2 Flotation tests

Flotation tests were conducted utilizing an XFG flotation machine. In a typical test, 2 g of molybdenite were added to 30 mL of deionized water and ultrasonically dispersed for 2 min. After the adjustment of pH, the slurry was introduced to a flotation cell. Following SIBX and MIBC addition, a 3 min flotation process was performed, and then flotation products were collected to determine floatability.

3.2.3 UV-vis spectrophotometry determination

For each adsorption experiment, 2 g of mineral particles were introduced into a certain concentration of SIBX solution and stirred for 30 min. Then 5 mL of the suspension was filtered for measurement. A UV-visible spectrophotometer (Lambda 750S, PerkinElmer, USA) was used to evaluate the filtrates at a wavelength of λ = 301 nm. The adsorption capacity was analyzed using the subsequent Eq (1):

$$Q_e = \frac{(C_0 - C_e)V}{1000m} \quad (1)$$

where Q_e denoted the adsorption capacity, mg/g; C_0 and C_e meant the initial and equilibrium concentration in solution, mg/L; V denoted solution volume, mL; m meant the mass of mineral samples, g.

Fig. 3.2 depicts a standard curve between absorbance and SIBX concentration of 5.81 × 10^{-6} to 5.81 × 10^{-5} mol/L. The standard curve with a correlation coefficient of 0.99989 was utilized to determine the residual SIBX concentration after adsorption.

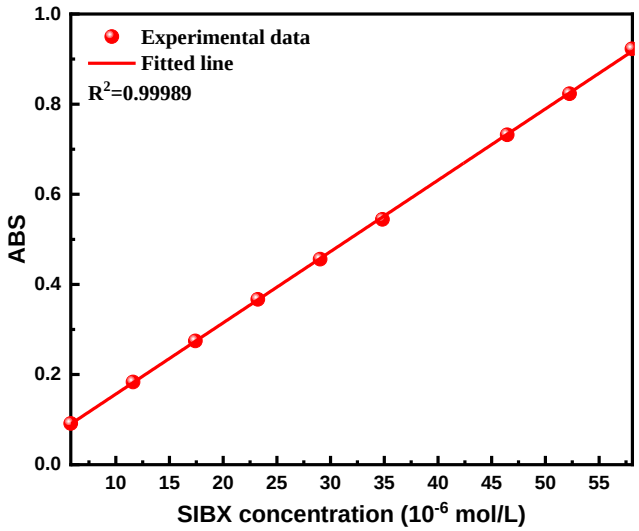

Fig. 3.2 The absorbance as a function of SIBX concentration.

3.2.4 Characterizations

FTIR spectra were acquired utilizing a UV-2600i spectrometer (Shimadzu, Japan). 0.15 g of molybdenite minerals were conditioned in 5.81 × 10^{-3} mol/L SIBX solution (pH = 5) for 30 min. After being filtered and freeze-dried, the minerals were mixed with KBr for FTIR measurement using the transmission method. XPS spectra were collected utilizing a K-alpha photoelectron spectrometer (Shimadzu, Japan). The spectra were analyzed by Thermo Avantage 5.9922 and calibrated at C 1 s (at 284.80 eV). The Tafel and rest potential tests were performed using an electrochemical workstation (CHI600E, China). Face and edge electrodes were prepared as the same processes described in previous literature [16]. A fresh face (0.78 cm^2) or edge (0.65 cm^2) plane was utilized as a working electrode. The counter electrode and reference electrode were Pt and Ag/AgCl (Saturated KCl) electrodes. Sodium chloride (NaCl, 0.1 mol/L) served as the supporting electrolyte. The contact angle on faces and edges was measured by a contact angle goniometer. Fresh edges and faces were prepared following the process described in previous literature [7]. The face or edge was treated in different SIBX solutions (pH = 5) for 30 min. Subsequently, the surface naturally dried at

room temperature. Three different locations were tested for each molybdenite surface, and the average contact angle value was reported. The topographic images of the edge and face treated and untreated with SIBX (3.48×10^{-3} mol/L at pH of 5) were captured by an atomic force microscope (Shimadzu, Japan). The detailed observation process was described in our previous literature [6, 17].

3.2.5 DFT calculation

The adsorption process of SIBX on molybdenite surfaces was investigated by Material Studio 2019 software. All models were simulated in the CASTEP module with the valence electron configurations of Mo $4s^2 4p^6 4d^5 5s^1$ and S $3s^2 3p^4$. The calculations employed a kinetic energy cutoff of 430 eV and utilized a k-point of $5 \times 5 \times 1$ to sample the Brillouin zone. The force, displacement, and tolerance values for energy, SCF and stress were set as 0.05 eV/Å, 0.002 Å, 2×10^{-5} eV/atom, 2×10^{-6} eV/atom and 0.1 GPa, respectively. A 15 Å vacuum slab was used in molybdenite optimizations. Faces were built along the (0 0 1) surface, and edges were created along the (1 0 0) surface.

3.3 Results and discussion

3.3.1 Micro-flotation tests

Fig. 3.3 (a) presents the impact of SIBX concentration on the floatability of molybdenite fines at pH 9. When SIBX was added, molybdenite floatability increased markedly with increasing SIBX concentration and then almost plateaued at an SIBX concentration of 3.48×10^{-3} mol/L. The floatability increased by 48% at an SIBX concentration of 5.81×10^{-3} mol/L, indicating that SIBX could enhance the flotation efficiency of molybdenite fines.

Fig. 3.3 (b) displays the influence of pH on the floatability of molybdenite fines with and without SIBX. For pure molybdenite, the floatability of molybdenite fines exhibited a gradual decline with increasing pH, which was ascribed to the formation of hydrophilic molybdate ionic species ($HMoO_4^-$ and MoO_4^{2-}) [18]. After being treated with SIBX, the floatability improved and then decreased slightly at pH 7–11. Compared with the case where SIBX was absent, the floatability increased by approximately 40% over the whole pH range, suggesting that SIBX could substantially enhance molybdenite flotation across a broad pH range.

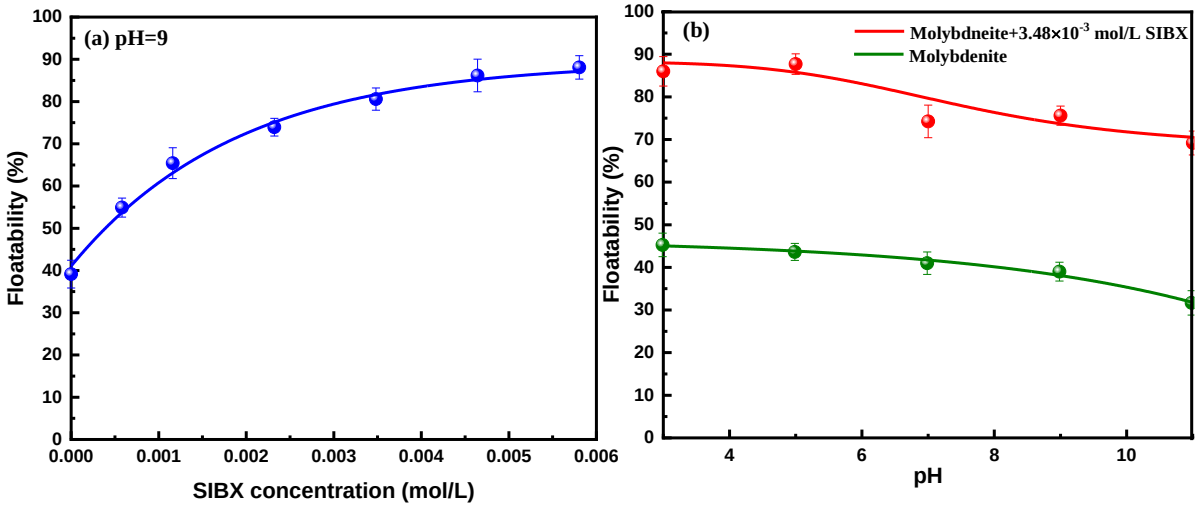

Fig. 3.3 Effect of SIBX concentration (a) and pH (b) on molybdenite flotation.

3.3.2 Contact angle

Fig. 3.4 illustrates the contact angles of molybdenite faces and edges treated with various concentrations of SIBX solution. Fresh faces exhibited good natural hydrophobicity with a contact angle of 63.75 °. As the concentration of SIBX increased, the contact angle increased steadily, reaching 88.25 ° at an SIBX concentration of 5.81 × 10^{-3} mol/L. In contrast, fresh edges were relatively hydrophilic with a contact angle of 40.75 °, and then the contact angle increased significantly to 82 ° at an SIBX concentration of 5.81 × 10^{-3} mol/L, indicating that substantial SIBX species were adsorbed on molybdenite edges. The results suggested that SIBX could enhance the hydrophobicity of both faces and edges, thus improving the flotation of molybdenite fines.

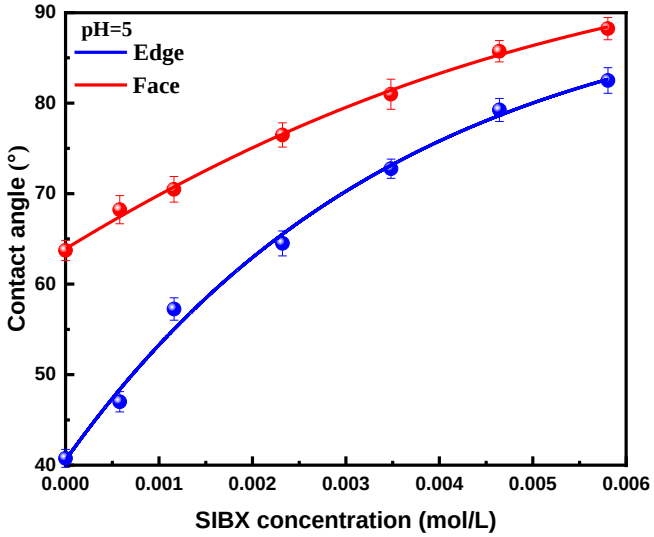

Fig. 3.4 Contact angle on faces and edges before and after SIBX adsorption.

3.3.3 UV-vis spectrophotometry analysis

The adsorption capacity of SIBX on molybdenite at various concentrations is presented in Fig. 3.5. The adsorption capacity increased significantly as SIBX concentration increased, and then remained nearly constant at an SIBX concentration of 3.48×10^{-3} mol/L. These results indicated that SIBX species were adsorbed on molybdenite surfaces, which accounted for the notable improvement in the flotation of molybdenite fines.

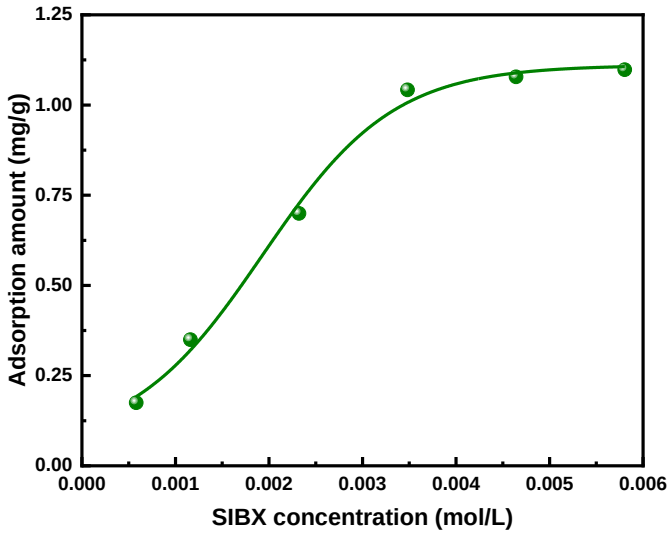

Fig. 3.5 Adsorption capacity of SIBX on molybdenite surfaces.

3.3.4 Tafel curves

Tafel curves of edge and face planes treated and untreated with SIBX are presented in Fig. 3.6. Before the introduction of SIBX, the face had a much lower corrosion current density (CCD) than the edge, indicating that the face has weaker electrochemical reactivity (Wu et al., 2023). After being treated with SIBX, the CCD of both face and edge was reduced. Generally, the decline of the CCD is due to the formation of a passivation coating on both the face and edge, which inhibits electrode corrosion [19]. In our case, the significant decrease in CCD was attributed to substantial adsorption of xanthate species on faces and edges.

In addition, the inhibition efficiency (IE) is determined using the following equation [20]:

$$IE\% = \frac{I_{corr}^{*} - I_{corr}}{I_{corr}^{*}} \times 100\% \quad (2)$$

where I_{corr}^{*} and I_{corr} represent the CCD of electrodes before and after SIBX treatment. As shown in Table 3.1, the IE of SIBX on faces and edges was 48.68% and 47.45%, respectively, which indicated that SIBX species were adsorbed on some reaction sites of molybdenite faces

and edges [21]. These results confirm the adsorption of SIBX species on both faces and edges, which is consistent with contact angle results.

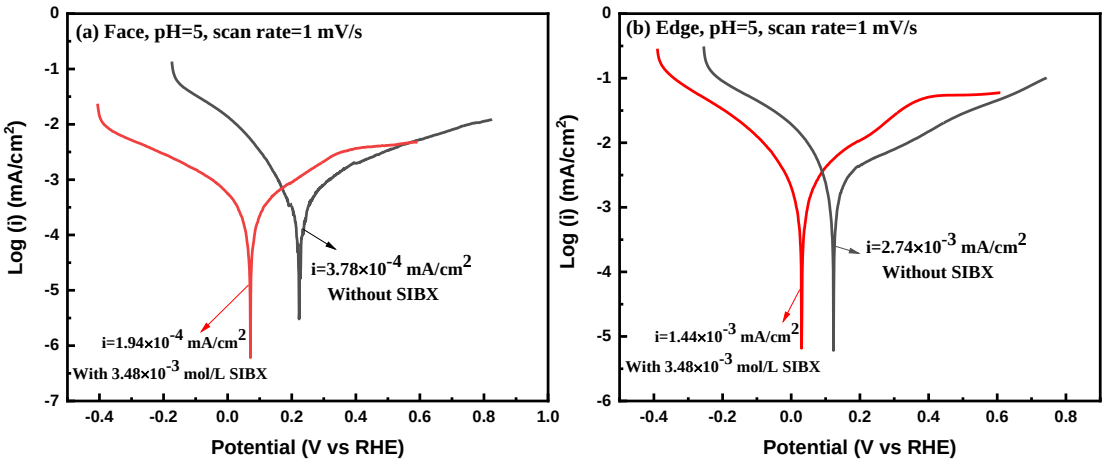

Fig. 3.6 Tafel curves of the face (a) and edge (b) planes treated and untreated with SIBX.

Table 3.1 The analysis of Tafel curves on edge and face planes

Plane	SIBX dosage (mol/L)	CCD (mA/cm^2)	IE (%)
Face	0	3.78×10^{-4}	48.68
	3.48×10^{-3} mol/L	1.94×10^{-4}	
Edge	0	2.74×10^{-3}	47.45
	3.48×10^{-3} mol/L	1.44×10^{-3}	

3.3.5 AFM observation

Fig. 3.7 presents AFM images (three-dimensional views) of molybdenite surfaces before and after SIBX modification. Fig. 3.7 (a) showed that the fresh molybdenite face and edge were clean and molecularly smooth. After SIBX treatment, numerous aggregates were distributed on the face and edge (Fig. 3.7 (b)), indicating that SIBX species or derivatives were present on both edges and faces, which was in agreement with the results of the Tafel curve and contact angle. Furthermore, denser agglomerates appeared on the edge than the face, which indicated that SIBX species were more prone to be adsorbed on the edge than the face.

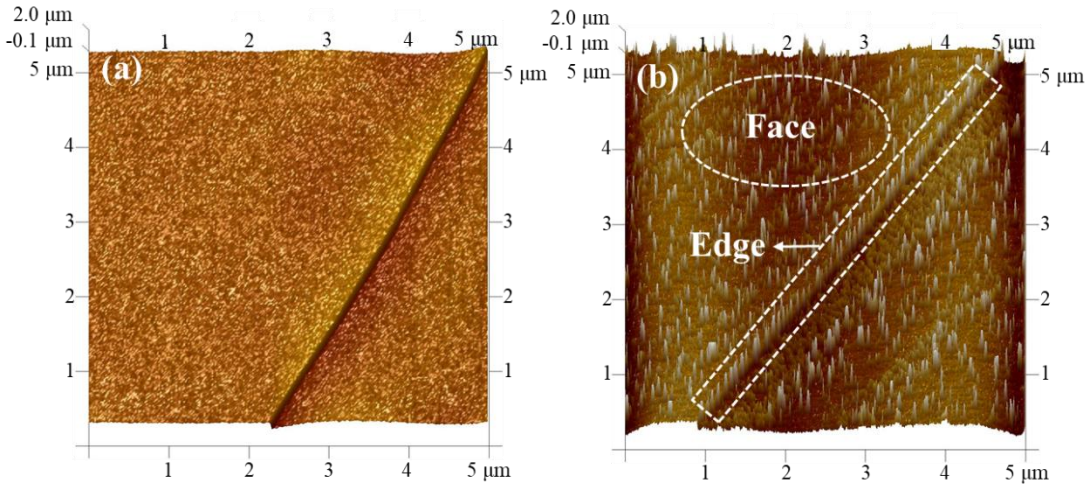

Fig. 3.7 The 3D AFM photographs of molybdenite surfaces without (a) and with (b) SIBX solution.

3.3.6 FTIR analysis

FTIR spectra of SIBX, molybdenite and SIBX-modified molybdenite are shown in Fig. 3.8. For the spectrum of SIBX (see Fig. 3.8 (a)), the absorption bands of –OH, $–CH_3$ and –CH stretching vibrations appeared at 3433, 2970 and 2872 cm^{-1} [22–24]. The absorption bands at 1460 and 1371 cm^{-1} were associated with the deformation vibration of $–CH_2$ and –CH groups [24]. Moreover, its C–O–C, C=S and C–S stretching vibrations appeared at 1184, 1054 and 902 cm^{-1} [25–27]. In Fig. 3.8 (b), the peak at 468 cm^{-1} corresponded to Mo–S vibration in molybdenite [28]. After interaction with SIBX, two new absorption bands appeared at 1029 and 1270 cm^{-1}, which were attributed to the C=S group of butyl xanthate (BX^-) and C–O–C group of dixanthogen (BX_2), respectively [25], indicating that both xanthate and its dixanthogen species were adsorbed on molybdenite surfaces. In addition, the peak at 1029 cm^{-1} exhibited a blue shift from 1054 cm^{-1}, which further indicated that BX^- might be chemisorb on the molybdenite surface.

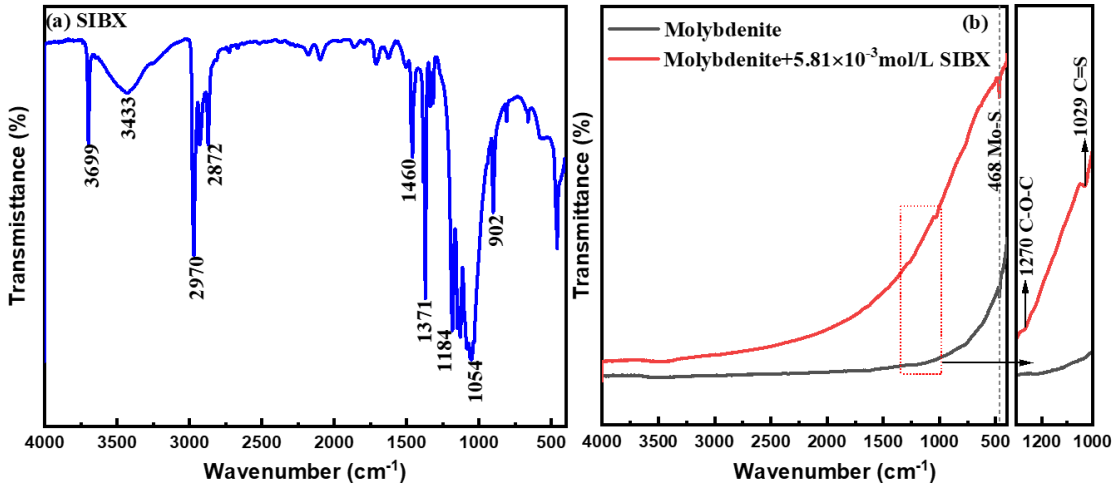

Fig. 3.8 FTIR results of SIBX (a) and molybdenite before and after SIBX addition (b).

3.3.7 XPS analysis

Fig. 3.9 presents the XPS spectra of C 1s, Mo 3d, S 2p and O 1s of molybdenite treated and untreated with SIBX. In Fig. 3.9 (a), C 1s peaks of molybdenite were centered at 284.80 eV (C–C) and 286.60 eV (C–O) [29]. For pure SIBX, the peaks at 284.80, 286.27, 287.83 and 288.98 eV were assigned to the C–C, C–O, S–C=S, and C=O groups [3, 27]. For molybdenite treated with SIBX, it was evident that a new peak appeared at 287.89 eV (S–C=S), which originated from SIBX, indicating that the derivative of SIBX was adsorbed on molybdenite surfaces.

The Mo 3d spectrum of molybdenite is shown in Fig. 3.9 (b). In pure molybdenite, the peaks were assigned to 226.88 eV (S 2s), 230.50 and 233.80 eV (Mo $3d_{5/2}$ and Mo $3d_{3/2}$ of MoO_2), 229.70 and 232.86 eV (Mo $3d_{5/2}$ and Mo $3d_{3/2}$ of MoS_2), 232.39 and 235.72 eV (Mo $3d_{5/2}$ and Mo $3d_{3/2}$ of MoO_3) [30, 31]. After being treated with SIBX, the MoS_2 peak shifted downward by 0.21 eV, indicating that SIBX species might interact with Mo atoms on molybdenite surfaces.

In Fig. 3.9 (c), the doublets at 162.44 eV and 163.60 eV denoted S $2p_{3/2}$ and S $2p_{1/2}$ of MoS_2 for the original molybdenite [1]. For SIBX, the peaks at 162.04 eV and 163.22 eV represented S $2p_{3/2}$ and S $2p_{1/2}$ of BX^- [32]. After the introduction of SIBX, new peaks appeared at 162.29 and 163.47 eV (S $2p_{3/2}$ and S $2p_{1/2}$ of BX^-), 164.46 and 165.56 eV (S $2p_{3/2}$ and S $2p_{1/2}$ of BX_2) [33, 34]. Notably, both BX^- and BX_2 originated from SIBX, suggesting that xanthate and dixanthogen species were adsorbed on molybdenite surfaces. In addition, the shifting of BX^- peaks on molybdenite surfaces was 0.25 eV after adsorption, which might indicate that SIBX was chemisorbed on molybdenite surfaces.

Fig. 3.9 (d) presents O 1s spectra. In pure molybdenite, the peaks at 530.57 and 531.89 eV were asssigned to MoO_2 and MoO_3 [35] For SIBX, the peaks at 531.34, 533.15 and 535.35 eV belonged to hydroxide, BX^- and sodium auger peak (Na KLL) [36–38], respectively. The hydroxide group might belong to sodium hydroxide used in the preparation of xanthate. The Na KLL could sometimes be observed around 535 eV according to the manual of Avantage. After adding SIBX, molybdenite exhibited three peaks at 530.45, 531.86 and 533.46 eV, which represented MoO_2, MoO_3 and BX^- of SIBX, respectively. The characteristic peak of BX^- appeared on the O 1s spectra of molybdenite, indicating that BX^- was adsorbed on molybdenite.

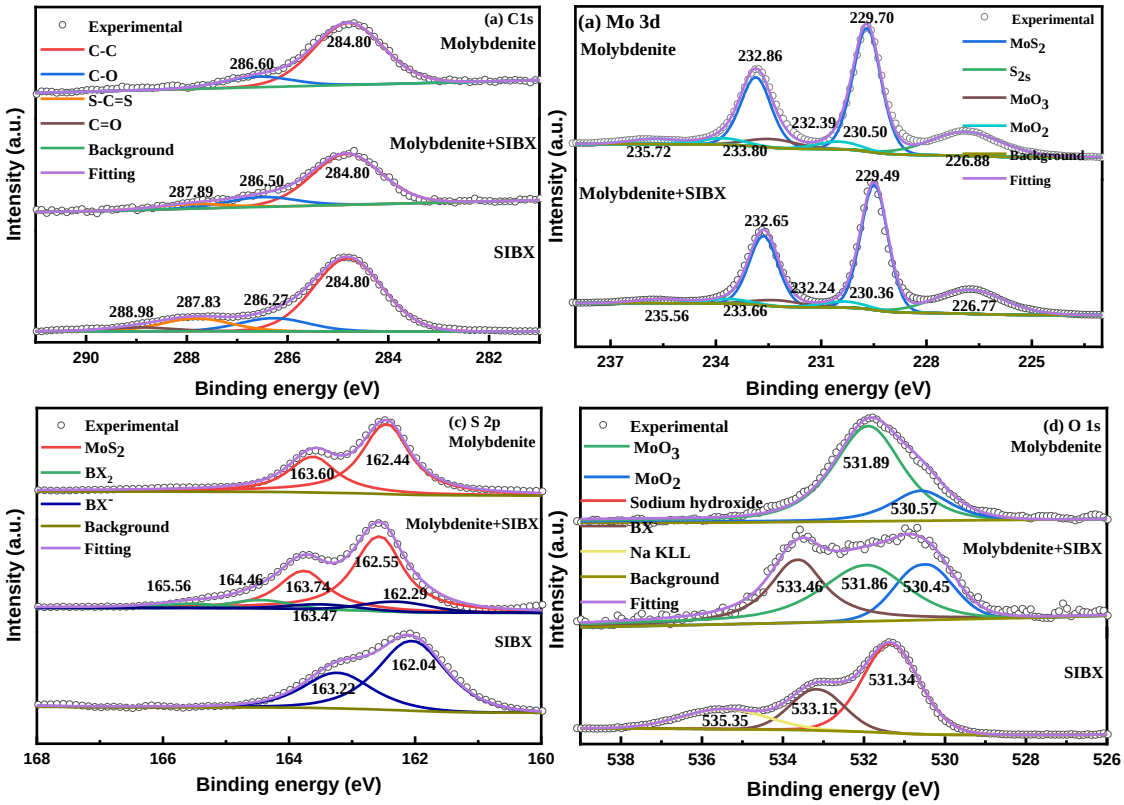

Fig. 3.9 C 1s (a); Mo 3d (b); S 2p (c) and O 1s (d) high-resolution spectra of molybdenite before and after SIBX introduction.

3.3.8 Rest potential measurement

Rest potential measurements were applied to evaluate the interactions between SIBX and molybdenite in an electrochemically altered solution. Fig. 3.10 displays the rest potential of the molybdenite face and edge before and after SIBX addition. Positive potentials relative to the dixanthogen couple (BX^-/BX_2) suggest the existence of BX_2 on sulfide ores. In

contrast, negative potentials relative to the (BX^-/BX_2) couple may indicate the presence of xanthate ions [12, 39]. The reversible potential for the (BX^-/BX_2) couple at 3.48 $\times 10^{-3}$ mol/L SIBX calculated from Reaction (3) was 17.33 mV [40]:

$$2BX^- \rightleftharpoons BX_2 + 2e^- \qquad E = -0.128 - 0.059\log[X^-] \qquad (3)$$

As shown in Fig. 3.10, the potential for the face was higher than that of the edge in the absence of SIBX, suggesting that the edge was more easily oxidized than the face. After treatment with SIBX, the potential of both the face and edge decreased, which was attributed to the adsorption of SIBX species that changed the structure of the electrical double layer at the solid-water surface. Notably, the potential of the face in 3.48 $\times 10^{-3}$ mol/L SIBX solution was higher than the reversible potential for the (BX^-/BX_2) couple, indicating that dixanthogen may form in this case. In contrast, the potential of the edge in 3.48 $\times 10^{-3}$ mol/L SIBX was lower than the reversible potential for the (BX^-/BX_2) couple, suggesting that xanthate ions were adsorbed on the edge, which was analogous to previous reports [41]. These results confirmed that dixanthogen and xanthate species maight be the dominant species formed on molybdenite faces and edges, which enhanced the hydrophobicity of both faces and edges, thereby improving the flotation of molybdenite fines.

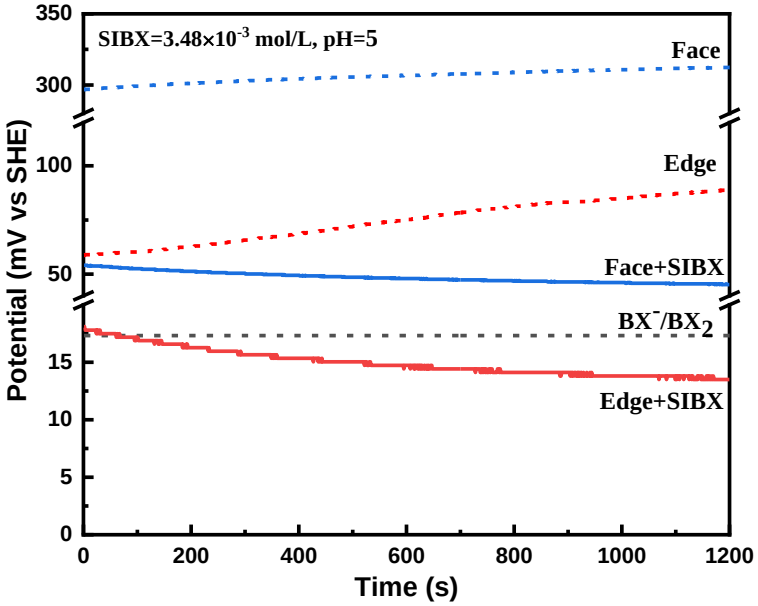

Fig. 3.10 Rest potential of face and edge planes before and after SIBX treatment.

3.3.9 DFT calculation

3.3.9.1 Adsorption of SIBX and dixanthogen on faces

As illustrated in Table 3.2, the adsorption energies of SIBX and dixanthogen on faces were 9.05 kJ/mol and −66.06 kJ /mol, respectively. The results also indicated the preferential

adsorption of dixanthogen on faces. In addition, Fig. 3.11 presents the electron cloud map of dixanthogen on faces. No overlap was observed between dixanthogen and faces, implying that no bond was formed during the adsorption. Meanwhile, the distance between the S atom within dixanthogen and the S atom on faces significantly increased to 3.219 Å (Table 3.2), which was far beyond the sum of the radii of two S atoms (2.12 Å), reconfirming no chemical bond was formed. These results indicated that dixanthogen might physically adsorb on faces, which was consistent with the results of rest potential measurements [42, 43].

Table 3.2 The calculated adsorption energies of two reagents on faces

Surface	Reagent	Adsorption energy（kJ·mol^{-1}）	D_{S-S} (Å)
Faces	SIBX	9.05	3.432
	Dixanthogen	−66.06	3.219

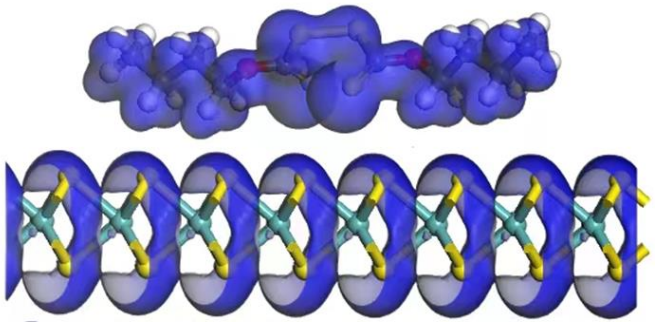

Fig. 3.11 Electron cloud map of dixanthogen on faces.

3.3.9.2 Adsorption of SIBX on edges

As discussed above, the rest potential of edges after treatment with SIBX was lower than the reversible potential for the (BX^-/BX_2) couple, indicating that only xanthate species were able to interact with edges. Therefore, the interaction between SIBX and edges was simulated. The adsorption energy of SIBX on edges was −235.62 kJ /mol, indicating that SIBX strongly interacted with edges.

Fig. 3.12 displays the electron density and electron density difference of SIBX on edges. In Fig. 3.12 (a), distinct overlap was observed across S_1–Mo_1 and S_2–Mo_2, indicating that the interaction between SIBX and molybdenite edges occurred through the bonding of two S atoms in SIBX with two Mo atoms on the edges. As shown in Fig. 3.12 (b), the blue color represented electron depletion, while the red color represented an electron accumulation. Blue regions around Mo atoms indicated electron depletion, while red regions near S atoms

showed electron accumulation. The red and blue areas were connected between S and Mo atoms, implying electron transfer from Mo to S atoms during the reaction.

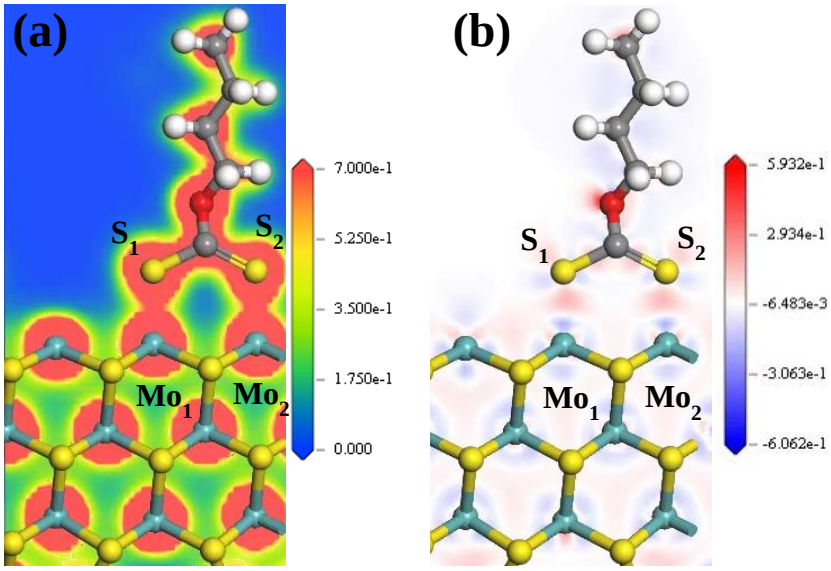

Fig. 3.12 Electron density (a) and electron density difference (b) of SIBX on edges.

Table 3.3 presents Mulliken bond populations of two newly formed Mo–S bonds. When SIBX adsorbed on edges, the lengths of two Mo–S bonds were 2.276 and 2.371 Å, respectively. Notably, both lengths were smaller than the radius sum of Mo–S (2.46 Å), implying a strong interaction between the atoms. Furthermore, two Mo–S bond populations were 0.57 and 0.54, elucidating the formation of highly covalent bonds between Mo and S atoms within SIBX.

Table 3.3 Mulliken population value of Mo–S bond

Bond	Population value	Length (Å)
Mo_1–S_1	0.57	2.276
Mo_2–S_2	0.54	2.371

Partial density of states (PDOS) for S_1, S_2, Mo_1 and Mo_2 before and after adsorption are displayed in Fig. 3.13. It was clear that Mo_1 and Mo_2 4d orbitals exhibited a shift towards the valence band, and the peak near the Fermi level showed a significant increase after adsorption, suggesting that Mo_1 and Mo_2 4d orbitals lost electrons and participated in the interaction (Fig. 3.13 (a) and (b)). As illustrated in Fig. 3.13 (c) and (d), S_1 and S_2 3p orbitals exhibited a movement towards the conduction band, and the peak near the Fermi level

displayed a notable decrease, indicating that S_1 and S_2 3p orbitals received electrons and took part in the interaction. Furthermore, a distinct orbital hybridization between Mo_1 and S_1, and Mo_2 and S_2 was observed in the energy range of –4.35 to –2.03 eV, implying a strong interaction between these atoms.

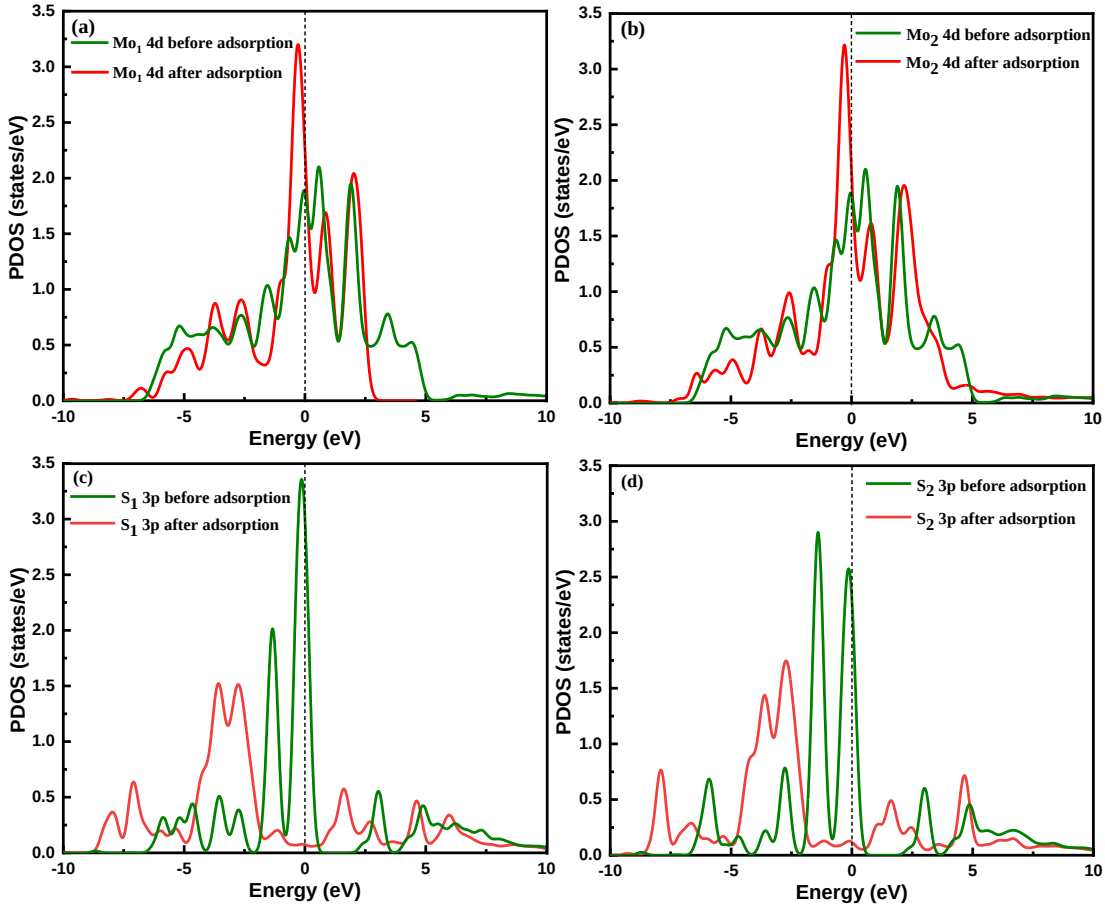

Fig. 3.13 PDOS analysis of Mo1 4d (a), Mo2 4d (b), S1 3p (c) and S2 3p (d) before and after adsorption.

3.3.10 Adsorption mechanism

To sum up, a possible adsorption mechanism could be inferred by the contact angle, adsorption capacity, Tafel curves, AFM, FTIR, XPS, rest potential and DFT calculations. As shown in Fig. 3.14, xanthate and its dixanthogen derivatives were adsorbed differently on molybdenite edges and faces. In particular, xanthate was chemisorbed on edges via the complexation of S 3p orbitals in SIBX with Mo 4d orbitals to generate two highly covalent bonds. On the other hand, dixanthogen was preferentially adsorbed on faces via physical

adsorption. The anisotropic adsorption of SIBX species on faces and edges improved their hydrophobicity.

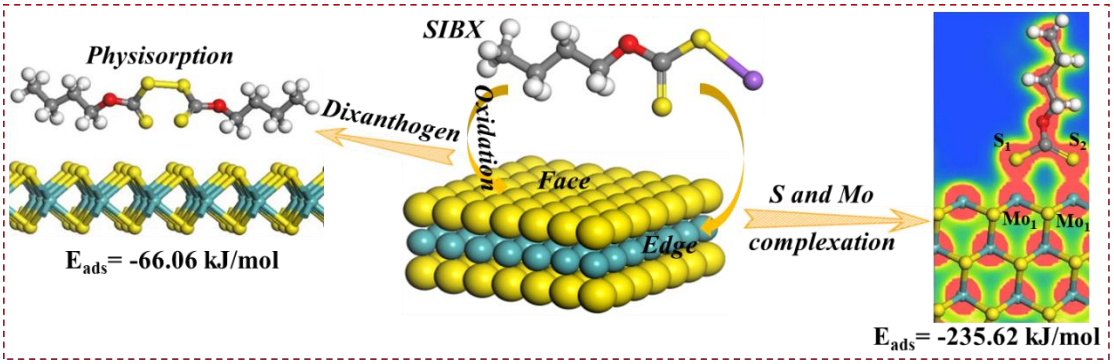

Fig. 3.14 Schematic diagram of SIBX species adsorption mechanism on molybdenite face and edge.

3.4 Conclusions

(1) SIBX species could significantly increase the flotation efficiency of molybdenite fines across a broad pH range.

(2) The anisotropic adsorption of dixanthogen and xanthate species on faces and edges improves their hydrophobicity.

(3) Xanthate species were preferentially chemisorbed on the edge to improve its hydrophobicity through the covalent bonding between Mo 4d orbitals and S 3p orbitals within SIBX.

(4) Dixanthogen was physically adsorbed on molybdenite faces, further improving the floatability of molybdenite fines.

Reference

[1] C. Wang, R. Liu, M. Wu, Z. Xu, M. Tian, Z. Yin, W. Sun, C. Zhang, Flotation separation of molybdenite from chalcopyrite using rhodanine-3-acetic acid as a novel and effective depressant, Miner. Eng. 162 (2021) 106747.

[2] B. Yang, H. Yan, M. Zeng, P. Huang, F. Jia, A. Teng, A novel copper depressant for selective flotation of chalcopyrite and molybdenite, Miner. Eng. 151 (2020) 106309.

[3] D. Yuan, K. Cadien, Q. Liu, H. Zeng, Adsorption characteristics and mechanisms of O-Carboxymethyl chitosan on chalcopyrite and molybdenite, J. Colloid Interface Sci. 552 (2019) 659–670.

[4] B. Ge, S. Liu, Q. Nie, Q. Li, C. Zhu, Applying one-stage grinding and flotation to improving copper recovery of a fine-grained Cu-Mo sulphide ore, Sep. Sci. Technol. 48 (2013) 1900–1905.

[5] J. Chen, L. Lan, X. Liao, Depression effect of pseudo glycolythiourea acid in flotation separation of copper–molybdenum, Trans. Nonferrous Met. Soc. China. 23 (2013) 824–831.

[6] J. Wu, B. Yang, S. Song, Q. Mildred, F. Jia, X. Tian, The efficient recovery of molybdenite fines using a novel collector: Flotation performances, adsorption mechanism and DFT calculation, Miner. Eng. 107848 (2022).

[7] J. Wang, L. Xie, Q. Lu, X. Wang, J. Wang, H. Zeng, Electrochemical investigation of the interactions of organic and inorganic depressants on basal and edge planes of molybdenite, J. Colloid Interface Sci. 570 (2020) 350–361.

[8] Z. Lu, Q. Liu, Z. Xu, H. Zeng, Probing Anisotropic Surface Properties of Molybdenite by Direct Force Measurements, Langmuir. 31 (2015) 11409–11418.

[9] S. Kelebek, Critical surface tension of wetting and of floatability of molybdenite and sulfur, J. Colloid Interface Sci. 124 (1988) 504–514.

[10] H. Li, T. He, H. Wan, Y. Han, Y. Guo, J. Jin, Insights into Selection of the Auxiliary Collector and Its Applicability Analysis for Improving Molybdenite Flotation, Minerals. 11 (2021) 528.

[11] L. Xie, J. Wang, J. Huang, X. Cui, X. Wang, Q. Liu, H. Zhang, Q. Liu, H. Zeng, Anisotropic polymer adsorption on molybdenite basal and edge surfaces and interaction mechanism with air bubbles, Front. Chem. 6 (2018) 1–11.

[12] S.A. Allison, L.A. Goold, M.J. Nicol, A. Granville, A determination of the products of reaction betweer various sulfide minerals and aqueous xanthate solution, and a correlation of the products with electrode rest potentials, Metall. Trans. 3 (1972) 2613–2618.

[13] S. Castro, A. Lopez-valdivieso, J.S. Laskowski, Review of the fl otation of molybdenite . Part I : Surface properties and fl oatability, Int. J. Miner. Process. 148 (2016) 48–58.

[14] P.M. Afenya, Adsorption of xanthate and starch on synthetic graphite, Int. J. Miner. Process. 9 (1982) 303–319.

[15] J. Zhang, X. Que, Mineral Reagent, Metallurgical Industry Press, Beijing, 2008.

[16] J. Wu, J. Feng, B. Yang, R. Martin, S. Song, M. Quintana, F. Jia, X. Tian, The anisotropic adsorption of potassium cetyl phosphate on molybdenite surface and its implication for improving the flotation of molybdenite fines, J. Mol. Liq. 378 (2023) 121616.

[17] B. Yang, D. Wang, T. Wang, H. Zhang, F. Jia, S. Song, Effect of Cu^{2+} and Fe^{3+} on the depression of molybdenite in flotation, Miner. Eng. 130 (2019) 101–109.

[18] M.C. Fuerstenau, B.J. Sabacky, On the natural floatability of sulfides, Int. J. Miner. Process. 8 (1981) 79–84.

[19] S. ke Li, G. hua Gu, G. zhou Qiu, Z. xiang Chen, Flotation and electrochemical behaviors of chalcopyrite and pyrite in the presence of N-propyl-N'-ethoxycarbonyl thiourea, Trans. Nonferrous Met. Soc. China. 28 (2018) 1241-1247.

[20] Y. Mu, Y. Peng, R.A. Lauten, The galvanic interaction between chalcopyrite and pyrite in the presence of lignosulfonate-based biopolymers and its effects on flotation performance, Miner. Eng. 122 (2018) 91–98.

[21] X. Qiu, H. Yang, G. Chen, W. Luo, An alternative depressant of chalcopyrite in cu–mo differential flotation and its interaction mechanism, Minerals. 9 (2019) 1–11.

[22] K. Zhao, X. Wang, Z. Wang, W. Yan, X. Zhou, L. Xu, C. Wang, A novel depressant for selective flotation separation of pyrite and pyrophyllite, Appl. Surf. Sci. 487 (2019) 9–16.

[23] R. Woods, G.A. Hope, G.M. Brown, Spectroelectrochemical investigations of the interaction of ethyl xanthate with copper, silver and gold: III. SERS of xanthate adsorbed on gold surfaces, Colloids Surfaces A Physicochem. Eng. Asp. 137 (1998) 339–344.

[24] C. Zhong, B. Feng, Y. Chen, M. Guo, H. Wang, Flotation separation of molybdenite and talc using tragacanth gum as depressant and potassium butyl xanthate as collector, Trans. Nonferrous Met. Soc. China. 31 (2021) 3879–3830.

[25] G.P.W. Suyantara, T. Hirajima, H. Miki, K. Sasaki, S. Kuroiwa, Y. Aoki, Effect of Na_2SO_3 on the floatability of chalcopyrite and enargite, Miner. Eng. 173 (2021) 107222.

[26] B. Luo, W. Nie, J. Dong, Effect of lead ions on the sulfidization flotation of smithsonite using sodium butyl xanthate as a collector, Miner. Eng. 185 (2022) 107710.

[27] Y. Chen, B. Feng, J. Peng, Z. Wang, Selective flotation of galena from sphalerite using a combination of $KMnO_4$ and carboxylated chitosan, Appl. Surf. Sci. 602 (2022) 154412.

[28] X. Tang, Y. Chen, K. Liu, Q. Peng, Z. Li, Reverse flotation separation of talc from molybdenite without addition of depressant: Effect of surface oxidation by thermal pre-treatment, Colloids Surfaces A Physicochem. Eng. Asp. 594 (2020) 124671.

[29] B. Yang, H. Yan, M. Zeng, H. Zhu, Tiopronin as a novel copper depressant for the selective flotation separation of chalcopyrite and molybdenite, Sep. Purif. Technol. 266 (2021) 118576.

[30] B. Yang, P. Huang, Q. An, An efficient chalcopyrite depressant for Cu-Mo separation and its interaction mechanism: Adsorption configuration and DFT calculations, J. Mol. Liq. 345 (2022) 118171.

[31] F. Jia, C. Liu, B. Yang, S. Song, Microscale control of edge defect and oxidation on molybdenum disulfide through thermal treatment in air and nitrogen atmospheres, Appl. Surf. Sci. 462 (2018) 471–479.

[32] K.C. Pillai, V.Y. Young, B. JO'M, XPS studies of xanthate adsorption on galena surfaces, Appl. Surf. Sci. 16 (1983) 322–344.

[33] I. Kartio, K. Laajalehto, E. Suoninen, Characterization of the ethyl xanthate adsorption layer on galena (PbS) by synchrotron radiation excited photoelectron spectroscopy, Colloids Surfaces A Physicochem. Eng. Asp. 154 (1999) 97–101.

[34] M. Deng, D. Karpuzov, Q. Liu, Z. Xu, Cryo-XPS study of xanthate adsorption on pyrite, Surf. Interface Anal. 45 (2013) 805 – 810.

[35] G.P.W. Suyantara, T. Hirajima, H. Miki, K. Sasaki, M. Yamane, E. Takida, S. Kuroiwa, Y. Imaizumi, Selective flotation of chalcopyrite and molybdenite using H2O2 oxidation method with the addition of ferrous sulfate, Miner. Eng. 122 (2018) 312–326.

[36] Z. Yang, G. Zhang, Q. Teng, X. Zhu, Removal of Pb^{2+} from aqueous solution by xanthan gum in the presence of xanthate, React. Funct. Polym. 175 (2022) 105288.

[37] J. Mielczarski, E. Suoninen, XPS study of ethyl xanthate adsorbed onto cuprous sulphide, Surf. Interface Anal. 6 (1984) 34–39.

[38] J. Szépvölgyi, A. Tüdös, I. Bertóti, X-ray photoelectron spectroscopy studies on solid xanthates, J. Electron Spectros. Relat. Phenomena. 50 (1990) 239–250.

[39] A.M. Buswell, D.J. Bradshaw, P.J. Harris, Z. Ekmekci, The use of electrochemical measurements in the flotation of a platinum group minerals (PGM) bearing ore, Miner. Eng. 15 (2002) 395–404.

[40] Y. Mu, Y. Cheng, Y. Peng, The interaction between grinding media and collector in pyrite flotation at neutral and slightly acidic pH, Miner. Eng. 145 (2020) 106063.

[41] N. Mhonde, L.S. Johansson, K. Corin, N. Schreithofer, The effect of sodium isobutyl xanthate on galena and chalcopyrite flotation in the presence of dithionite ions, Miner. Eng. 169 (2021) 106985.

[42] H. Peng, D. Wu, M. Abdalla, W. Luo, W. Jiao, X. Bie, Study of the Effect of Sodium Sulfide as a Selective Depressor in the Separation of Chalcopyrite and Molybdenite, Minerals. 7 (2017) 51.

[43] S. Grano, J. Ralston, R.S.C. Smart, Influence of electrochemical environment on the flotation behaviour of Mt. Isa copper and lead-zinc ore, Int. J. Miner. Process. 30 (1990) 69–97.

The main content in this chapter was published in *Minerals Engineering.*

Chapter IV. The efficient recovery of molybdenite fines using a novel collector: Flotation performances, adsorption mechanism and DFT calculation

4.1 Introduction

Molybdenite is a valuable sulfide mineral, which has attracted much interest in broad fields such as electronics, catalysts and lubrication due to its outstanding optical and electronic properties [1, 2]. With the rapid depletion of high-grade molybdenite ores, it is urgent to explore low-grade and fine-disseminated molybdenite deposits to satisfy the increasing market demands [3]. Commonly, these ores need to be finely ground to liberate fine molybdenite particles from other minerals.

As a laminar crystalline structure, molybdenite exhibits two types of surface, namely non-polar faces and polar edges. The non-polar faces are formed through the breakage of weak van der Waals interaction between S–Mo–S layers, which are hydrophobic. While the polar edges are generated by the rupture of Mo–S bonds, which are hydrophilic [4, 5]. The hydrophobicity of molybdenite particles depends on the particle size. As particle size reduces, the face/edge ratio decreases, thus the hydrophobicity of molybdenite particles declines [6]. Molybdenite particle (>20 um) is regarded as a naturally hydrophobic mineral that is primarily concentrated through flotation [7]. However, molybdenite fines (–20 um) exhibit poor floatability because hydrophilic edges dominate.

The anisotropic surface properties of molybdenite are of significant importance in determining the surface wettability and floatability of molybdenite. Thus, considerable efforts have been made to reveal the difference between face and edge planes. For example, the surface free energy of the molybdenite edge (0.1952 J/m^2) is nearly 5-fold higher than the face (0.0426 J/m^2) [8]. Molybdenite edge exhibits a higher chemical activity than the face [7]. The oxidation occurs preferentially at Mo sites on the edge because of the lower energy barrier [9]. Molybdenite edges carried more negative charge than faces in a neutral or alkaline environment, and no hydrophobic force has been detected on the edges over the pH range [10]. The distinction between faces and edges can be employed to improve the flotation performance of molybdenite. Li et al. found that polyethylene oxide (PEO) could improve the flotation of molybdenite fines compared to kerosene, because the O atoms of PEO had a strong affinity toward Mo atoms of edges. Meanwhile, it could facilitate molybdenite fines to flocculate, both of which enhanced the floatability of molybdenite fines [3]. He et al. pointed

out that polycyclic aromatic hydrocarbon (PAH) adsorbed on molybdenite edges through its polar group and rendered them hydrophobic, and then promoted the floatability of molybdenite fines compared to kerosene [11]. Previous researches mainly focused on the anisotropic surface properties and adsorption difference on faces and edges planes. Few studies reported the flotation of molybdenite fines through the targeted regulation of edges.

Non-polar hydrocarbon oils, such as kerosene and diesel, are generally employed as traditional molybdenite collectors. These reagents can improve the hydrophobicity of molybdenite faces because they are readily adsorbed on the faces through van der Waals forces and hydrophobic interactions [12, 13]. However, these reagents can't be used as efficient collectors for molybdenite fines due to the poor affinity between non-polar oils and edges. Thus, the targeted regulation of molybdenite edges is essential to enhance the flotation of molybdenite fines.

In this study, N-(N-butyl) thiophosphoric triamide (NBPT) was first introduced as a molybdenite collector. NBPT is a non-toxic chemical, which is widely used as an urease inhibitor in aerobic soils [14]. As shown in Fig. 4.1, NBPT contains -NH, $-NH_2$ and P=S groups. Within NBPT, both the S and N atoms have lone pair electrons, which make it possible to complex with metal atoms [15]. Thus, NBPT was tested as a potential collector to improve the flotation of molybdenite fines. The flotation behaviros and mechanims were investigated via flotation, Zeta potential, FTIR, adsorption capacity, ToF-SIMS, XPS, AFM tests and DFT calculations.

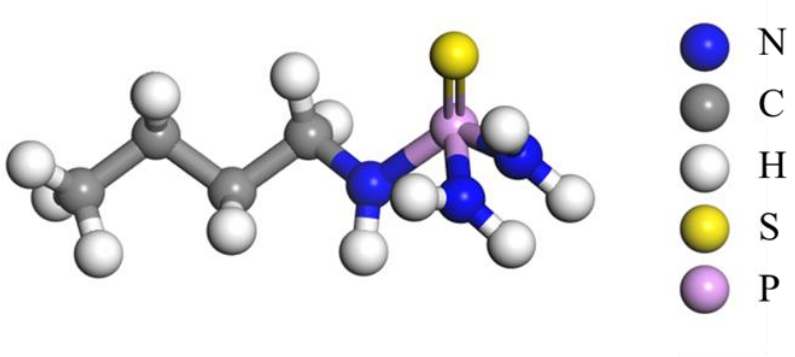

Fig. 4.1 Molecular structure of NBPT

4.2 Experimental

4.2.1 Materials and reagents

Molybdenite samples were acquired from Guangxi province, China. The bulk samples were selected by hand first, then ground and screened to obtain particle less than –20 μm. The

X-ray diffraction (XRD) spectrum of the sample is depicted in Fig. 4.2. XRD result and chemical assay indicated that purity of the molybdenite sample was 97 %.

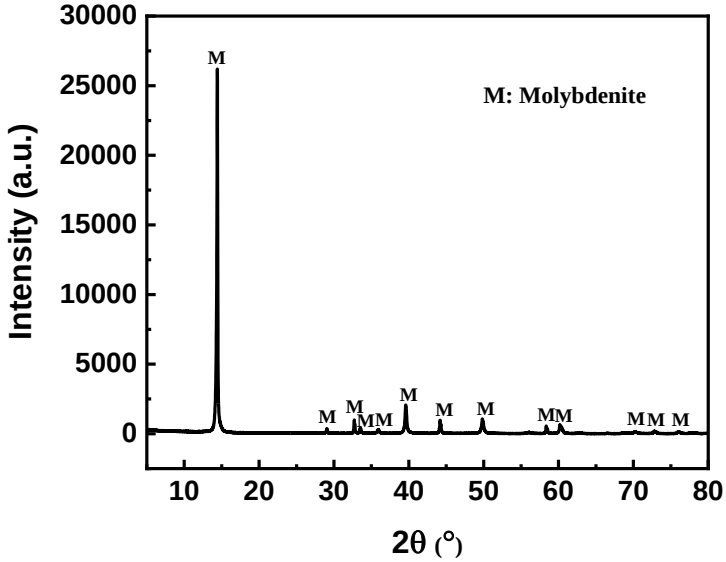

Fig. 4.2 XRD pattern of raw molybdenite material.

NBPT purchased from Aladdin, China, was used as a flotation collector. Sodium hydroxide (NaOH, Aladdin, China) and hydrochloric acid (HCl, Aladdin, China) were applied as pH regulators. Methyl isobutyl carbinol (MIBC, Aladdin, China) was employed as a frother. Ultrapure water with a resistivity of 18.25 MΩ·cm was used.

4.2.2 Flotation tests

Flotation tests were conducted using the XFG flotation machine. 2 g of molybdenite samples (–20 μm) were ultrasonically dispersed for 2 min, and the slurry was then transferred to a flotation cell and conditioned for 2 min. NBPT and MIBC were introduced in sequence after the adjustment of pH. Subsequently, the flotation was performed for 3 min. The concentrates and tailings were filtered, dried and weighed separately to calculate floatability. The flow sheet of flotation is presented in Fig. 4.3. The average floatability plot represented three repeat experiments.

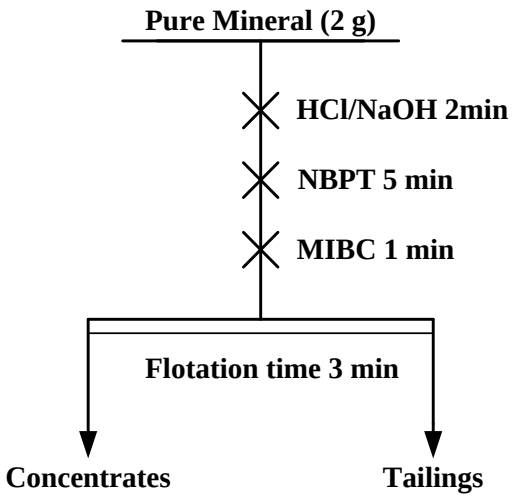

Fig. 4.3 Flow sheet of molybdenite flotation tests.

4.2.3 Characterizations

Zeta potential was measured using a Zetasizer Nano analyzer (Malvern, UK). 0.15 g of molybdenite samples were added into NBPT solution (0.001 M NaCl) and conditioned for 5 min. 1 mL of suspension was taken for measurements. The FTIR spectra of molybdenite and NBPT were recorded through FTIR-50 spectrometer (Nicolet, USA) at room temperature. The molybdenite samples were stirred in 1000 ppm NBPT solutions at pH of 4 for 30 min. Subsequently, the suspension was filtered and dried for measurements. The adsorption capacity was determined based on TOC method. 2 g of molybdenite samples were introduced in a 70 mL NBPT solutions (pH = 4) and stirred for 30 min. Then the TOC content of centrifugated supernatant was determined by a total organic carbon analyzer (TOC-L, Japan). The following equation was used to calculate the adsorption capacity:

$$q=\frac{(C_1-C_2)V}{m} \quad (1)$$

Where q means the adsorption amount (mg/g), C_1 means the initial concentration of NBPT solution (mg/L), C_2 means the concentration of NBPT supernatant (mg/L), V means the volume of NBPT solution (L), and m means the weight of molybdenite (g). Time-of-Flight Secondary Ion Mass Spectrometry (ION-TOF GmbH, Germany) equipped with 30 kV acceleration voltage and a Bi primary ion source was employed to characterize the surface chemical compositions of molybdenite. X-ray photoelectron spectra (Thermo ESCALAB 250, USA) were measured with Al Kα radiation at vacuum of 8×10^{-10} Pa. Molybdenite sample was treated in 1000 ppm NBPT solution at pH of 4 for 30 min. The binding energy was calibrated at the C1s peak at 284.80 eV. The molybdenite samples were prepared by

mechanical exfoliation. The bulk molybdenite sample with dimensions around 0.5 cm × 0.5 cm × 0.1 cm was prepared first. Then a fresh molybdenite surface was cleaved using Scotch tape. After that, one drop of 1000 ppm NBPT solutions was placed on the surface and allowed for adsorption for 5 min. After washing with ultrapure water to remove unabsorbed NBPT species the molybdenite surface was dried for 5 min. The morphology of molybdenite before and after NBPT treatment was observed by Brucker Multimode 8 AFM system, using a ScanAsystair N-type silicon probe. The surface images were captured in automatically optimized scan parameters with 512 pixels, and then NanoScope Analysis software was used to analyze the images [16].

4.2.4 DFT calculation

All computational calculations were computed using the CASTEP module. For adsorption geometry optimization, a cutoff energy of 430 eV and the Brillouin zone with a k-point of a 5×1×1 grid were used. The convergence tolerances of energy, displacement, stress, force and the SCF tolerance were 2×10^{-5} eV/atom, 0.002 Å, 0.1 GPa, 0.05 eV/Å and 2×10^{-6} eV/atom, respectively [8, 17].

In all calculations and stimulations, the 2H–MoS_2 model was used, with a 5×5×1 super cell and a 15 Å vacuum layer. The face and edge were built along the (0 0 1) and (1 0 0) cleavage plane, respectively. In the calculation, the valence electron configurations of Mo and S atoms were Mo $4s^2 4p^6 4d^5 5s^1$ and S $3s^2 3p^4$. According to density functional theory, quantitative calculations were conducted to unveil the adsorption mechanism of NBPT. The adsorption energy is calculated by the following:

$$E_{ads} = E_{system} - E_{slab} - E_{NBPT} \quad (2)$$

Where E_{ads} represents the adsorption energy, E_{system} represents the total energy of the molybdenite with NBPT, E_{slab} represents the energy of molybdenite slab, and E_{NBPT} represents the energy of NBPT.

4.3. Results and discussions

4.3.1 Flotation tests

Fig. 4.4 (a) shows the effect of NBPT concentration on molybdenite floatability at pH 4. The floatability increased significantly as NBPT concentration increased and then almost reached a plateau at an NBPT concentration of 600 ppm. The floatability increased by about 50% after the introduction of NBPT, which indicated that NBPT could efficiently collect molybdenite fines.

Fig. 4.4 (b) presents the floatability of molybdenite fines with and without NBPT. In the absence of NBPT, molybdenite floatability fluctuated around 45% as pH varied. After adding NBPT, the floatability considerably increased. The floatability was higher in acidic conditions than in alkaline conditions, indicating NBPT was more suitable for collecting molybdenite at acidic conditions.

Fig. 4.4 (c) displays the molybdenite floatability as a function of kerosene concentration. Without NBPT, the floatability of molybdenite fines was slightly improved as kerosene concentration increased. After NBPT was introduced, molybdenite floatability was greatly improved and remained at about 80% as kerosene concentration increased. The results indicated that NBPT could efficiently improve the flotation of molybdenite fines.

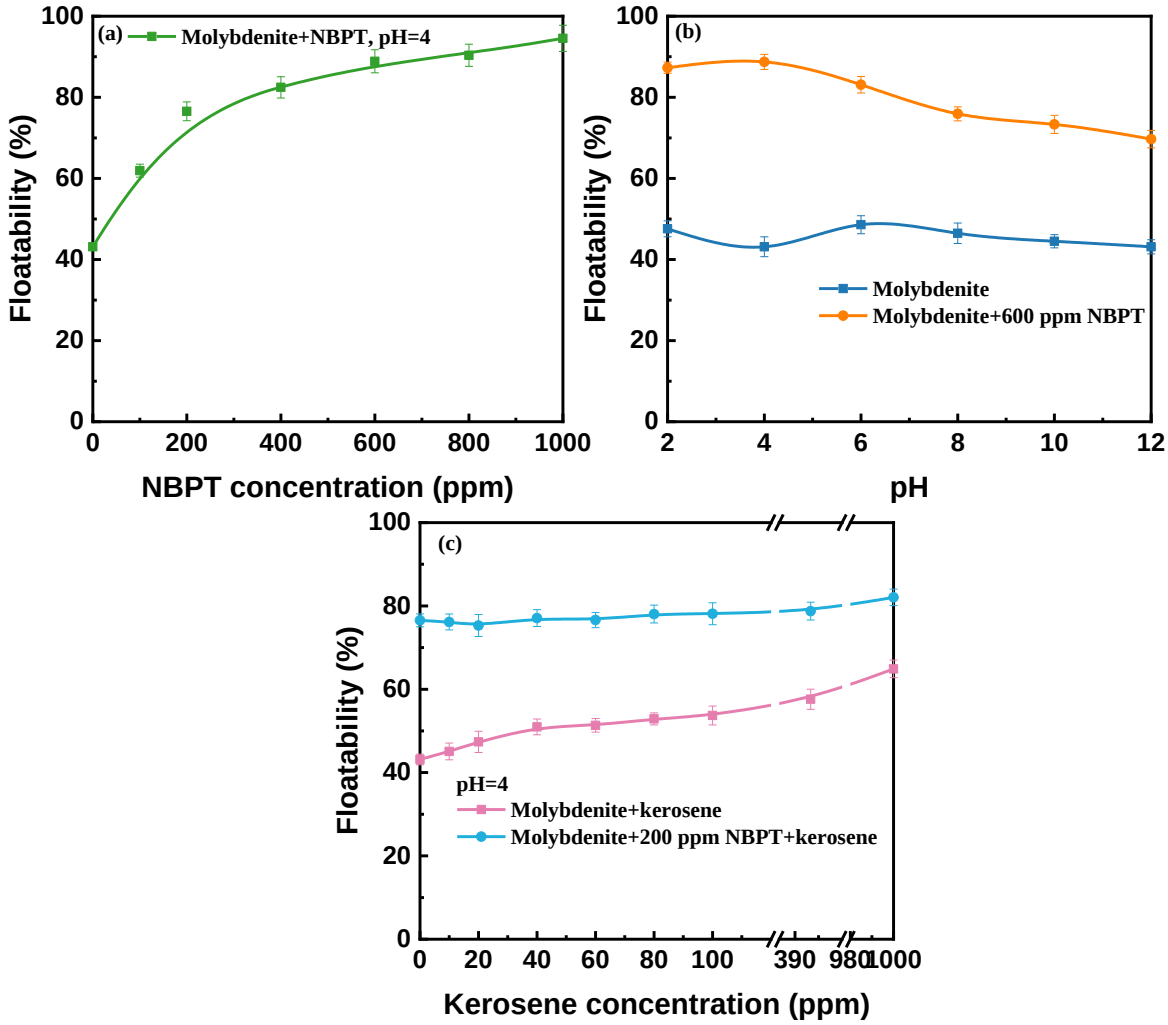

Fig. 4.4 The effect of: (a) NBPT concentration, (b) pH, (c) kerosene concentration on the floatability of molybdenite fines.

4.3.2 Zeta potential measurements

Fig. 4.5 shows the effect of pH on Zeta potential of molybdenite. Pure molybdenite was negatively charged over the pH range, which originated from molybdate ionic species ($HMoO^{4-}$ and MoO_4^{2-}) [18, 19]. After the treatment of NBPT, Zeta potential of molybdenite became more negative throughout the pH range, suggesting that substantial NBPT species adsorbed on molybdenite surface. The NBPT molecular contains both anions (P=S groups) and cations (–NH and $–NH_2$). The insignificant shift of Zeta potential may due to the offset between anions and cations [20, 21].

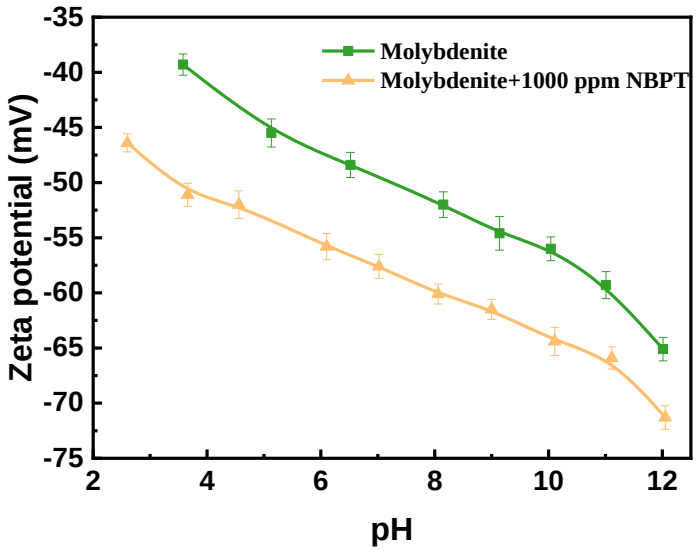

Fig. 4.5 Zeta potential of molybdenite in the presence and absence of NBPT.

4.3.3 FTIR spectra measurement

Fig. 4.6 displays the FTIR spectra of molybdenite before and after treatment with NBPT. The characteristic peaks of NBPT are shown in Table 4.1, which included –NH, $–NH_2$, P=S, $–CH_3$ and $–CH_2$ groups. After the addition of NBPT, two new peaks appeared near 1062 cm^{-1} and 1618 cm^{-1}, which were assigned to the $–CH_2–$ rocking and scissoring vibration of $–NH_2$, respectively. The results indicated that NBPT was adsorbed on molybdenite surfaces.

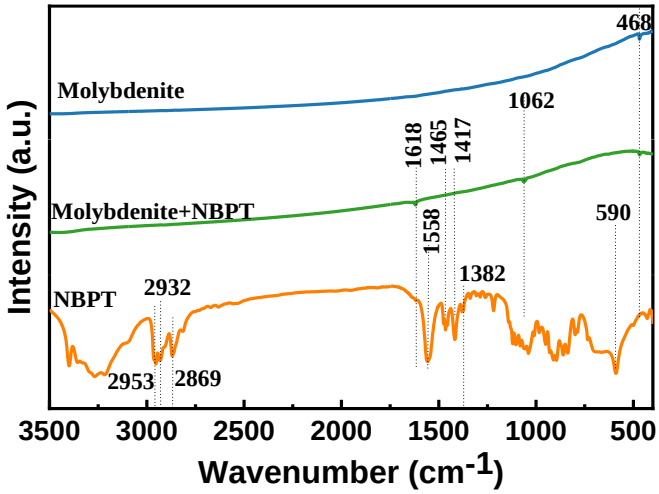

Fig. 4.6 FTIR spectra of molybdenite before and after NBPT addition.

Table 4.1 Major functional groups of NBPT

Wavenumber (cm^{-1})	Groups
3250-3400	N–H stretching [22]
2953	$–CH_3$ stretching [23]
2932	$–CH_2$ asymmetric stretching [24]
2869	$–CH_3$ stretching [23]
1618	$–NH_2$ scissor vibration [25]
1558	$–NH_2$ bending vibration [26]
1465	$–CH_2$ symmetric stretching [22]
1417	P=S stretching vibration [27]
1382	$–CH_3$ symmetric stretching [24]
1062	$–CH_2$-rocking [28]
590	P=S bending vibration [27]

4.3.4 Adsorption capacity of NBPT on molybdenite

Fig. 4.7 shows the adsorption amount of NBPT on molybdenite at different concentrations. The adsorption amount of NBPT on molybdenite significantly increased as NBPT concentration increased. Specifically, it could be seen the adsorption amount reached a plateau at an NBPT concentration of 600 ppm, which was consistent with the flotation results.

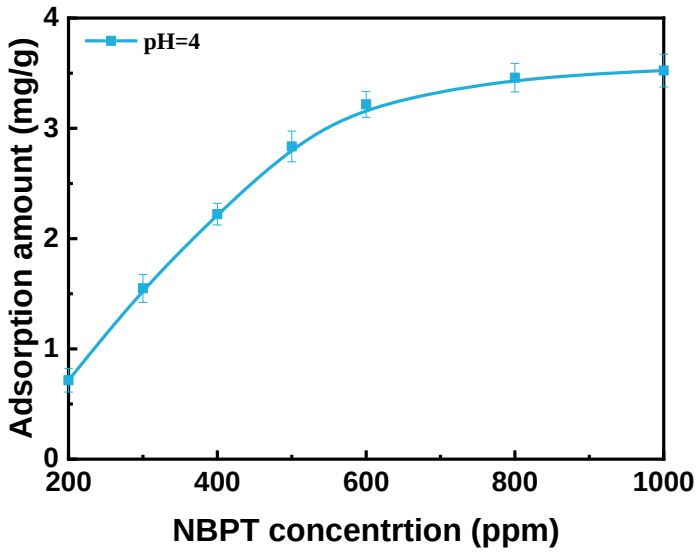

Fig. 4.7 Adsorption amount of NBPT on molybdenite.

4.3.5 ToF-SIMS analysis

ToF-SIMS measurements were performed to investigate the chemical composition of molybdenite after NBPT addition. Fig. 4.8 presents the spectra of negative ions (a) and positive ions (b) (m/z 1-300). In the negative ions, the possible ions include CH^- (m/z 13), O^- (m/z 16), CN^- (m/z 26), S^- (m/z 32), SO_3^- (m/z 80), $MoSO^-$ (m/z 146), MoS_2^- (m/z 162), MoS_2O^- (m/z 178), MoS_3^- (m/z 194), $CH_3MoS_3O^-$ (m/z 261) and $Mo_2S_3^-$ (m/z 292). In the positive ions, the molybdenum isotopes with m/z values of 92, 96 and 98 were also detected on molybdenite surfaces. The other positive ions included NH_4^+ (m/z 18), $C_2H_5^+$ (m/z 29), CH_4N^+ (m/z 30), $C_3H_5^+$ (m/z 41), $C_2H_8N^+$ (m/z 46), $C_4H_9^+$ (m/z 57), $C_3H_{10}N^+$ (m/z 60), $C_4H_{12}N^+$ (m/z 74), $C_4H_9N_2^+$ (m/z 85), MoS^+ (m/z 130), Mo_2S^+ (m/z 228), $Mo_2S_2^+$ (m/z 260) and $Mo_2S_3^+$ (m/z 292). The presence of fragments of O^-, SO_3^-, $MoSO^-$, MoS_2O^- and $CH_3MoS_3O^-$ indicated that some molybdenite particles were oxidized.

The molecular fragments such as CH^-, NH_4^+, CN^-, $C_2H_5^+$, $C_4H_4N^+$, $C_3H_5^+$, $C_2H_8N^+$, $C_4H_9N_2^+$, and $C_4H_{12}N^+$ of NBPT were detected, which further indicated that NBPT adsorbed on molybdenite surfaces.

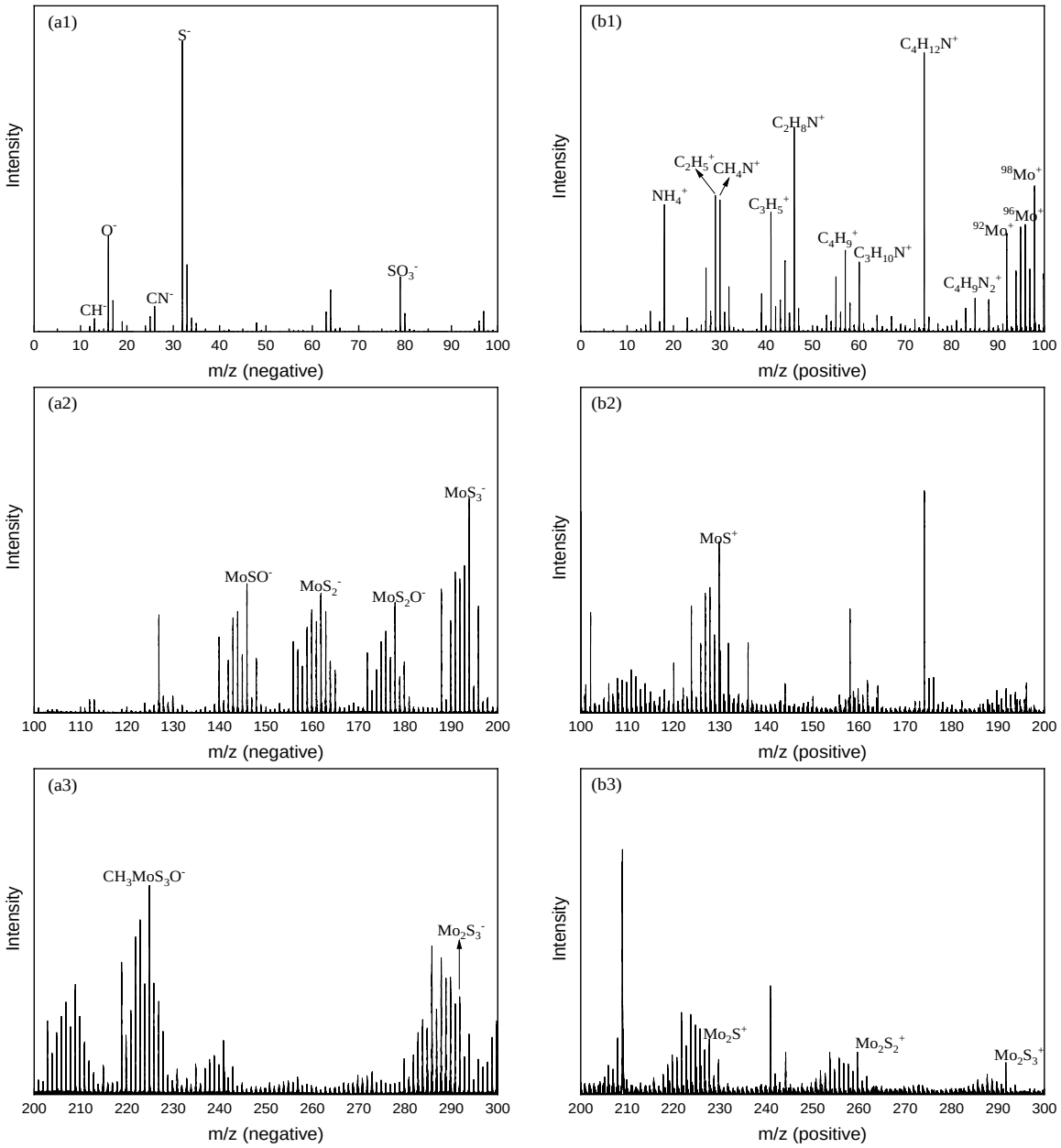

Fig. 4.8 The ToF-SIMS spectra of molybdenite treated with NBPT (a) negative; (b) positive.

4.3.6 XPS result

Fig. 4.9 displays the high-resolution XPS spectra of Mo 3d, S 2p, N 1s and P 2p of molybdenite in the absence and presence of NBPT. The Mo 3d spectra are shown in Fig. 4. 9 (a). For molybdenite, the peaks at 227.16 eV, 229.04, 230 and 232.35 eV were attributed to S 2s, Mo $3d_{5/2}$ of MoO_2, Mo $3d_{5/2}$ of MoS_2 and Mo $3d_{5/2}$ of MoO_3; the peaks located at 234.04, 233.17 and 236.36 eV were assigned to Mo $3d_{3/2}$ of MoO_2, Mo $3d_{3/2}$ of MoS_2, and Mo $3d_{3/2}$ of

MoO_3 [29, 30], respectively. After the addition of NBPT, the peaks of MoS_2 moved to 229.55 and 232.70 eV, representing shifts of 0.45 eV and 0.47 eV. The apparent decrease might be attributed to the change in electron density of Mo atoms, indicating NBPT might be chemically adsorbed on molybdenite surfaces through coordinating with Mo atoms.

The S 2p spectra are given in Fig. 4.9 (b). For NBPT, the peaks at 161.82 eV and 163.05 eV were assigned to P=S [31]. In pure molybdenite, the peaks at 162.64 eV and 163.83 eV were attributed to S $2p_{3/2}$ and S $2p_{1/2}$ of MoS_2 [32]. When NBPT was introduced, the peaks of S $2p_{3/2}$ and S $2p_{1/2}$ of MoS_2 moved to 162.46 eV and 163.65 eV, and the insignificant shifts indicated that S atoms of molybdenite did not participate in the reaction with NBPT. Meanwhile, the new peaks at 162.14 eV and 163.28 eV were assigned to S $2p_{3/2}$ and S $2p_{1/2}$ of P–S bonds [33], which originated from P=S groups of NBPT, reconfirming that NBPT was adsorbed on molybdenite surfaces.

The N 1s spectra are presented in Fig. 4.9 (c). For NBPT, the peaks at 398.95, 400.80 and 401.63 eV correspond to $–NH_2$ [34], –NH– [32] and C–N groups [35], respectively. After treatment with NBPT, the N 1s region was partially overlapped with Mo $3p_{3/2}$ (393.08 eV) region. The peak at 395.32 eV was assigned to the Mo–S bonds of molybdenite [36–38], the peaks at 396.54, 398.87 eV were corresponded to Mo $3p_{3/2}$ of MoO_2 [39], $–NH_2$ [34], respectively. The insignificant shift of the $–NH_2$ peak suggested that $–NH_2$ might not participate in the reaction.

In Fig. 4.9 (d), the P 2p spectra of NBPT were fitted into two peaks located at 133.48 eV and 134.35 eV, which belonged to P–N [40] and P=S [41], respectively. After the addition of NBPT, no apparent shift of P 2p was detected, suggesting that P atoms did not participate in the reaction between NBPT and molybdenite.

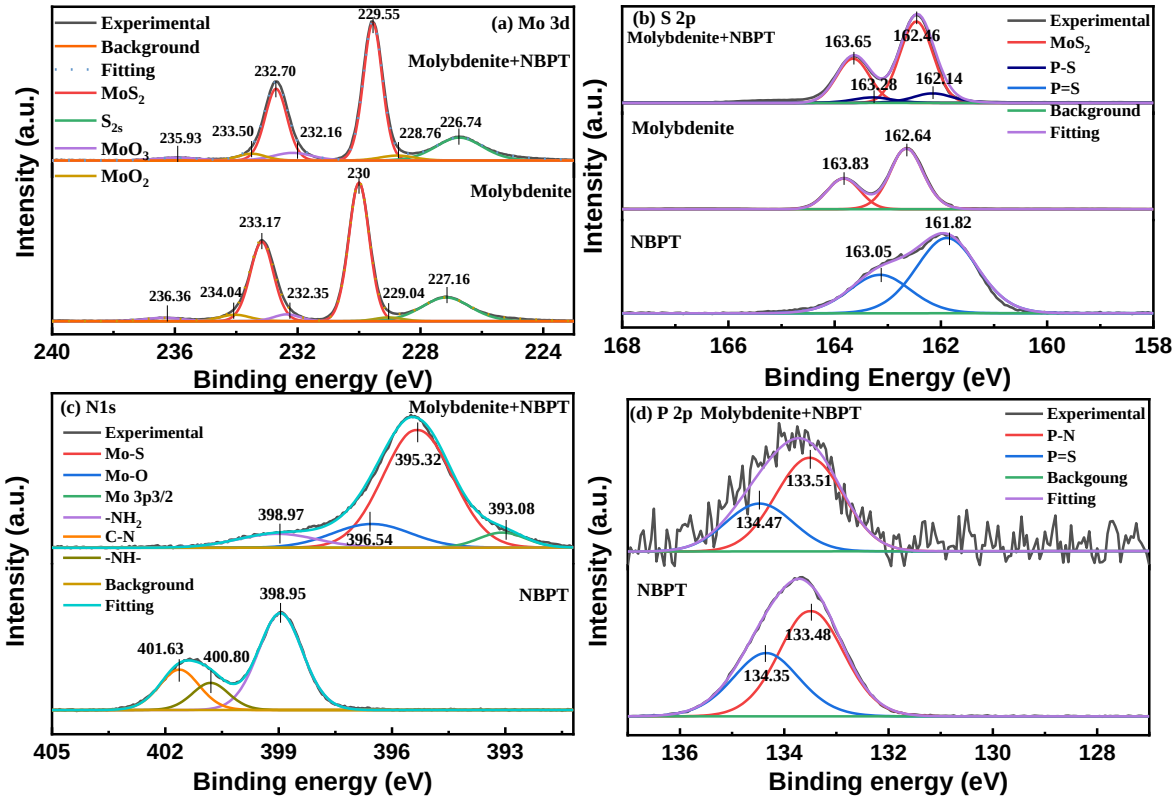

Fig. 4.9 High-resolution XPS spectra of the molybdenite in the absence and presence of NBPT: (a) Mo 3d; (b) S 2p; (c) N 1s; (d) P 2p

4.3.7 AFM analysis

Two-dimensional (2D) and three-dimensional (3D) AFM images of molybdenite before and after addition of NBPT are presented in Fig. 4. 10. Smooth faces and edges were clearly observed in air (Fig. 4.10a). After the adsorption of NBPT, pine tree-like and sheet-like aggregates covered molybdenite face and edge, respectively (Fig. 4.10b), but more aggregates appeared on edges. These results showed NBPT was more readily adsorbed on edges rather than faces, suggesting that NBPT had preferential affinity for edges.

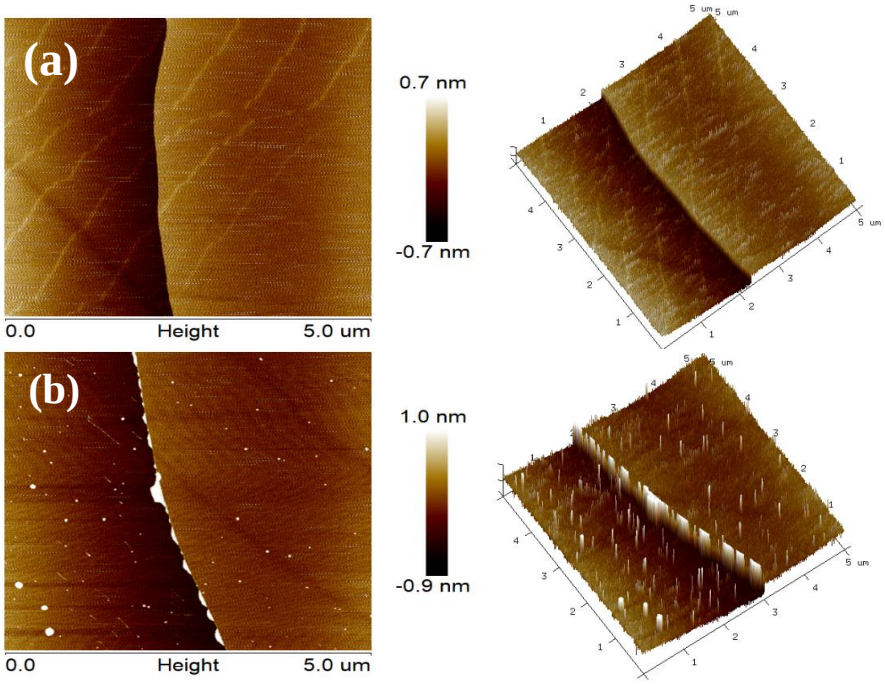

Fig. 4.10 AFM images of molybdenite in the absence (a) and presence (b) of NBPT.

4.3.8 DFT calculation

4.3.8.1 Analysis of adsorption energy

The adsorption energy of NBPT on different adsorption models is shown in Table 4.2. As expected, the adsorption energy of NBPT on (1 0 0) surfaces was much higher than that on (0 0 1) surfaces, suggesting that NBPT preferentially adsorbed on (1 0 0) surfaces, which was in agreement with AFM measurements. The different adsorption models before and after geometry optimization on molybdenite (1 0 0) surface are shown in Fig. 4.11. The large adsorption energy indicated that the adsorption of NBPT on edges was thermodynamically stable. In addition, "S–Mo_1" model was more favorable compared with other models.

Table 4.2 Adsorption energy of NBPT on molybdenite

Crystal surface	Adsorption model	Adsorption energy/(kJ • mol^{-1})
(0 0 1)	/	–39.96
(1 0 0)	S–Mo_1	–657.69
	N–Mo_1	–638.68
	S–N–Mo_1	–646.75
	N–Mo_1–S–Mo_2	–650.39

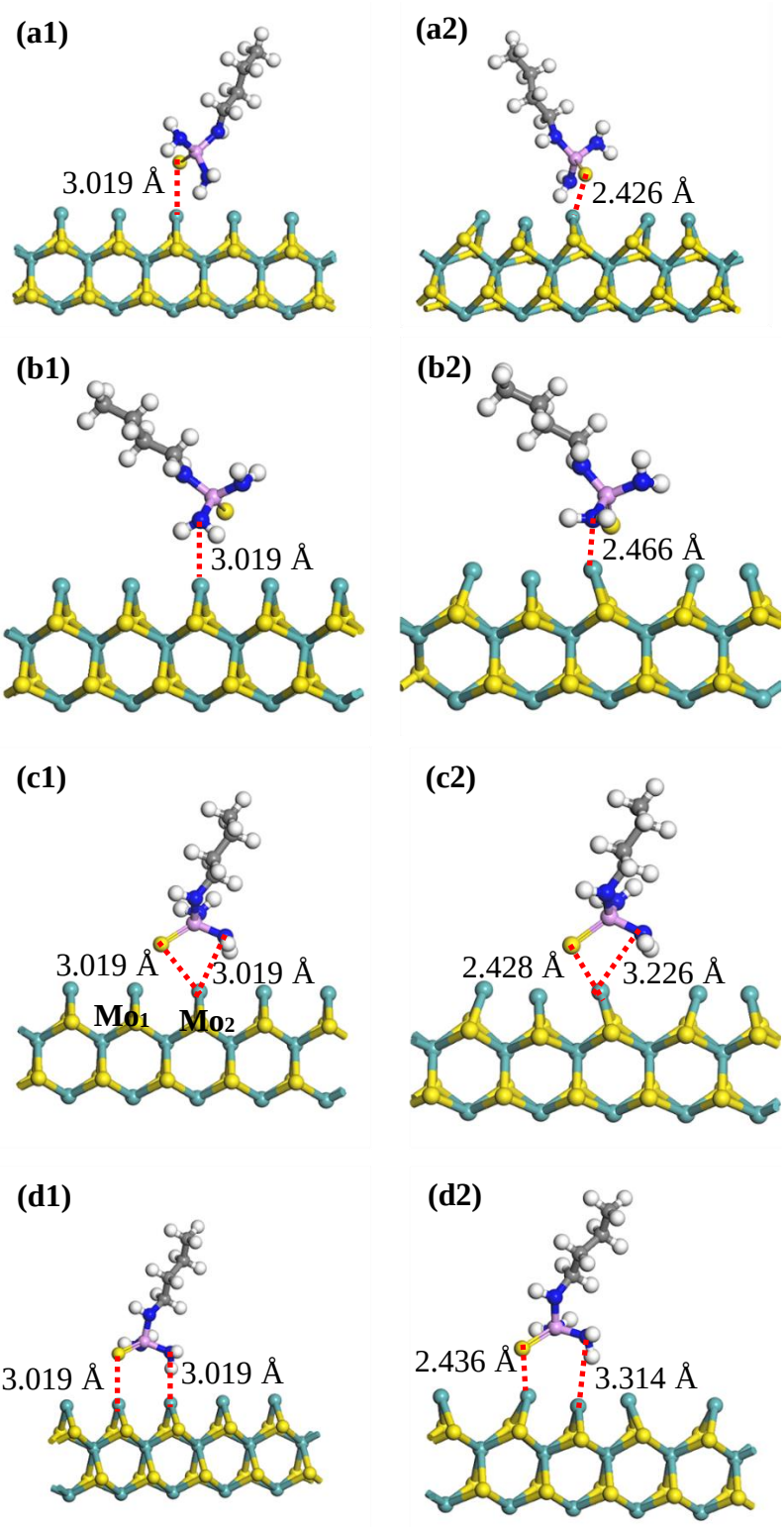

Fig. 4.11 The adsorption models of NBPT on molybdenite (1 0 0) surface before (1) and after (2) geometry optimization: (a) S–Mo_1, (b) N–Mo_1, (c) S–N–Mo_1, (d) N–Mo_1–S–Mo_2.

4.3.8.2 Analysis of electron density and electron density difference

The electron density map and electron density difference were analyzed to investigate the bonding mechanism. Fig. 4.12 shows the electron density map of NBPT and molybdenite (0 0 1) and (1 0 0) surfaces. Different color represent different electron density. As expected, no overlap of the electron distribution was found between NBPT and molybdenite (0 0 1) surface (Fig. 4.12 (a)), while the electron distributions of the S atom within NBPT were apparently overlapped with those Mo atoms on molybdenite (1 0 0) surface (Fig. 4.12 (b)), indicating the adsorption between NBPT and (1 0 0) surface much more stronger than that on (0 0 1) surface, which was consistent with the adsorption energy results.

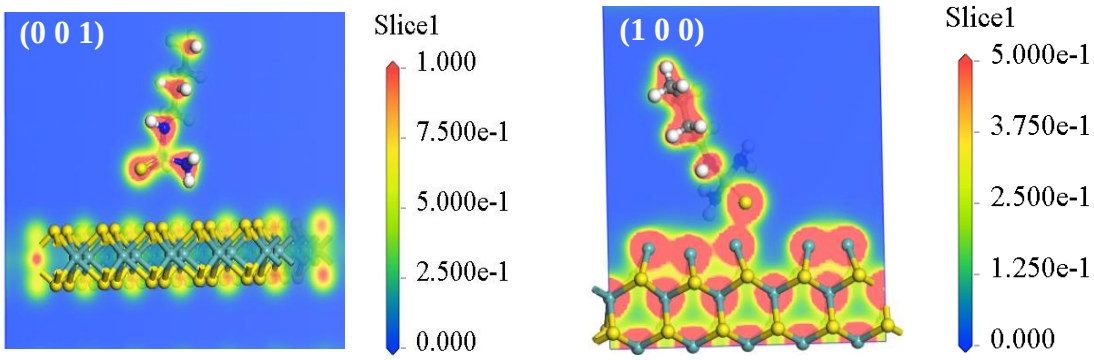

Fig. 4.12 Electron density map of: (a) (0 0 1) surface, (b) (1 0 0) surface of molybdenite.

Fig. 4.13 depicts the electron density difference of NBPT on molybdenite (1 0 0) surface. The red area indicates the gain of electrons while the blue area represents the deleption of electrons. The S and Mo atoms connected in the blue–red region, suggesting that the possible electron transfer between NBPT and Mo atoms.

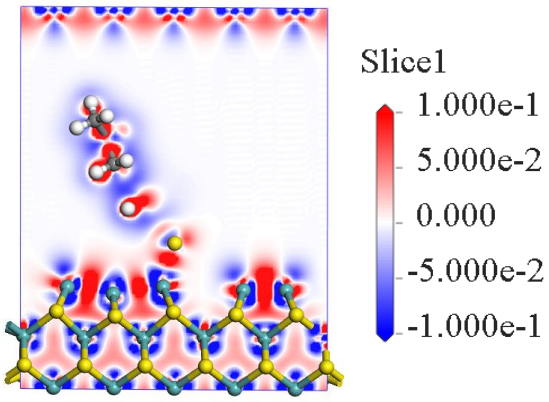

Fig. 4. 13 Electron density difference of NBPT on molybdenite (1 0 0) surface.

3.8.3 Analysis of Mulliken populations and density of states

Table 4.3 shows the Mulliken population and bond length of "S–Mo_1" adsorption model. The bond length between the S and Mo atoms was 2.426 Å, which was smaller than the sum of atomic radii of S–Mo (2.44 Å), suggesting that a strong bond was formed between these two atoms. The result was also observed in the electron density map. The S–Mo bond population was 0.52, indicating that S–Mo bond had strong covalent character [42].

Table 4.3 Mulliken population and bond length of the stable adsorption model

Bond	Population	Bond Length/Å
S–Mo	0.52	2.426

Table 4.4 presents the Mulliken charge population of atoms before and after NBPT adsorption. The S atom of NBPT gained electrons (i.e. –0.46 e to –0.63 e) while the Mo atom lost electrons (i.e. –0.18 e to –0.05 e), suggesting there was a strong bonding interaction between these two atoms.

Fig. 4.14 shows the PDOS results of S 3p of NBPT, Mo 4d of molybdenite before and after adsorption. An intense peak around the Fermi level was found in the PDOS of S 3p orbital of NBPT, suggesting that the S 3p orbital had high chemical activity. The S 3p orbital of NBPT peak around the Fermi level decreased significantly after adsorption, indicating that the S 3p orbital of NBPT gained electrons and participated in the bonding reaction (Fig. 4.14 (a)). After adsorption, the PDOS of Mo 4d orbital moved toward the conduction band, and the peak around the Fermi level increased, suggesting that Mo atoms lost electrons and involved in the bonding interaction (Fig. 4.14 (b)) [25]. These results were in agreement with above results. Moreover, the S 3p orbital of NBPT and Mo 4d orbital apparently overlapped in the range of −7.8 to −5.2, −3.2 to −1.6 and 0.4 to 3.1 eV after adsorption, indicating the S 3p orbital of NBPT hybridized with Mo 4d orbital of molybdenite [43].

Table 4.4 Mulliken charge population of atoms before and after adsorption

Atom	Mulliken charge (e)		
	Before	After	Change
S of NBPT	–0.46	–0.63	–0.17
Mo	–0.18	–0.05	0.13

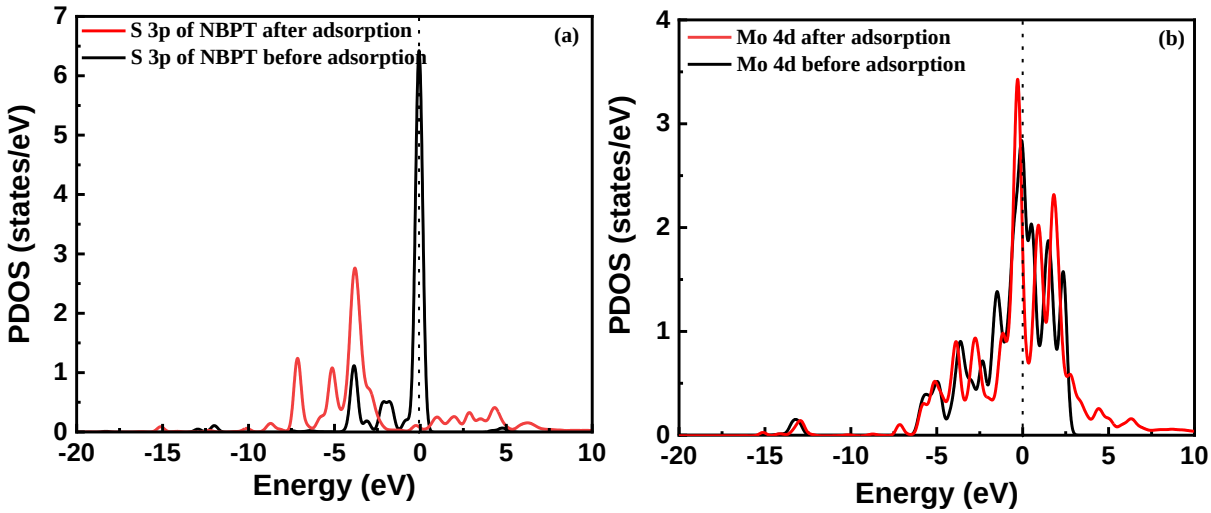

Fig. 4.14 PDOS results of: (a) S 3p of NBPT; (b) Mo 4d before and after adsorption.

4.3.9 Adsorption model

To sum up, the adsorption capacity, XPS, ToF-SIMS, AFM and DFT results collectively indicate that NBPT preferentially adsorbed on molybdenite edges via the hybridization of the S 3p orbital of NBPT with the Mo 4d orbital, as shown in Fig. 4.11 (a), orienting non-polar groups toward the bulk solutions, thus rendering the edges hydrophobic.

4.4. Conclusions

(1) NBPT could be used as an effective collector to enhance the flotation of molybdenite fines at a broad pH range.

(2) NBPT had a much stronger affinity for edges than faces.

(3) NBPT was chemically adsorbed on molybdenite edges through the hybridization of the S 3p orbital of NBPT with the Mo 4d orbital to form a strong covalent bond.

(4) NBPT had promising application prospects because of its high selectivity and environmental compatibility.

References

[1] Q. Zhang, X. Li, M. Li, C. Yuan, Study on flotation separation experiment of molybdenite using new type collector, Adv. Mater. Res. 753–755 (2013) 81–84.

[2] D. Malhotra, R.M. Rowe, A.K. Bhasin, Evaluation of collectors for molybdenite flotation, Mining, Metall. Explor. 3 (1986) 184–186.

[3] S. Li, X. Ma, J. Wang, Y. Xing, X. Gui, Y. Cao, Effect of polyethylene oxide on flotation of molybdenite fines, Miner. Eng. 146 (2020) 106146.

[4] M.C. Fuerstenau, B.J. Sabacky, On the natural floatability of sulfides, Int. J. Miner. Process. 8 (1981) 79–84.

[5] T.F. Jaramillo, K.P. Jørgensen, J. Bonde, J.H. Nielsen, S. Horch, I. Chorkendorff, Identification of active edge sites for electrochemical H2 evolution from MoS2 nanocatalysts, Science (80-.). 317 (2007) 100–102.

[6] Q. Lin, G. hua Gu, H. Wang, Y. cai Liu, J. gang Fu, C. qing Wang, Flotation mechanisms of molybdenite fines by neutral oils, Int. J. Miner. Metall. Mater. 25 (2018) 1–10.

[7] S. Castro, A. Lopez-valdivieso, J.S. Laskowski, International Journal of Mineral Processing Review of the fl otation of molybdenite . Part I : Surface properties and floatability, Int. J. Miner. Process. 148 (2016) 48–58.

[8] Z. Wei, Y. Li, L. Huang, New insight into the anisotropic property and wettability of molybdenite: A DFT study, Miner. Eng. 170 (2021) 107058.

[9] J.R. Lince, P.P. Frantz, Anisotropic oxidation of MoS_2 crystallites studied by angle-resolved X-ray photoelectron spectroscopy, Tribol. Lett. 9 (2001) 211–218.

[10] Z. Lu, Q. Liu, Z. Xu, H. Zeng, Probing Anisotropic Surface Properties of Molybdenite by Direct Force Measurements, Langmuir. 31 (2015) 11409–11418.

[11] T. He, H. Li, J. Jin, Y. Peng, Y. Wang, H. Wan, Improving fine molybdenite flotation using a combination of aliphatic hydrocarbon oil and polycyclic aromatic hydrocarbon, Results Phys. 12 (2019) 1050–1055.

[12] S. Song, X. Zhang, B. Yang, A. Lopez-Mendoza, Flotation of molybdenite fines as hydrophobic agglomerates, Sep. Purif. Technol. 98 (2012) 451–455.

[13] R.C. Santana, J.A. Ribeiro, M.A. Santos, A.S. Reis, C.H. Ataíde, M.A.S. Barrozo, Flotation of fine apatitic ore using microbubbles, Sep. Purif. Technol. 98 (2012) 402–409.

[14] R.E. Engel, B.D. Towey, E. Gravens, Degradation of the Urease Inhibitor NBPT as Affected by Soil pH, Soil Sci. Soc. Am. J. 79 (2015) 1674–1683.

[15] C. Wang, R. Liu, M. Wu, Z. Xu, M. Tian, Z. Yin, W. Sun, C. Zhang, Flotation separation of molybdenite from chalcopyrite using rhodanine-3-acetic acid as a novel and effective depressant, Miner. Eng. 162 (2021) 106747.

[16] B. Yang, D. Wang, T. Wang, H. Zhang, F. Jia, S. Song, Effect of Cu^{2+} and Fe^{3+} on the depression of molybdenite in flotation, Miner. Eng. 130 (2019) 101–109.

[17] Y. Hu, Z. Gao, W. Sun, X. Liu, Anisotropic surface energies and adsorption behaviors of scheelite crystal, Colloids Surfaces A Physicochem. Eng. Asp. 415 (2012) 439–448.

[18] H. Yan, B. Yang, M. Zeng, P. Huang, A. Teng, Selective flotation of Cu-Mo sulfides using xanthan gum as a novel depressant, Miner. Eng. 156 (2020) 106486.

[19] P.F.A. Braga, A.P. Chaves, A.B. Luz, S.C.A. Fran ça, The use of dextrin in purification by flotation of molybdenite concentrates, Int. J. Miner. Process. 127 (2014) 23–27.

[20] Z. Yin, W. Sun, Y. Hu, R. Liu, W. Jiang, C. Zhang, Q. Guan, C. Zhang, Synthesis of acetic acid-[(hydrazinylthioxomethyl)thio]-sodium and its application on the flotation separation of molybdenite from galena, J. Ind. Eng. Chem. 52 (2017) 82–88.

[21] N. Mhonde, M. Smart, K. Corin, N. Schreithofer, Investigating the electrochemical interaction of a thiol collector with chalcopyrite and galena in the presence of a mixed microbial community, Minerals. 10 (2020) 1–17.

[22] Tsukamoto, Tatsuya, Matsuoka, Masaya, Kondo, Atsushi, Takeuchi, Masato, Investigation of NH_3 and NH_4^+ adsorbed on ZSM-5 zeolites by near and middle infrared spectroscopy, Catal. Sci. Technol. (2015) 4587–4593.

[23] M. Thomas, H.H. Richardson, Two-dimensional FT-IR correlation analysis of the phase transitions in a liquid crystal, 4'-n-octyl-4-cyanobiphenyl (8CB), Vib. Spectrosc. 24 (2000) 137-146.

[24] H. Wang, S. Gu, Y. Bai, S. Chen, N. Zhu, C. Wu, F. Wu, Anion-effects on electrochemical properties of ionic liquid electrolytes for rechargeable aluminum batteries, J. Mater. Chem. A. 3 (2015) 22677–22686.

[25] B. Yang, P. Huang, Q. An, An efficient chalcopyrite depressant for Cu-Mo separation and its interaction mechanism: Adsorption configuration and DFT calculations, J. Mol. Liq. 345 (2022) 118171.

[26] B. Shanta, T.U. Rashid, A.K. Mallik, I.M. Minhajul, K.M. Nuruzzaman, H. Papia, K. Mala, R.M. Mizanur, Facile Preparation of Biocomposite from Prawn Shell Derived Chitosan and Kaolinite-Rich Locally Available Clay, Int. J. Polym. Ence. 2017 (2017) 1–8.

[27] Y. Zhang, Research on synthesis of N-(n-Butyl) thiophosphoric triamide and its derivatives, Southwest University of Science and Technology, 2016.

[28] J. Zhuang, M. Li, Y. Pu, A.J. Ragauskas, C.G. Yoo, Observation of potential contaminants in processed biomass using fourier transform infrared spectroscopy, Appl. Sci. 10 (2020) 1–13.

[29] F. Jia, C. Liu, B. Yang, S. Song, Microscale control of edge defect and oxidation on molybdenum disulfide through thermal treatment in air and nitrogen atmospheres, Appl. Surf. Sci. 462 (2018) 471–479.

[30] C. Liu, S. Zeng, B. Yang, F. Jia, S. Song, Simultaneous removal of Hg^{2+}, Pb^{2+} and Cd^{2+} from aqueous solutions on multifunctional MoS2, J. Mol. Liq. 296 (2019) 111987.

[31] J. Auvergniot, A. Cassel, D. Foix, V. Viallet, V. Seznec, R. Dedryvère, Redox activity of argyrodite Li_6PS_5Cl electrolyte in all-solid-state Li-ion battery: An XPS study, Solid State Ionics. 300 (2017) 78–85.

[32] B. Yang, H. Yan, M. Zeng, H. Zhu, Tiopronin as a novel copper depressant for the selective flotation separation of chalcopyrite and molybdenite, Sep. Purif. Technol. 266 (2021) 118576.

[33] Y. Hu, B. Li, X. Jiao, C. Zhang, X. Dai, J. Song, Stable Cycling of Phosphorus Anode for Sodium‐Ion Batteries through Chemical Bonding with Sulfurized Polyacrylonitrile, Adv. Funct. Mater. 28 (2018) 1801010.

[34] A.L. Schwaner, E.D. Pylant, J.M. White, Electron-induced surface chemistry: Synthesis of NH x fragments on Ag (111), J. Vac. Sci. Technol. A Vacuum, Surfaces, Film. 14 (1996) 1453–1456.

[35] H. Zarrok, A. Zarrouk, B. Hammouti, R. Salghi, C. Jama, F. Bentiss, Corrosion control of carbon steel in phosphoric acid by purpald–weight loss, electrochemical and XPS studies, Corros. Sci. 64 (2012) 243–252.

[36] S. Li, Z. Zhao, T. Ma, P. Pachfule, A. Thomas, Superstructures of Organic–Polyoxometalate Co-crystals as Precursors for Hydrogen Evolution Electrocatalysts, Angew. Chemie-Int. Ed. 61 (2022) 1–8.

[37] P. Basu, K. Mukherjee, S. Khamrui, S. Mukherjee, M. Ahmed, K. Acharya, D. Banerjee, P.M.G. Nambissan, K. Chatterjee, Oxygen, nitrogen co-doped molybdenum disulphide nanoflowers for an excellent antifungal activity, Mater. Adv. 1 (2020) 1726–1738.

[38] P. Basu, J. Chakraborty, N. Ganguli, K. Mukherjee, K. Acharya, B. Satpati, S. Khamrui, S. Mandal, D. Banerjee, D. Goswami, Defect-engineered MoS_2 nanostructures for reactive oxygen species generation in the dark: antipollutant and antifungal performances, ACS Appl. Mater. Interfaces. 11 (2019) 48179–48191.

[39] D.D. Sarma, C.N.R. Rao, XPES studies of oxides of second-and third-row transition metals including rare earths, J. Electron Spectros. Relat. Phenomena. 20 (1980) 25–45.

[40] G.L. Chai, K. Qiu, M. Qiao, M.M. Titirici, C. Shang, Z. Guo, Active sites engineering leads to exceptional ORR and OER bifunctionality in P,N Co-doped graphene frameworks, Energy Environ. Sci. 10 (2017) 1186–1195.

[41] A. Rossi, F.M. Piras, D. Kim, A.J. Gellman, N.D. Spencer, Surface reactivity of tributyl thiophosphate: effects of temperature and mechanical stress, Tribol. Lett. 23 (2006) 197–208.

[42] M. Castell à-Ventura, A. Moissette, E. Kassab, DFT Study of Si/Al Ratio and Confinement Effects on the Energetics and Vibrational Properties of some Aza-Aromatic Molecules Adsorbed on H-ZSM-5 Zeolite, Computation. 8 (2020) 81.

[43] X. Long, Y. Chen, J. Chen, Z. Xu, Q. Liu, Z. Du, The effect of water molecules on the thiol collector interaction on the galena (PbS) and sphalerite (ZnS) surfaces: A DFT study, Appl. Surf. Sci. 389 (2016) 103–111.

The main content in this chapter was published in *Minerals Engineering.*

Chapter V. The anisotropic adsorption of potassium cetyl phosphate on molybdenite surface and its implication for improving the flotation of molybdenite fines

5.1 Introduction

Molybdenite (MoS_2) is a primary source to extract molybdenum, which is extensively used in metallurgy, machinery, chemical and aerospace due to its excellent lubricity, thermal stability, catalysis and photoelectric performance [1, 2]. With the increasing demand for molybdenum and the rapid depletion of molybdenite deposits, it is imperative to efficiently treat the low-grade and finely-disseminated molybdenite ores [3]. However, these refractory molybdenite ores require fine grinding to liberate molybdenite from other minerals. As a typical anisotropic mineral with a layered structure, molybdenite exhibits two kinds of surfaces, namely hydrophobic faces and hydrophilic edges, respectively [4]. The hydrophobicity of molybdenite particles relies on the edge /face ratio. As particle size decreases, the edge/face ratio increases, hence molybdenite hydrophobicity reduces significantly [5, 6]. Molybdenite particles bigger than +20 μm are commonly considered naturally hydrophobic with good floatability [7], but the flotation of molybdenite fines (–20 μm) is inefficient because of its poor hydrophobicity. Therefore, the targeted regulation of the edges is essential to improve the flotation of molybdenite fines [8].

In recent decades, many efforts have been devoted to investigating the interfacial properties of faces and edges in relation to flotation. For example, Lucay et al. found that Na^+ decreased electrostatic repulsion between molybdenite edges and bubbles, thus improving molybdenite flotation [9]. Lu et al. demonstrated that Ca^{2+} interacted with the MoO_4^{2-} or $HMoO_4^-$ groups on the edges, which adversely affected molybdenite flotation [10]. Yang et al. reported that Fe^{3+} strongly depressed molybdenite due to its precipitate $Fe(OH)_3$ preferentially adsorbed on molybdenite edges, rendering molybdenite hydrophilic [11]. In addition, sodium metabisulfite (MBS) depressed molybdenite because sulphite ions oxidized and adsorbed on molybdenite edges, forming sulphate complexations that prevented collector's adsorption [12]. Carboxymethyl cellulose (CMC) mainly adsorbed on the face rather than the edge due to the strong hydrophobic attraction and weak electrostatic repulsion between CMC and the face, which weakened molybdenite hydrophobicity and its floatability [13]. Polyethylene oxide (PEO) was preferentially adsorbed on the edges due to the strong affinity between O atoms and Mo atoms, thus promoting the flotation of molybdenite fines [14]. Although much work has been done, little attention has been paid to enhancing the flotation of molybdenite fines based on the targeted regulation of molybdenite edges. As

previously mentioned, the edge surface dominates the hydrophobicity of molybdenite fines. Thus, the development of novel collectors that selectively interact with the edges is a promising approach to improve the flotation of molybdenite fines.

Potassium cetyl phosphate (PCP) is a stable and environmentally-friendly surfactant, commonly used as a cleansing agent and emulsifier in skin care products. As shown in Fig. 5.1, PCP contains one phosphate group and a cetyl chain. The phosphorous-bearing functional group within PCP exhibits strong complexation with cationic sites on various minerals such as rare-earth minerals, oxidized minerals and carbonate minerals [15–17]. In this study, PCP was first explored as a potential molybdenite collector. The flotation performances and the interaction mechanisms were investigated by micro-flotation tests, Zeta potential, Fourier Transform Infrared Spectrometer (FTIR), X-ray Photoelectron Spectroscopy (XPS), atomic force microscopy (AFM), Tafel curves, cyclic voltammetry (CV), contact angle and density functional theory (DFT) calculations.

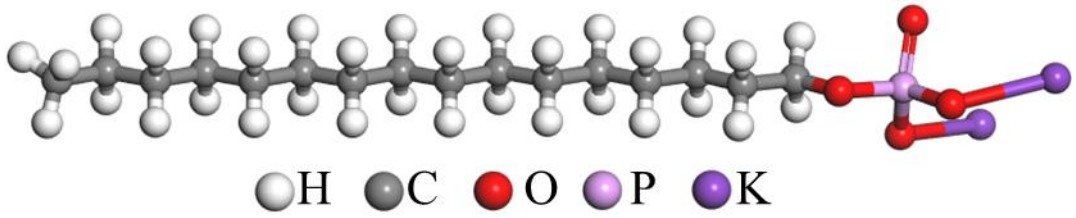

Fig. 5.1 Molecular structure of PCP.

5.2 Experimental

5.2.1Materials

Bulk molybdenite from Wuzhou Mine (Guangxi province, China) was utilized in this study. The ores were selected, crushed, ground and sieved to obtain –20 μm molybdenite particles for micro-flotation tests. The X-ray diffraction (XRD) pattern of raw molybdenite minerals is shown in Fig. 5.2. The chemical assay and XRD pattern demonstrated that molybdenite samples were highly pure (97%).

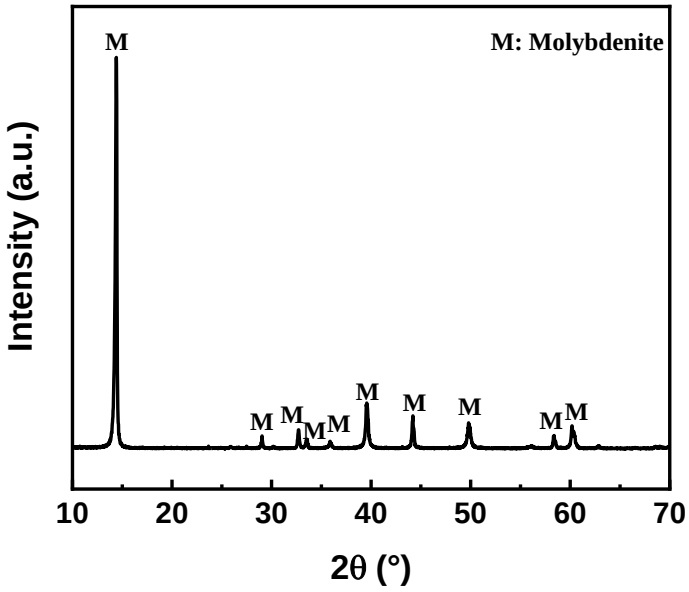

Fig. 5.2 The XRD pattern of molybdenite samples.

All reagents were acquired from Sigma-Aldrich, China. PCP was applied as a collector, methyl isobutyl carbinol (MIBC) was used as a frother, HCl and NaOH were employed as pH regulators, respectively. Deionized water was utilized in all tests.

5.2.2 Flotation tests

An XFG flotation machine (Wuhan exploration machinery factory, China) was utilized to perform all flotation tests. 2 g of molybdenite minerals were added to 40 mL deionized water and dispersed by ultrasonic cleaner (KunShan Ultrasonic Instrument Co., Ltd, China) for 2 min, and then the pulp was transferred to a flotation cell. After the adjustment of pH, PCP and MIBC were subsequently introduced. Finally, the flotation was conducted for 3 min, and the flotation products were filtered, dried and weighed successively to calculate floatability.

5.2.3 Characterizations

Zeta potential measurements were conducted using a NanoPlus3 analyzer (Micromeritics, USA). Briefly, 0.1 g of molybdenite was dispersed in a PCP solution containing 0.001 M NaCl as the background electrolyte and stirred for 5 min. Subsequently, 1 mL of the suspension was withdrawn for zeta potential analysis. Fourier transform infrared (FTIR) spectra of molybdenite were recorded using an MMC 274 spectrometer (Nexus, Germany). Prior to measurement, 0.2 g of mineral samples were conditioned in a 1000 ppm PCP solution (pH = 10) for 30 min. The treated samples were then filtered and dried before

FTIR analysis. X-ray photoelectron spectroscopy (XPS) measurements were performed using a K-Alpha photoelectron spectrometer (Thermo Scientific, USA). The spectra were analyzed using Thermo Avantage software (version 5.9922), and the binding energies were calibrated with reference to the C 1s peak at 284.80 eV. The surface topography of molybdenite faces and edges, both with and without PCP treatment, was characterized using an atomic force microscope (AFM, Bruker, USA) operating in ScanAsyst air mode. The detailed characterization procedure followed our previous studies [11]. Electrochemical measurements, including Tafel polarization and cyclic voltammetry (CV), were carried out using a VersaSTAT 4 electrochemical workstation (Princeton Applied Research, USA). The preparation of molybdenite face and edge electrodes followed the procedures reported in previous studies [18]. During the tests, freshly prepared molybdenite face and edge electrodes were mounted on the electrode holder with exposed geometric surface areas of 0.75 cm^2 and 0.66 cm^2, respectively, and immersed in a 0.1 M NaCl electrolyte solution. A platinum electrode served as the counter electrode, while an Ag/AgCl (1 M KCl) electrode was used as the reference electrode. The wettability of molybdenite edges was evaluated by contact angle measurements using a Dataphysics OCA20 goniometer (Germany) via the sessile drop method. Fresh molybdenite edge surfaces were prepared according to previously reported methods [18, 19]. The samples were immersed in PCP solutions at pH 10 for 30 min and then naturally dried prior to measurement. During the measurements, contact angles were recorded at three different locations on each molybdenite edge surface, and the average value was reported.

5.2.4 DFT calculation

The simulation of PCP adsorption was conducted utilizing CASTEP. Ultrasoft pseudopotentials were used to describe electron configurations of Mo $4s^2 4p^6 4d^5 5s^1$ and O $2s^2 2p^4$. The Brillouin zone was sampled utilizing a k-point of $5 \times 5 \times 1$ and the kinetic energy cutoff of 430 eV was used for molybdenite calculations [20]. The tolerance value of energy, force, stress, displacement and SCF tolerance were 2×10^{-5} eV/atom, 0.05 eV/Å, 0.1 GPa, 0.002 Å and 2×10^{-6} eV/atom. The optimizations of molybdenite were calculated in a 30 Å vacuum slab. The molybdenite (0 0 1) surface (MS001) was cleaved to create the face. The edge was built along the molybdenite (1 0 0) surface (MS100).

5.3 Results and discussion

5.3.1 Micro-flotation tests

Fig. 5.3 (a) displays molybdenite floatability at pH 10 as a function of collector dosage. When PCP was introduced, the floatability increased by about 64% at a PCP dosage of 1000 ppm. While kerosene was added , the floatability of molybdenite fines barely changed. The results suggested that kerosene could not improve the hydrophobicity of molybdenite edges, because of its poor affinity for edges [19]. These results indicated that PCP could effectively enhance the flotation of molybdenite fines, which might be a potential collector for molybdenite flotation.

Fig. 5.3 (b) shows the impact of pH on the flotation performance of molybdenite. Without PCP, the floatability decreased gradually as the pH increased, which was attributed to the presence of electrical charges on edges that originated from the transformation of molybdate ionic species ($HMoO_4^-$ and MoO_4^{2-}) in solution and on molybdenite surfaces [9, 21]. After the introduction of PCP, the floatability improved as pH increased, and then remained nearly constant in the pH range of 10–12. These results indicated that PCP exhibited powerful collecting ability under alkaline conditions.

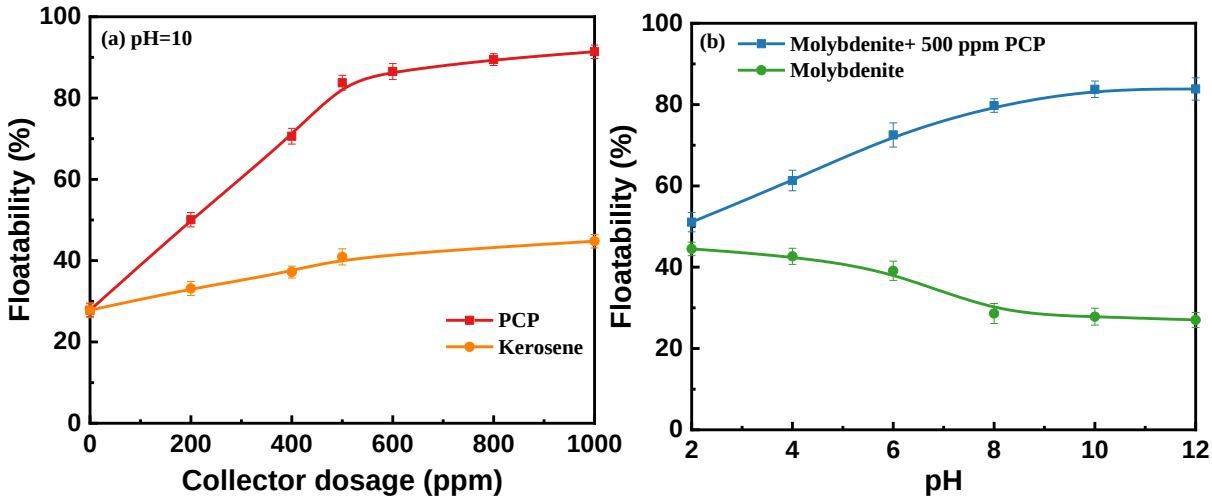

Fig. 5.3 The impact of collector dosage (a) and pH (b) on the floatability of molybdenite fines.

The dissociation equilibria of cetyl phosphate (CP) species were calculated using Eqs. (1) and (2). Fig. 5.4 shows the effect of PCP solution on the distribution diagram [22]. CP molecules were predominant at pH below 2, which tended to disappear at pH ≈ 5. CP^- species were the main species in the pH range of 2–7.5, and the first dissociation of CP was almost

complete at pH 10.5. In addition, CP^{2-} species appeared at pH 5 and gradually dominated in solution equilibria as the pH increased under an alkaline environment, which was the only species above pH 10.5.

$$CP \leftrightharpoons CP^{-} \qquad pK_{a1} = 2.02 \qquad (1)$$

$$CP^{-} \leftrightharpoons CP^{2-} \qquad pK_{a1} = 7.49 \qquad (2)$$

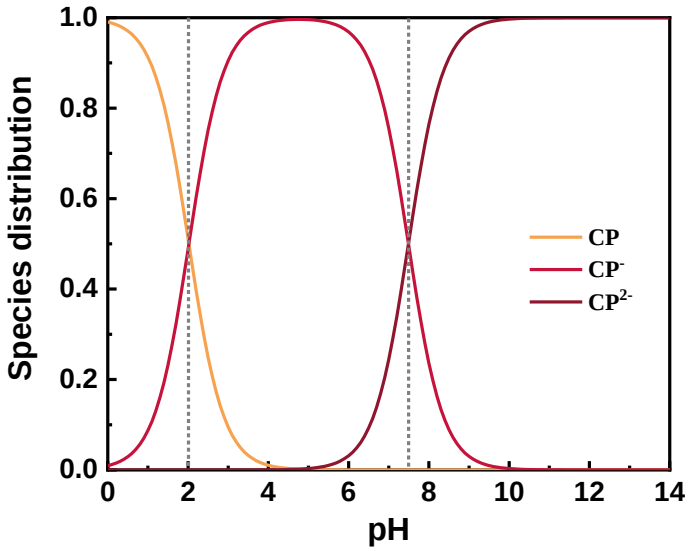

Fig. 5.4 Species distribution of CP solution as a function of pH.

5.3.2 Zeta potential

Fig. 5.5 presents the zeta potential of molybdenite with and without PCP under various pH values. For pure molybdenite, the zeta potential was negative throughout the pH range, which was in accordance with previous studies [11]. After the introduction of PCP, the Zeta potential decreased significantly toward the more negative direction, indicating a strong adsorption of PCP on molybdenite surfaces. Based on the distribution diagram of PCP, it could be deduced that substantial PCP anions were adsorbed on molybdenite surfaces.

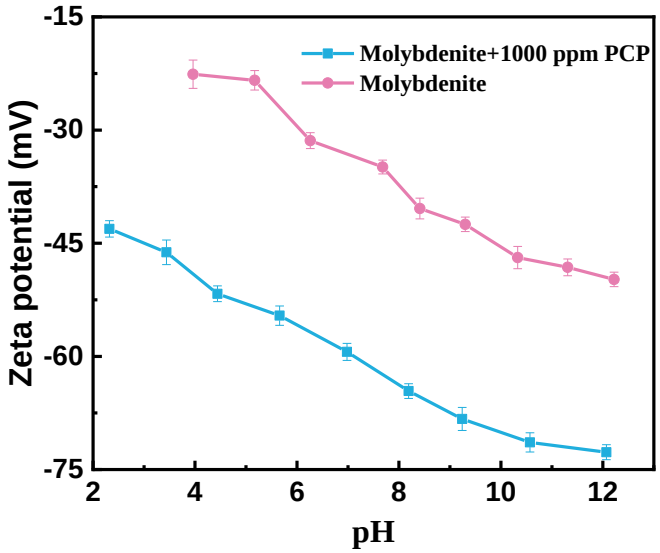

Fig. 5.5 Zeta potential of molybdenite with or without PCP at various pH.

5.3.3 FTIR tests

Fig. 5.6 shows the FTIR spectra of PCP, molybdenite in the presence and absence of PCP. Table 5.1 provides the characteristic peaks of PCP. For pure PCP, the characteristic peaks at 1080, 2848 and 2919 cm^{-1} were ascribed ssigned to the vibration of $–CH_3$, $–CH_2$ and –PO– groups, respectively. For molybdenite treated with PCP, the peaks of $–CH_3$ and $–CH_2$ vibrations still existed. Meanwhile, the –PO– group exhibited a blue shift from 1080 cm^{-1} to 1088 cm^{-1}. These results indicated that PCP might be chemically adsorbed on molybdenite surfaces via the phosphate groups [23].

Table 5.1 Major functional groups of PCP

Wavenuumber (cm^{-1})	Functional group
3399	O–H stretching vibration
2921	$–CH_3$ stretching vibration
2848	$–CH_2$ stretching vibration
1460	–CH stretching vibration
1214	C–O stretching vibration
1154	$(PO_3)^{2–}$ stretching vibration
1080	–PO– stretching vibration
835	C–H bending vibration
569	O–P–O bending vibration

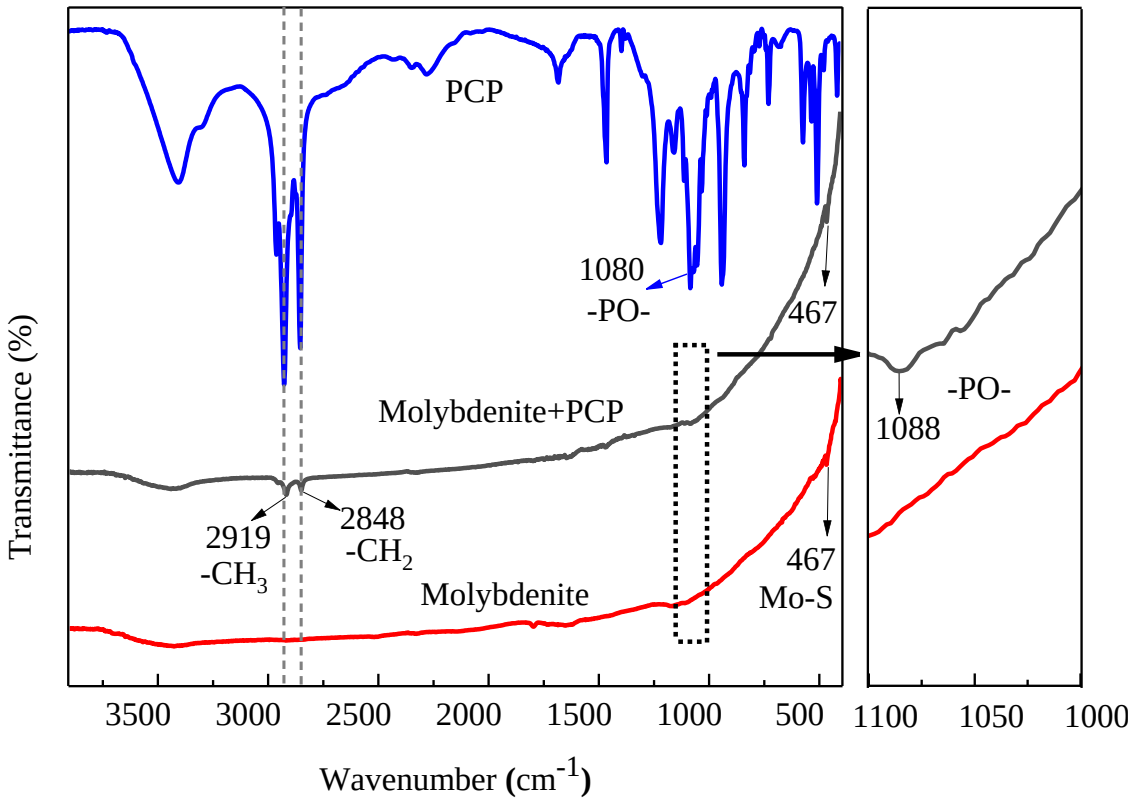

Fig. 5.6 FTIR results of PCP, molybdenite with and without PCP treatment.

5.3.4 XPS analysis

Fig. 5.7 shows the high-resolution spectra of P 2p, O 1s, Mo 4d and S 2p on treated and untreated molybdenite. The spectra of P 2p of PCP, molybdenite with and without PCP are presented in Fig. 5.7 (a). For pure PCP, two doublets centered at 133.13eV and 134.10 eV, which were assigned to HPO_4^{2-} [24] and PO_4^{3-} [25]. For molybdenite treated with PCP, the spectra of P 2p were fitted into four peaks, located at 132.53 eV, 133.38 eV, 134.09 eV and 134.99 eV, which were assigned to P–O–Mo [26], HPO_4^{2-}, PO_4^{3-} and $H_2PO_4^-$ [27], respectively. Moreover, the appearance of P–O–Mo peak reconfirmed that the chemisorption was due to the coordination between phosphate groups and Mo atoms on molybdenite surfaces.

Fig. 5.7 (b) displays the O 1s spectra. For PCP, two peaks at 532.30 eV and 530.53 eV were derived from P–O [28] and P=O [29] bonds, respectively. For bare molybdenite, two doublets at 531.99 eV and 533.22 eV were assigned to C=O [30] and C=O groups [31], which originated from the reference carbon. After treatment with PCP, the peaks of P–O (532.72 eV), P=O (530.68 eV), C=O (533.34 eV) and C–O (531.58 eV) were observed in the spectrum. In addition, a movement of 0.42 eV in the P–O bond was observed after the

introduction of PCP, elucidating that the chemisorption occurred on the molybdenite surfaces.

Mo 3d spectra of molybdenite with and without PCP are illustrated in Fig. 5.7 (c). In the absence of PCP, the peaks located at 227.01, 228.76, 229.90, 232.35, 233.06, 233.65 and 236.14 eV were assigned to S 2s, Mo $3d_{5/2}$ of MoO_2, Mo $3d_{5/2}$ of MoS_2, Mo $3d_{5/2}$ of MoO_3, Mo $3d_{3/2}$ of MoO_2, Mo $3d_{3/2}$ of MoS_2, Mo $3d_{3/2}$ of MoO_3 [32–34], respectively. After the addition of PCP, the shifting of 0.22 eV was detected in the Mo $3d_{5/2}$ and Mo $3d_{3/2}$ of MoS_2, suggesting that PCP chemisorbed on molybdenite surfaces.

Fig. 5.7 (d) exhibits the spectra of S 2p of molybdenite. For bare molybdenite, the peaks at 163.98 eV and 162.78 eV were assigned to S $2p_{1/2}$ and S $2p_{3/2}$ of MoS_2 [32, 35]. After being treated with PCP, the peaks of S $2p_{1/2}$ and S $2p_{3/2}$ did not shift significantly, indicating that S atoms might not be involved in the reaction between PCP and molybdenite.

XPS results clearly demonstrated that the phosphate groups within PCP chemisorbed on Mo atoms, forming P–O–Mo bonds, which was in line with FTIR results.

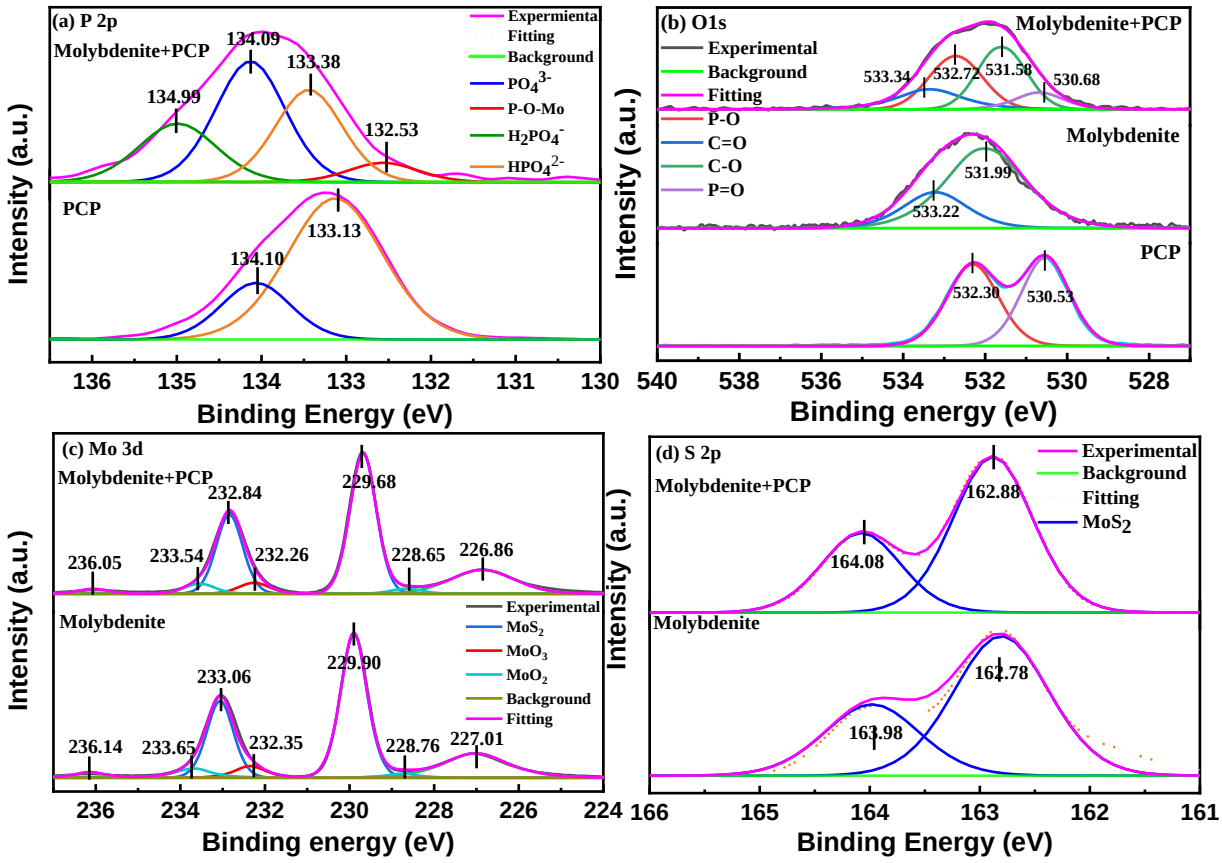

Fig. 5.7 XPS spectra of molybdenite treated/untreated with PCP.

5.3.5 AFM measurement

Fig. 5.8 displays the two-dimensional (2D) and three-dimensional (3D) AFM images of treated and untreated molybdenite with 1000 ppm PCP. Before the addition of PCP, an atomically smooth face and edge were detected in air (Fig. 5.8 (a)). Upon treatment with PCP solution for 5 min, many tree-like aggregates accumulated on molybdenite edges while a few appeared on faces (Fig. 5.8 (b)). These results indicated that PCP was preferentially adsorbed on edges rather than faces, demonstrating PCP had a stronger affinity for edges.

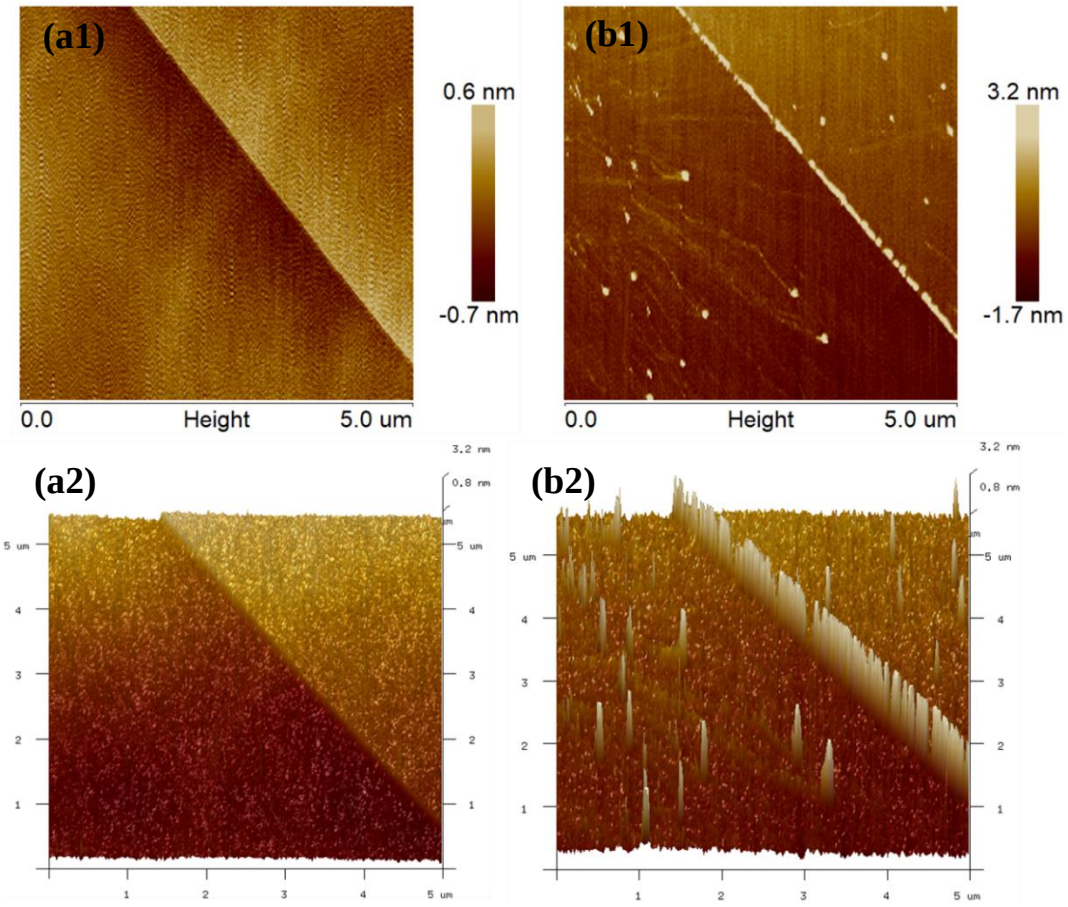

Fig. 5.8 2D and 3D AFM images of molybdenite surfaces before (a) and after adsorption (b).

5.3.6 Electrochemical study

5.3.6.1 Tafel curves

Fig. 5.9 displays the Tafel curves of the molybdenite face and edge electrode in 0 and 1000 ppm PCP solution. The inhibition efficiency (IE) could be calculated from the corrosion

current density using equation (3), and the analysis results of Tafel curves are shown in Table 5.2 [36, 37]:

$$IE\% = \frac{I^*_{corr} - I_{corr}}{I^*_{corr}} \times 100\%$$

Where I^*_{corr} and I_{corr} denote the corrosion current densities of molybdenite electrodes in 0 and 1000 ppm PCP, respectively.

The Tafel plot of molybdenite face in 0 and 1000 ppm PCP is presented in Fig. 5.9 (a). The corrosion current densities were 2.043 × 10^{-4} mA/cm^2 and 1.707 × 10^{-4} mA/cm^2 in 0 ppm and 1000 ppm PCP solution, respectively. Meanwhile, the *IE%* of PCP on the molybdenite face was only 16.45%, suggesting that PCP inhibited a small number of reaction sites on the molybdenite face.

Fig. 5.9 (b) shows the Tafel curves of molybdenite edge in 0 and 1000 ppm PCP solution. After adding PCP, the corrosion current density declined from 2.543 × 10^{-3} mA/cm^2 to 3.151 × 10^{-4} mA/cm^2, indicating that PCP adsorbed on molybdenite edge and thus inhibiting the corrosion of edge electrode. In addition, the *IE%* of PCP on molybdenite edge was 87.6%, demonstrating that PCP adsorbed most reaction sites of molybdenite edge.

The higher corrosion current density of the edge than the face without PCP indicated that the edge had higher electrochemical reactivity than the face [30]. Moreover, the much higher *IE%* showed PCP tended to react with molybdenite edges, which was consistent with AFM results. Combined with AFM and Tafel curve results, molybdenite edge had more affinity to PCP than the face. Therefore, the interaction between PCP and molybdenite edge should only be considered in CV and contact angle analysis.

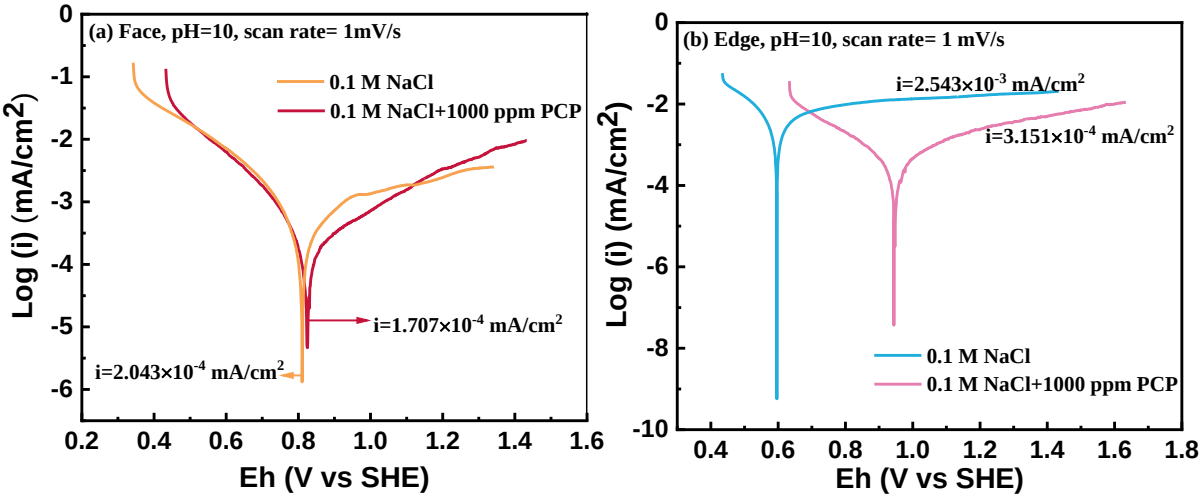

Fig. 5.9 Tafel curves of molybdenite: (a) face, (b) edge electrode with and without PCP.

Table 5.2 The results of Tafel curves on face and edge

Surface	PCP concentration (ppm)	Corrosion current densities (mA/cm^2)	IE%
Face	0	2.043×10^{-4}	16.45
	1000	1.707×10^{-4}	
Edge	0	2.543×10^{-3}	87.6
	1000	3.151×10^{-4}	

5.3.6.2 Cyclic voltammetry

Fig. 5.10 presents the cyclic voltammetry (CV) curves of the edge in 0.1 M NaCl with and without PCP. Before the introduction of PCP, the edge exhibited inherent surface redox reactions. An oxidation current peak appeared at 0.5 V in the positive direction, and a reduction current peak appeared at –0.45 V in the negative direction. CV peaks commonly occur at molybdenite edge due to the transformation between Mo^{2+}/Mo^{3+}, Mo^{4+} and Mo^{6+} when active Mo atoms are exposed to the solution [38]. Therefore, the oxidation peak was ascribed to the conversion of Mo^{2+}/Mo^{3+} to Mo^{4+}, and the reduction peak was due to the transformation of Mo^{6+} to Mo^{4+} [18]. After the addition of PCP, the CV curves of the edge showed slightly decreased redox peaks, indicating that PCP complexed with the active electrochemical sites (Mo^{4+}) and thereby influenced the redox reactions on molybdenite edges.

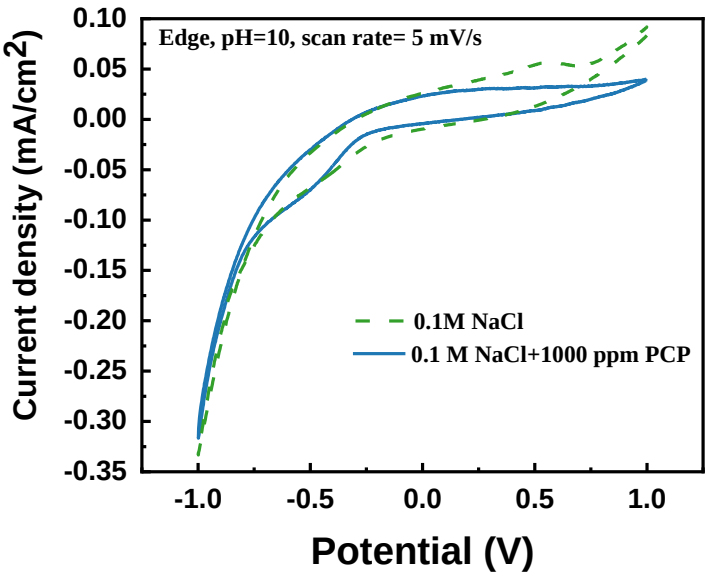

Fig. 5.10 Cyclic voltammetry diagrams of molybdenite edge with and without PCP.

5.3.7 Contact angle

Fig. 5.11 shows the contact angle on molybdenite edge before and after treatment with different concentrations of PCP. The contact angle of molybdenite edge increased from 41.75 ° to 62.75 ° as PCP concentration increased from 0 to 1000 ppm, indicating that PCP could significantly enhance the hydrophobicity of molybdenite edge. Taking AFM and electrochemical results into consideration, it is reasonable to conclude that the significant improvement in the flotation of molybdenite fines was attributed to the targeted regulation of the edge hydrophobicity.

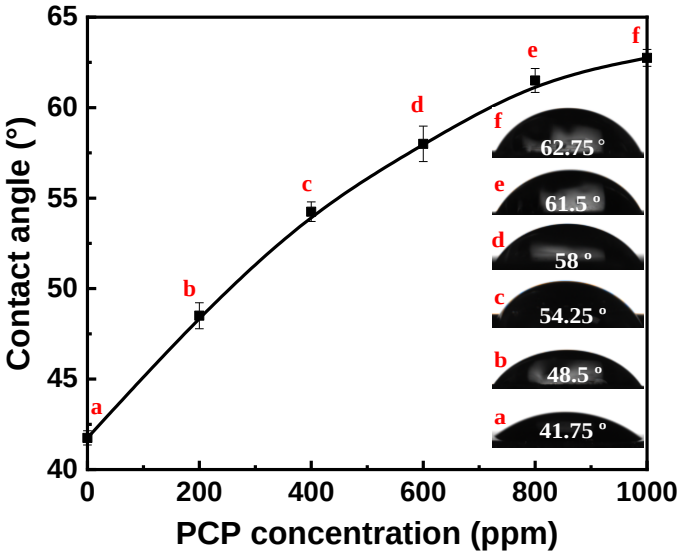

Fig. 5.11 Contact angle of molybdenite edge after various concentrations of PCP treatment.

5.3.8 DFT calculations

5.3.8.1 Adsorption energy

Table 5.3 shows that the adsorption energies of PCP on MS001 and MS100. Fig. 5.12 displays the possible adsorption model of PCP on MS001. The adsorption energy of PCP on MS001 was 33.5 kJ/mol, which meant it was thermodynamically unfavorable for PCP to adsorb on MS001. While the adsorption energy of PCP on MS100 was –735.14 kJ/mol and –728.61 kJ/mol for "Mo_1+Mo_2" and "Mo_2" models, respectively, which meant the adsorption of PCP on MS100 surface was thermodynamically favorable. Moreover, in comparison with "Mo_2" model, "Mo_1+Mo_2" model was more thermodynamically stable due to more negative adsorption energy. The finding confirmed AFM and Tafel curve results that PCP selectively adsorbed on molybdenite edges.

Table 5. 3 Adsorption energies on molybdenite surfaces

Surface	Adsorption site	Adsorption energy（kJ/mol）
(0 0 1)	S	33.5
(1 0 0)	Mo_1+Mo_2	–735.14
	Mo_2	–728.61

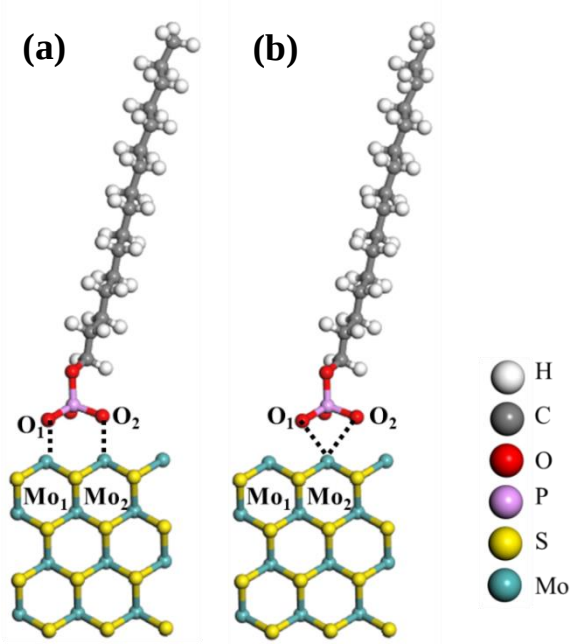

Fig. 5.12 Suggested adsorption model on MS100: (a) Mo1+Mo2; (b) Mo2.

5.3.8.2 Electron density

Fig. 5.13 presents the electron density of PCP on MS001 and MS100. Obviously, no overlap of the electron distribution appeared between PCP and MS001. However, the electron distribution of O atoms within PCP evidently overlapped with the Mo atoms on MS100, reconfirming the strong interaction between Mo atoms and O atoms in phosphate groups, which was in line with the adsorption energy results. Since the adsorption of PCP on MS100 was more favorable, only this case will be discussed in the following analysis.

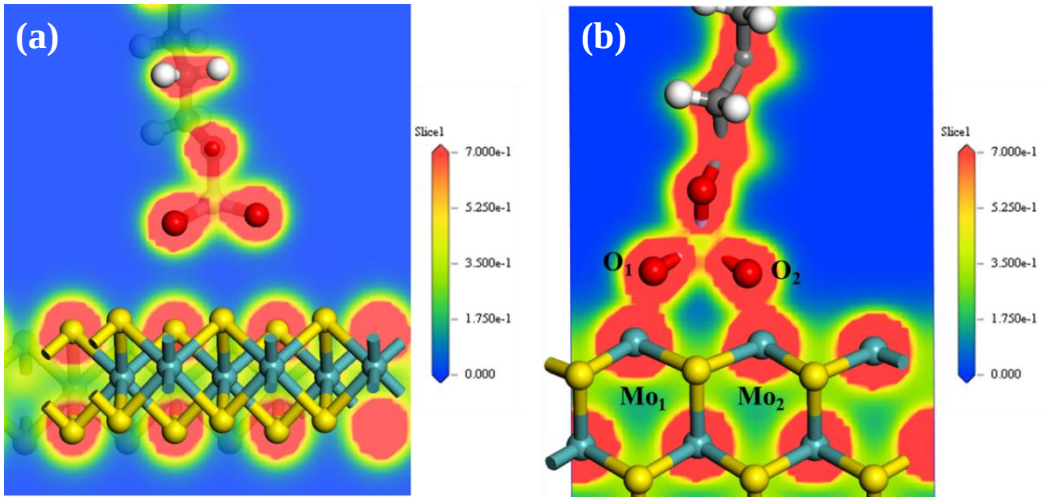

Fig. 5.13 Electron density of PCP on: (a) MS001; (b) MS100.

5.3.8.3 Electron density difference

Fig. 5.14 displays the electron density difference of PCP on MS100. The blue color means the reduction of electrons, whereas the red color means an increase of electrons. Note that the areas near the Mo atoms were blue, indicating the decrease in electron density. While the areas near the O atoms were red, demonstrating an accumulation in electron density. The blue and red regions are connected between Mo atoms and O atoms, suggesting that the electrons might transfer from Mo atoms to O atoms during the adsorption.

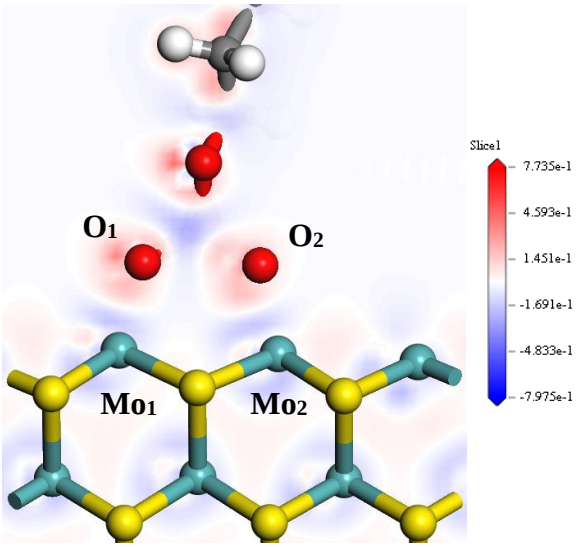

Fig. 5.14 The electron density difference of PCP on MS100.

3.8.4 Mulliken population of bond and atom

Table 5.4 shows the Mulliken bond population of the two O–Mo bonds. When PCP interacted with MS100, the length of the two O–Mo bonds was 1.99 Å and 1.974 Å, both of which were smaller than the sum of radium of O and Mo atoms (2.06 Å), indicating strong bonds were formed between O atoms of PCP and Mo atoms. In addition, the bond populations of the two O–Mo bonds were 0.43 and 0.46, elucidating that O atoms within PCP and Mo atoms formed two high ionicity bonds.

Table 5.4 Mulliken bond population of O-Mo

Bond	Population	Bond length (Å)
O_1–Mo_1	0.43	1.99
O_2–Mo_2	0.46	1.974

Table 5.5 presents the Mulliken charges of O and Mo atoms before and after PCP adsorption on MS100. The data showed that the O atoms were the electron receiver, with O_1 2p and O_2 2p orbitals mainly receiving electrons, 0.06 and 0.08 e, respectively. Meanwhile, Mo atoms were the electron donor, with Mo_1 4d orbital and Mo_2 4d orbital losing electrons, 0.31 and 0.32 e, respectively. These results proved that phosphate groups within PCP strongly interacted with Mo atoms on molybdenite.

Table 5.5 Mulliken atomic population of O and Mo atoms

Atom	Adsorption state	s	p	d	f	Total	Charge (e)
O_1	Before	1.93	4.85	0	0	6.81	0.06
	After	1.86	5.01	0	0	6.87	
O_2	Before	1.93	4.85	0	0	6.78	0.08
	After	1.87	5	0	0	6.86	
Mo_1	Before	2.48	6.25	5.16	0	13.9	–0.31
	After	2.46	6.31	4.82	0	13.59	
Mo_2	Before	2.48	6.25	5.16	0	13.9	–0.32
	After	2.47	6.3	4.82	0	13.58	

5.3.8.5 Partial density of states

Fig. 5.15 displays the partial density states (PDOS) of O_1 and Mo_1 atoms before and after adsorption. After adsorption, the Mo_1 4d orbital shifted to higher energy and the peak near the Fermi level enhanced significantly, implying Mo_1 4d orbital lost electrons and took part in the bonding reaction (Fig. 5.15 (a)). As presented in Fig. 5.15 (b), the O_1 2p orbital moved to lower energy and the peak around the Fermi level declined apparently, demonstrating the O_1 2p orbital was involved in the bonding reaction and received electrons. In addition, the Mo_1 4d and O_1 2p orbitals overlapped in the range of −5.1 to −3.7, −2.8 to −2.1 and 0.8 to 1.4 eV, indicating the O_1 2p orbital hybridized with Mo_1 4d orbital and the strong reaction occurred between the two atoms.

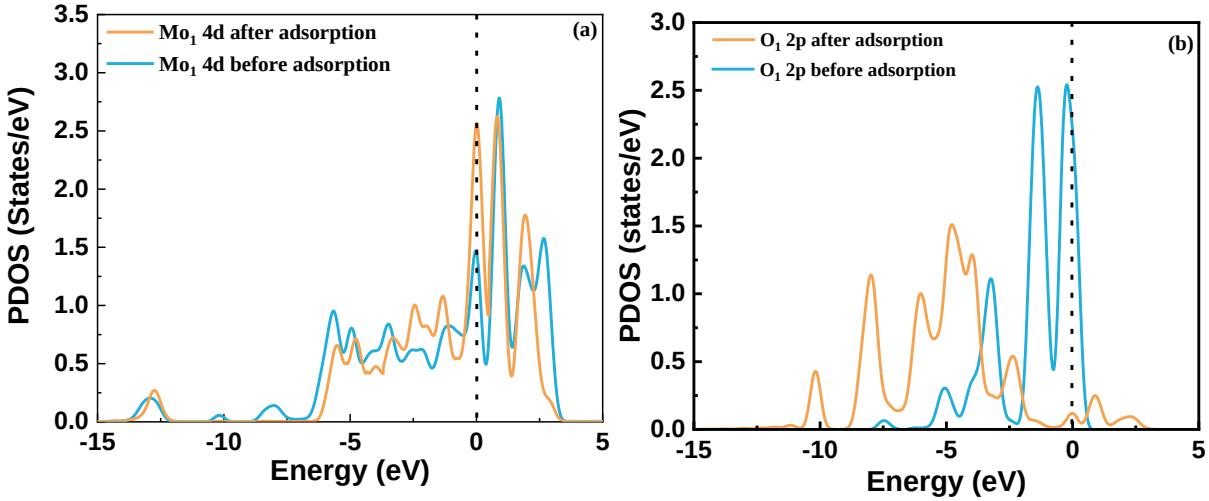

Fig. 5.15 PDOS of: (a) Mo1 4d; (b) O1 2p before and after adsorption.

5.3.9 Adsorption model

In brief, an adsorption model is proposed according to the zeta potential, FTIR spectroscopy, XPS, AFM, Tafel curves, cyclic voltammetry, contact angle and DFT calculations. Due to the particular preference toward the edges, PCP chemisorbed on molybdenite edges through the hybridization of the O 2p orbital with the Mo 4d orbital, formation of six-membered chelating rings, as illustrated in Fig. 5.12 (a), exposing the hydrocarbon chain toward the bulk solution, thus making the molybdenite edge hydrophobic.

5.4 Conclusion

(1) PCP could effectively promote the flotation of molybdenite fines over a wide pH range due to the targeted regulation of edge hydrophobicity.

(2) PCP was more favorably adsorbed at edges through the strong complexation between the phosphate group and the Mo sites.

(3) PCP was chemisorbed on the edges via the hybridization of the O 2p orbital and the Mo 4d orbital to form two high ionicity bonds.

(4) PCP was a promising collector of molybdenite fines because of its high efficiency and environmental sustainability.

Reference

[1] V.P. Kumar, D.K. Panda, Next generation 2D material molybdenum disulfide (MoS_2): properties, applications and challenges, ECS J. Solid State Sci. Technol. 11 (2022) 33012.

[2] H.K. Feng, Z.Y. Cai, Y.G. Li, Y.F. Qi, Domestic and overseas research status on molybdenum resources and its use, in: Adv. Mater. Res., Trans Tech Publ, 2014: pp. 401–406.

[3] Q. Lin, G.U. Guo-Hua, H. Wang, C.Q. Wang, Y.C. Liu, F.U. Jian-Gang, R.F. Zhu, An effective approach for improving flotation recovery of molybdenite fines from a finely-disseminated molybdenum ore, J. Cent. South Univ. 25 (2018) 1326–1339.

[4] S. Castro, A. Lopez-valdivieso, J.S. Laskowski, Review of the flotation of molybdenite . Part I : Surface properties and fl oatability, Int. J. Miner. Process. 148 (2016) 48–58.

[5] S. Song, X. Zhang, B. Yang, A. Lopez-Mendoza, Flotation of molybdenite fines as hydrophobic agglomerates, Sep. Purif. Technol. 98 (2012) 451–455.

[6] Q. Lin, G. hua Gu, H. Wang, Y. cai Liu, J. gang Fu, C. qing Wang, Flotation mechanisms of molybdenite fines by neutral oils, Int. J. Miner. Metall. Mater. 25 (2018) 1–10.

[7] B. Yang, S. Song, A. Lopez-Valdivieso, Kinetics of hydrophobic agglomeration of molybdenite fines in aqueous suspensions, Physicochem. Probl. Miner. Process. 51 (2015) 181–189.

[8] T. Miettinen, J. Ralston, D. Fornasiero, The limits of fine particle flotation, Miner. Eng. 23 (2010) 420–437.

[9] M.C. Fuerstenau, B.J. Sabacky, On the natural floatability of sulfides, Int. J. Miner. Process. 8 (1981) 79–84.

[10] Z. Lu, J. Ralston, Q. Liu, Face or Edge? Control of molybdenite surface interactions with divalent cations, J. Phys. Chem. C. 124 (2020) 372–381.

[11] B. Yang, D. Wang, T. Wang, H. Zhang, F. Jia, S. Song, Effect of Cu^{2+} and Fe^{3+} on the depression of molybdenite in flotation, Miner. Eng. 130 (2019) 101–109.

[12] Y. Chen, X. Chen, Y. Peng, The depression of molybdenite flotation by sodium metabisulphite in fresh water and seawater, Miner. Eng. 168 (2021) 106939.

[13] L. Xie, J. Wang, J. Huang, X. Cui, X. Wang, Q. Liu, H. Zhang, Q. Liu, H. Zeng, Anisotropic polymer adsorption on molybdenite basal and edge surfaces and interaction mechanism with air bubbles, Front. Chem. 6 (2018) 1–11.

[14] S. Li, X. Ma, J. Wang, Y. Xing, X. Gui, Y. Cao, Effect of polyethylene oxide on flotation of molybdenite fines, Miner. Eng. 146 (2020) 106146.

[15] F. Li, H. Zhong, G. Zhao, S. Wang, G. Liu, Flotation performances and adsorption mechanism of α-hydroxyoctyl phosphinic acid to cassiterite, Appl. Surf. Sci. 353 (2015) 856–864.

[16] Y. Tang, W. Yin, S. Kelebek, Magnesite-dolomite separation using potassium cetyl phosphate as a novel flotation collector and related surface chemistry, Appl. Surf. Sci. 508 (2020) 145191.

[17] G. Zhou, J. Luo, Mechanism of flotation using citric acid for separating monazite from bastnaesite, Nonferrous Met. 41 (1989) 33–40.

[18] J. Wang, L. Xie, Q. Lu, X. Wang, J. Wang, H. Zeng, Electrochemical investigation of the interactions of organic and inorganic depressants on basal and edge planes of molybdenite, J. Colloid Interface Sci. 570 (2020) 350–361.

[19] Z. Lu, Q. Liu, Z. Xu, H. Zeng, Probing Anisotropic Surface Properties of Molybdenite by Direct Force Measurements, Langmuir. 31 (2015) 11409–11418.

[20] Z. Wei, Y. Li, L. Huang, New insight into the anisotropic property and wettability of molybdenite: A DFT study, Miner. Eng. 170 (2021) 107058.

[21] P.F.A. Braga, A.P. Chaves, A.B. Luz, S.C.A. Fran ça, The use of dextrin in purification by flotation of molybdenite concentrates, Int. J. Miner. Process. 127 (2014) 23–27.

[22] Y. Tang, J. Yao, W. Yin, S. Kelebek, Molecular dynamics simulation of cetyl phosphate adsorption in flotation of magnesite and pertinent chemical aspects, Minerals. 10 (2020) 1–11.

[23] Y. Tang, W. Yin, S. Kelebek, Molecular dynamics simulation of magnesite and dolomite in relation to flotation with cetyl phosphate, Colloids Surfaces A Physicochem. Eng. Asp. 610 (2021) 125928.

[24] K. Rokosz, T. Hryniewicz, S. Raaen, D. Matysek, L. Dudek, K. Pietrzak, SEM, EDS, and XPS characterization of coatings obtained on titanium during AC plasma electrolytic process enriched in magnesium, Adv. Mater. Sci. 18 (2018) 68–78.

[25] B. Hou, L. Ma, X. Zang, N. Shang, J. Song, X. Zhao, C. Wang, J. Qi, J. Wang, R. Yu, Design and construction of 3D porous $Na_3V_2(PO_4)_3$/C as high performance cathode for sodium ion batteries, Chem. Res. Chinese Univ. 37 (2021) 265–273.

[26] K. Rokosz, T. Hryniewicz, S. Gaiaschi, P. Chapon, S. Raaen, D. Matýsek, Ł. Dudek, K. Pietrzak, Novel porous phosphorus–calcium–magnesium coatings on titanium with copper or zinc obtained by DC plasma electrolytic oxidation: fabrication and characterization, Materials. 11 (2018) 1680.

[27] X. Guo, Z. Feng, B. Hurley, R. Buchheit, Entrapped molybdate in phytate film and the corresponding anodic corrosion inhibition on AA2024-T3, J. Electrochem. Soc. 163 (2016) 260–268.

[28] M. Nocuń, Structural studies of phosphate glasses with high ionic conductivity, J. Non. Cryst. Solids. 333 (2004) 90–94.

[29] G.D. Khattak, M.A. Salim, A.S. Al-Harthi, D.J. Thompson, L.E. Wenger, Structure of molybdenum-phosphate glasses by X-ray photoelectron spectroscopy (XPS), J. Non. Cryst. Solids. 212 (1997) 180–191.

[30] Y. Chen, X. Chen, Y. Peng, The effect of sodium hydrosulfide on molybdenite flotation in seawater and diluted seawater, Miner. Eng. 158 (2020).

[31] C. Zhong, H. Wang, L. Zhang, M. Guo, B. Feng, Flotation separation of molybdenite and talc by xanthan gum, Powder Technol. 388 (2021) 158–165.

[32] B. Yang, H. Yan, M. Zeng, H. Zhu, Tiopronin as a novel copper depressant for the selective flotation separation of chalcopyrite and molybdenite, Sep. Purif. Technol. 266 (2021) 118576.

[33] P. Chen, Y. Gou, J. Ni, Y. Liang, B. Yang, F. Jia, S. Song, Efficient ofloxacin degradation with Co (II)-doped MoS_2 nano-flowers as PMS activator under visible-light irradiation, Chem. Eng. J. 401 (2020) 125978.

[34] C. Wang, R. Liu, M. Wu, Z. Xu, M. Tian, Z. Yin, W. Sun, C. Zhang, Flotation separation of molybdenite from chalcopyrite using rhodanine-3-acetic acid as a novel and effective depressant, Miner. Eng. 162 (2021) 106747.

[35] B. Yang, H. Yan, M. Zeng, P. Huang, F. Jia, A. Teng, A novel copper depressant for selective fl otation of chalcopyrite and molybdenite, Miner. Eng. 151 (2020) 106309.

[36] Y. Mu, Y. Peng, R.A. Lauten, The galvanic interaction between chalcopyrite and pyrite in the presence of lignosulfonate-based biopolymers and its effects on flotation performance, Miner. Eng. 122 (2018) 91–98.

[37] X. Qiu, H. Yang, G. Chen, W. Luo, An alternative depressant of chalcopyrite in Cu-Mo differential flotation and its interaction mechanism, Minerals. 9 (2019) 1–11.

[38] S.M. Tan, A. Ambrosi, M. Pumera, Pristine basal-and edge-plane-oriented molybdenite MoS_2 exhibiting highly anisotropic properties, Chem. a Eur. J. (2015) 7170–7178.

The main content in this chapter was published in *Journal of Molecular Liquid*

Chapter VI. Improving the flotation of molybdenite fines based on the targeted regulation of edges using a novel chelating collector

6.1 Introduction

Molybdenite (MoS_2), as an important sulfide mineral, has been extensively used in metallurgy, lubrication, catalysis and batteries owing to its superior thermal stability, lubricity and electronic properties [1]. As high-grade molybdenite deposits diminish, the exploitation of fine-disseminated and low-grade ores is vital to meet huge market demands. Nevertheless, these ores need fine grinding to liberate molybdenite from gangues before flotation can take place. As a typical layer-structured mineral with distinct anisotropic properties, molybdenite manifests two kinds of surfaces: hydrophilic edges and hydrophobic faces [2]. Edges are formed by the break of covalent S–Mo bonds while faces are derived from the rupture of van der Waals force between layers [3]. As molybdenite particle size reduces, the edge/face ratio increases, thus molybdenite hydrophobicity declines, causing a sharp decrease in floatability [4]. Commonly, molybdenite particles coarser than 20 μm are regarded as hydrophobic and exhibit satisfactory floatability, whereas molybdenite fines (less than 20 μm) show poor floatability due to the dominance of hydrophilic edges [5]. Consequently, improving the hydrophobicity of edges is vital for enhancing the recovery of molybdenite fines.

In practice, hydrocarbon oils such as kerosene are utilized as the conventional collector in molybdenite flotation. They favorably adsorb on molybdenite faces via van der Waals force and hydrophobic interaction [6], thereby improving face hydrophobicity and enhancing flotation efficiency. Nevertheless, they cannot effectively collect molybdenite fines owing to their poor affinity for molybdenite edges. To solve the problem in the flotation of molybdenite fines, oil agglomeration, hydrophobic (or shear) flocculation, carrier flotation and column flotation have been explored [6]. For instance, Fu et al. achieved 95% recovery of ultrafine molybdenite using oil agglomerate flotation [7]. Song et al. reported that the floatability of molybdenite fines reached 90% after the formation of hydrophobic agglomerates [8]. Wan et al. found that fine particles adhered to coarse particle carriers, thereby enhancing the flotation efficiency of molybdenite fines to nearly 90% [9]. Kim et al. pointed out that the recovery and grade of molybdenite obtained by column flotation exceeded 95% [10]. Though these approaches can improve the flotation efficiency of molybdenite fines to certain extent, none of them have been applied in large-scale practice due to strict limitations and high operations costs. In addition, conventional techniques emphasize on the regulation of molybdenite faces or the fluid properties, but little consideration has been taken into adjusting the hydrophobicity of edges [4]. Notably,

improving the hydrophobicity of edges is a more promising and effective strategy to promote the flotation of molybdenite fines.

2-Mercaptobenzothiazole (MBT) is a heterocyclic thioamide containing both nitrogen and sulfur as electron donor atoms (as shown in Fig. 6.1), which is employed as a new collector in the flotation of copper minerals, tarnished or oxidized lead minerals [11]. Meanwhile, MBT can form hydrophobic complexes with some metals such as copper, iron, nickel and cobalt, and thus is widely applied as a corrosion inhibitor [12]. Previous studies reported that the exocyclic S or N atoms within MBT chemisorbed on iron atoms of pyrite surfaces, thus achieving a satisfactory recovery of pyrite [13, 14]. However, the effect of MBT on molybdenite flotation is barely discussed. Due to its strong complexing ability with metal ions, MBT may be an effective collector for molybdenite fines. In this work, MBT was first introduced as a possible molybdenite collector. The flotation performance and interaction mechanism were probed via flotation tests, contact angle, SEM-EDS, adsorption capacity, Zeta potential, XPS and DFT calculation, with the purpose to exploit an effective collector to recover molybdenite fines efficiently.

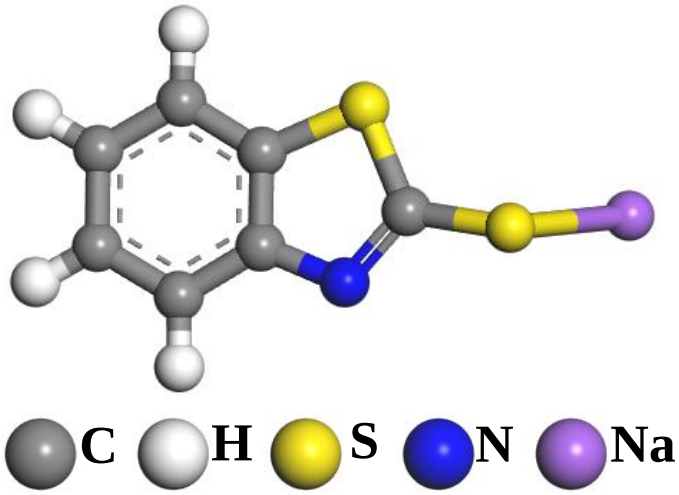

Fig. 6.1 The molecular structure of MBT.

6. 2Materials and methods

6.2.1 Materials

Bulk molybdenite minerals were collected from Liuzhou City, China. These minerals were hand-selected, ground and screened to prepare –20 μm particles for flotation tests and other measurements. XRD pattern indicated no purity peak was detected (Fig. 6.2). The chemical assay revealed the purity of the molybdenite samples was 97%.

Methyl isobutyl carbinol (MIBC), NaOH and HCl with analytical grade were purchased from Macklin, China, which were employed as frother and pH modifiers. Kerosene and MBT obtained from Aladdin were used as molybdenite collectors in flotation. Ultra-pure water was used in all tests.

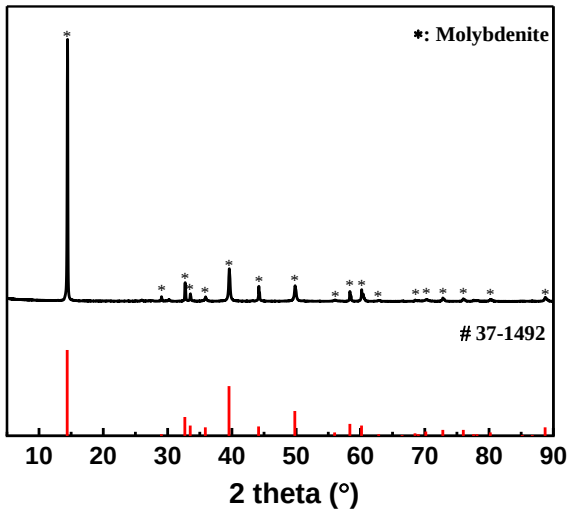

Fig. 6.2 XRD pattern of molybdenite minerals

6.2.2 Micro-flotation test

The micro-flotation was performed in a flotation cell with an effective volume of 70 mL in an open-air condition. 2 g minerals were mixed with deionized water and dispersed by ultrasonic treatment for two minutes. After the regulation of pH, MBT (or kerosene) and MIBC were introduced into the pulp in order at the interval of five minutes and one minute. After flotation, concentrates and tailings were collected and dried to count floatability.

6.2.3 Adsorption measurement

A Cary 60 spectrophotometer (Agilent, USA) was employed to measure the absorbance of MBT solution at a wavelength of 301 nm. Before the measurement, a standard curve between absorbance and MBT concentration was established first (Fig. 6.3). After that, molybdenite particles (2 g) were introduced into different concentrations of MBT solutions and stirred for five minutes. Afterward, the suspension was filtered and the absorbance of the filtrate was determined. The adsorption amount was calculated as a previous study reported [4].

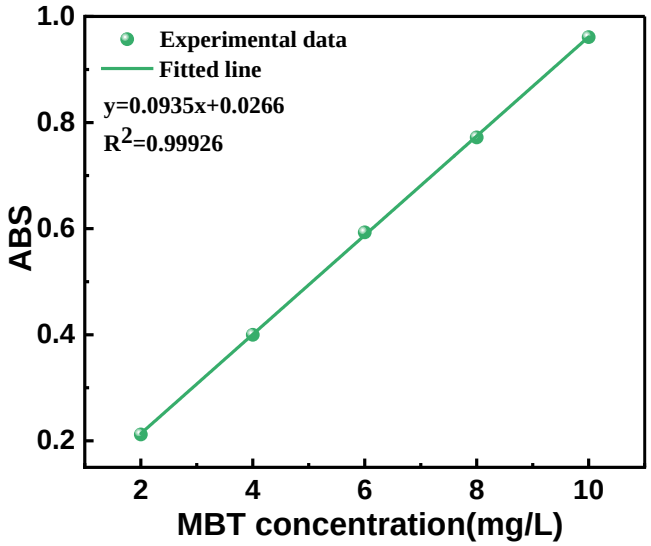

Fig. 6.3 The correlation between MBT concentration and absorbance.

6.2.4 Characterizations

Contact angle measurements were performed with both faces and edges samples by a contact angle goniometer (JC2000C1, Powereach, China). Molybdenite samples with good crystallinity were selected to prepare faces and edges samples. Faces samples were obtained by mechanical exfoliation using Scotch tape. Edges samples were prepared as described in the previous study [15]. A Zeta Potential Finder Analyzer was applied to determine Zeta potential. Molybdenite powders (0.1 g) were introduced into an MBT solution (10^{-3} M NaCl) and stirred for 5 min. Afterward, 1 mL of the suspension was extracted for measurement. SEM (JEM-2100F, Japan) was employed to investigate the morphology characteristic. The element distribution was detected with an Energy Dispersive Spectrometer (EDAX Elite, USA). XPS spectra were collected by an ESCALAB 250Xi spectrometer (Thermo, USA). Molybdenite samples were treated in MBT solutions (100 mg/L, pH = 4) for 5 min, and then minerals were filtered and dried for measurement. The standard C 1s binding energy was calibrated to 284.80 eV, and Advantage software was used to fit the spectra.

6.2.5 Computational method

The adsorption of MBT on molybdenite surfaces was calculated using CASTEP program within Materials Studio 2019 based on the density functional theory (DFT). All configurations were stimulated under the exchange correlation function of GGA-PBE. Ultrasoft pseudopotentials were performed to describe the valence configuration of Mo 4 $s^2 4p^6 4d^5 5s^1$, S $3s^2 3p^4$, N $2s^2 2p^3$. The (1 0 0) and (0 0 1) surfaces of molybdenite were cleaved and called edges and faces. Edges and faces before and after MBT adsorption were optimized

using a 15 Å vacuum slab and a cutoff energy of 430 eV. The convergence tolerances of 2 × 10^{-5} eV/atom, 0.002 Å, 0.1 GPa and 0.05 eV/Å for energy, displacement, stress and force were performed to ensure converged calculation [16].

6.3 Results and discussion

6.3.1 Flotation behavior

The effect of pH on the floatability of molybdenite fines is illustrated in Fig. 6.4 (a). Without a collector, the floatability of molybdenite fines declined slowly with an increase in pH. In the presence of collectors, the floatability improved greatly at pH 2−10. Compared with kerosene, a low dosage of MBT achieved much higher floatability, suggesting that MBT was more efficient than kerosene in collecting molybdenite fines.

Fig. 6.4 (b) depicts the floatability of molybdenite fines as a function of collector dosage. At pH 4, the floatability improved sharply as MBT or kerosene dosage increased. At an MBT dosage of 100 mg/L, the floatability increased to 95.53%, which was much higher than that (68.47%) achieved at a kerosene dosage of 400 mg/L. These results indicated that MBT was more effective than kerosene in the recovery of molybdenite fines. In addition, it was evident that less MBT was needed to achieve equivalent results under acidic conditions than alkaline conditions, which may be attributed to the presence of more amine ions in acidic solutions [17], indicating that MBT had a stronger collecting ability to molybdenite fines under acidic conditions.

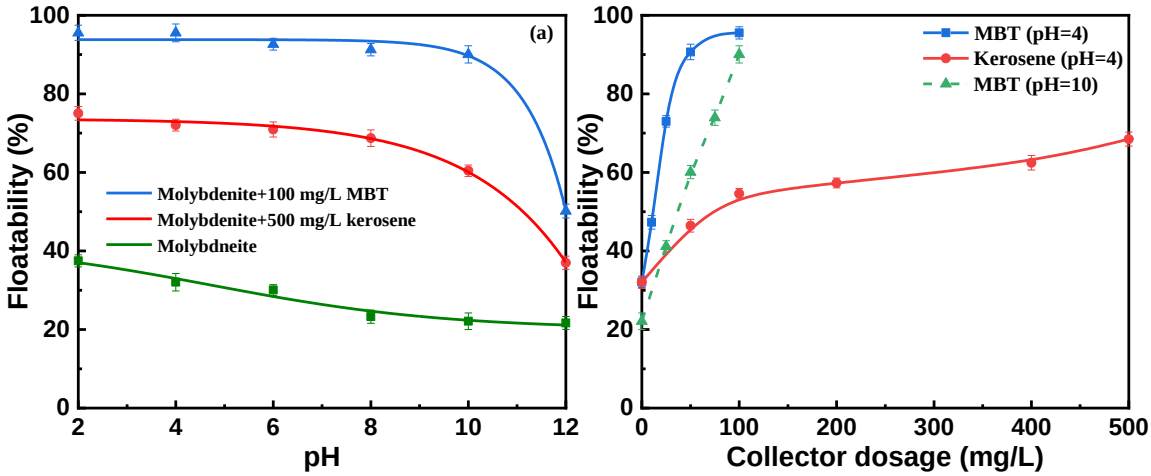

Fig. 6.4 Effects of pH (a) and collector dosages (b) on molybdenite flotation.

6.3.2 Contact angle

Fig. 6.5 displays contact angles of faces and edges before and after MBT treatment at pH 4 and 10. At pH 4, the contact angle of fresh faces and edges was 77.5 °and 43.5 °, which

was slightly higher than that at pH 10. After MBT treatment, the contact angle of faces increased slowly and that of edges surged significantly, indicating that MBT could improve the hydrophobicity of both faces and edges. Moreover, the contact angle of faces and edges at pH 4 was greater than that at pH 10, which was consistent with flotation results.

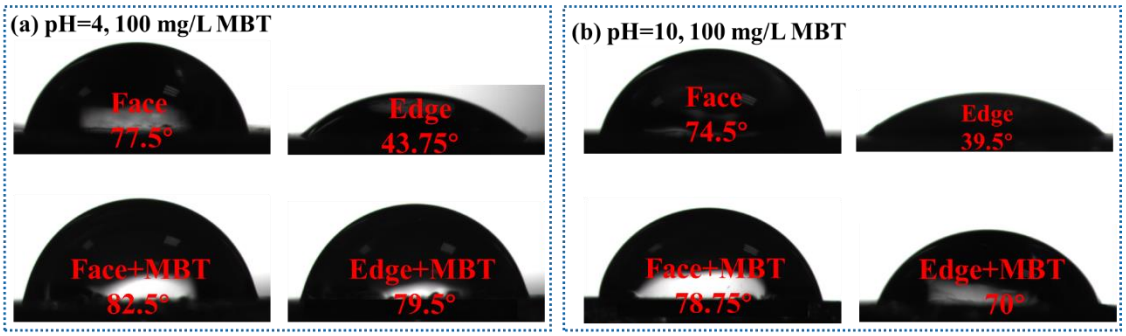

Fig. 6.5 Contact angles of faces and edges with and without MBT at pH of 4 (a) and 10 (b).

6.3.3 Adsorption capacity results

Fig. 6.6 depicts the adsorption amount of MBT on molybdenite surfaces at pH 4 and 10. It was clear that the adsorption amount increased with increasing MBT concentration. Meanwhile, the adsorption amount of MBT on molybdenite surface at pH 4 was consistently higher than that at pH 10, which explained why MBT achieved a higher floatability under acid conditions than alkaline environments. These results were in accordance with the contact angle results.

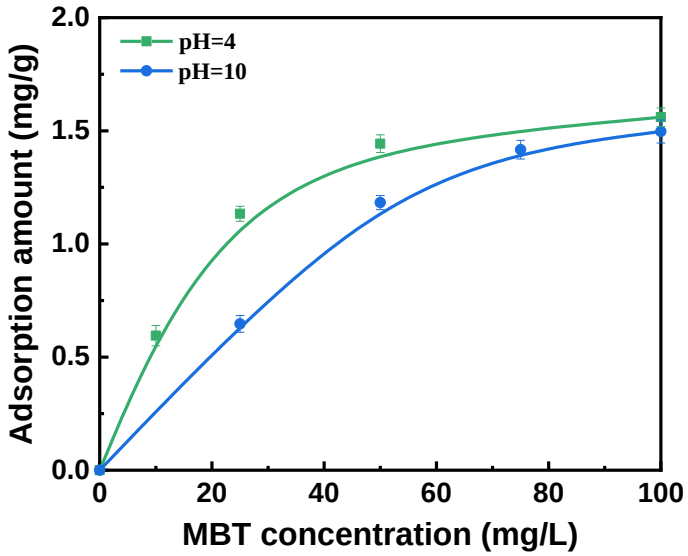

Fig. 6.6 Adsorption amount of MBT on molybdenite surface.

6.3.4 Zeta potential

The zeta potential of molybdenite in the absence and presence of MBT is illustrated in Fig. 6.7. In Fig. 6.7 (a), the zeta potential was negative in the entire pH range for pure molybdenite, which was attributed to the presence of molybdate ions [18]. For molybdenite treated with MBT, zeta potential shifted to the positive direction in acidic conditions while moving to the more negative direction in alkaline environments. The significant change suggested that MBT species were adsorbed on molybdenite surface. In Fig 6.7 (b), it was clear that the zeta potential of molybdenite shifted upwards at pH 4 while became more negative at pH 10 as MBT dosage increased, which depended on the extent to which the amino group combined to protons or the extent to which the –SH lost the protons. It is known that –SH loses a proton and becomes negatively charged at pH > 1.6 [19]. Moreover, the N atom is likely to be protonated even at pH as high as 12 [20]. Therefore, the positive movement of zeta potential might be ascribed to more protonation of amino groups than deprotonation of –SH in acid conditions. Conversely, the negative shift might result from less amino group protonation than –SH deprotonation under alkaline conditions.

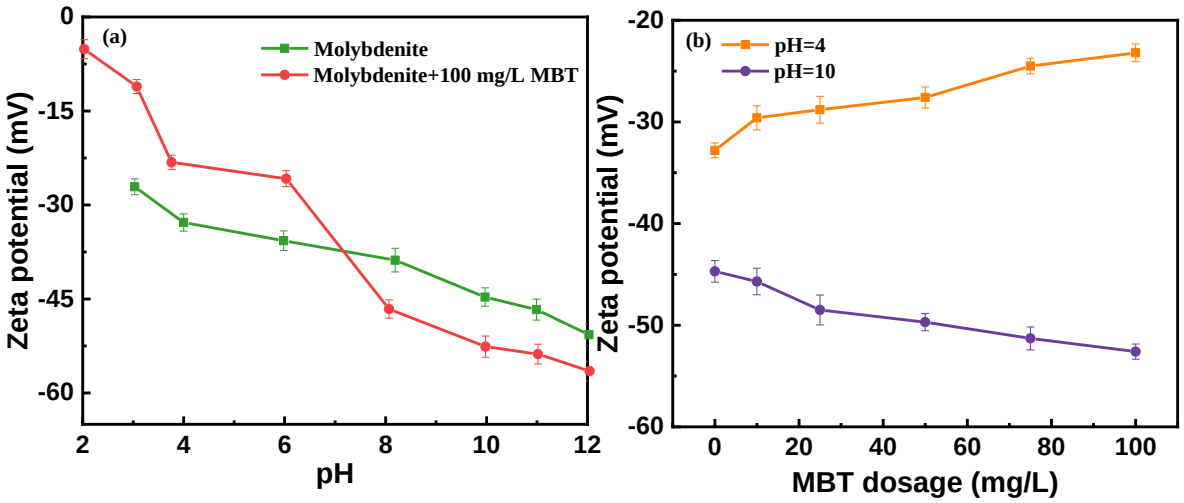

Fig. 6.7 Zeta potential of molybdenite fines before and after MBT addition (a), at pH 4 and 10 (b).

6.3.5 SEM-EDS result

The SEM-EDS images of molybdenite faces and edges treated with MBT are shown in Fig. 6.8. Compared with faces, the N element detected was much denser and more uniformly on edges possibly due to its stronger affinity for edges. These results also explained the difference in contact angle between faces and edges.

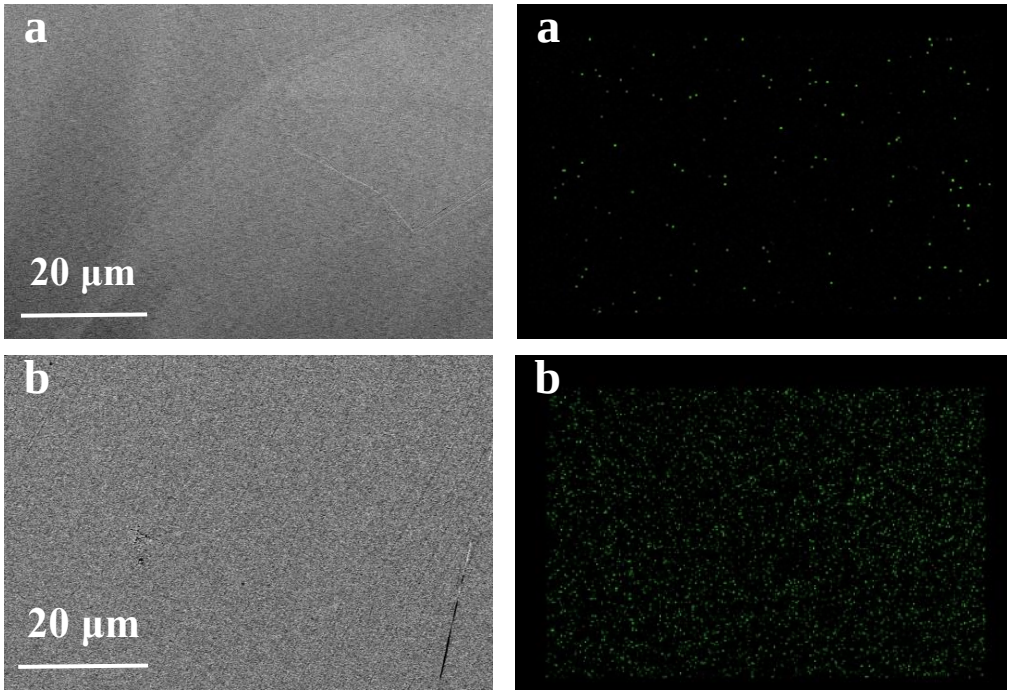

Fig. 6.8 SEM-EDS images of molybdenite faces (a) and edges (b) after MBT addition (1 meant the photograph, 2 denoted the N element mapping).

6.3.6 XPS result

Fig. 6.9 shows the XPS spectra of Mo 3d, S 2p and N 1s of molybdenite in the presence and absence of MBT. In Fig. 6.9 (a), for pure molybdenite, the peaks at 226.61, 229.36, 232.49, 230.17, 233.47, 232.20 and 235.50 eV denoted S 2s [21], Mo (IV) $3d_{5/2}$of MoS_2, Mo (IV) $3d_{3/2}$of MoS_2, [22] Mo (IV) $3d_{5/2}$of MoO_2, Mo (IV) $3d_{3/2}$of MoO_2 [23], Mo (VI) $3d_{5/2}$of MoO_3, Mo (VI) $3d_{3/2}$of MoO_3 [10], respectively. After treatment with MBT, the shifting of MoS_2 peaks was 0.24 eV, indicating that MBT possibly adsorbed on Mo sites of molybdenite surface. Fig. 6.9 (b) illustrates the S 2p spectra. The peaks of MBT located at 162, 163.2, 163.94 and 164.98 eV, which were assigned to S $2p_{3/2}$ and S $2p_{1/2}$ of exocyclic S atom, S $2p_{3/2}$ and S $2p_{1/2}$ of endocyclic S atom [24], respectively. For bare molybdenite, the peaks centered at 162.35 and 163.51 eV, which were assigned to S $2p_{3/2}$ and S $2p_{1/2}$ of MoS_2 [25]. For molybdenite treated with MBT, new peaks were detected at 162.22 and 163.42 eV, which were derived from the exocyclic S atom within MBT. Furthermore, the movement of the exocyclic S atom peaks on molybdenite was 0.22 eV, indicating that MBT possibly chemically adsorbed on molybdenite. Fig. 6.9 (c) depicts the N 1s spectra. For MBT, the peak at 398.42 eV represented C–N [26]. After the treatment of MBT, three peaks at 395.24, 397.17 and 398.70 eV were observed, which represented Mo 3p of MoS_2 [27], Mo–N [28]

and C–N, respectively. Notably, the appearance of the Mo–N group indicated that the N atom within MBT interacted with the Mo atom on molybdenite surface.

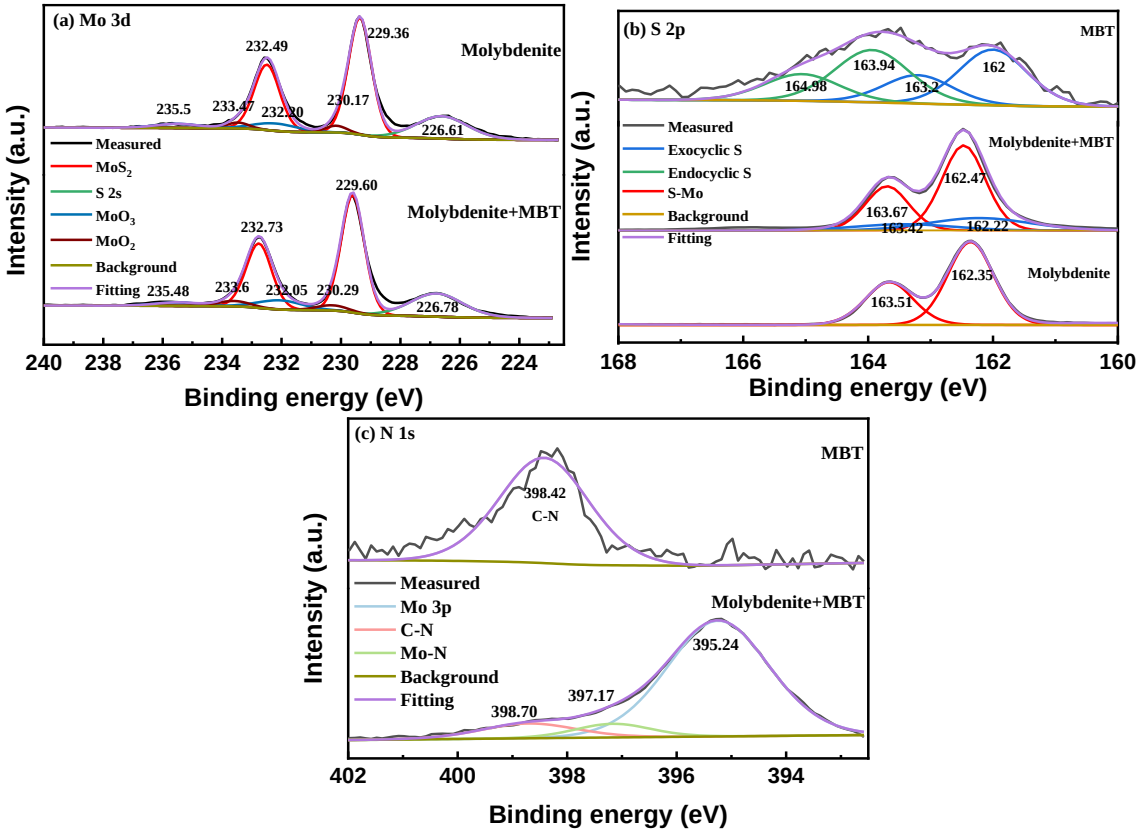

Fig. 6.9 XPS spectra of Mo 3d (a), S 2p (b), N 1s (c) and O 1s (d) for treated and untreated molybdenite.

6.3.7DFT calculations

6.3.7.1 Adsorption energy

The different adsorption models of molybdenite faces and edges before and after MBT adsorption are shown in Fig. 6.10. The adsorption energies of MBT on faces and edges are displayed in Table 6.1. It was clear that the “b” model was more stable when MBT adsorbed on faces. For all adsorption models, the adsorption energy of MBT on edges was higher than on faces, indicating that MBT was more readily adsorbed on edges, which was in agreement with SEM-EDS results. Compared with other models, the “f” model was more energetically stable with the lowest adsorption energy of –268.87 kJ/mol, which indicated MBT was most likely to interact with edges in this configuration. Therefore, the “b” and “f” model were discussed carefully in the following sections.

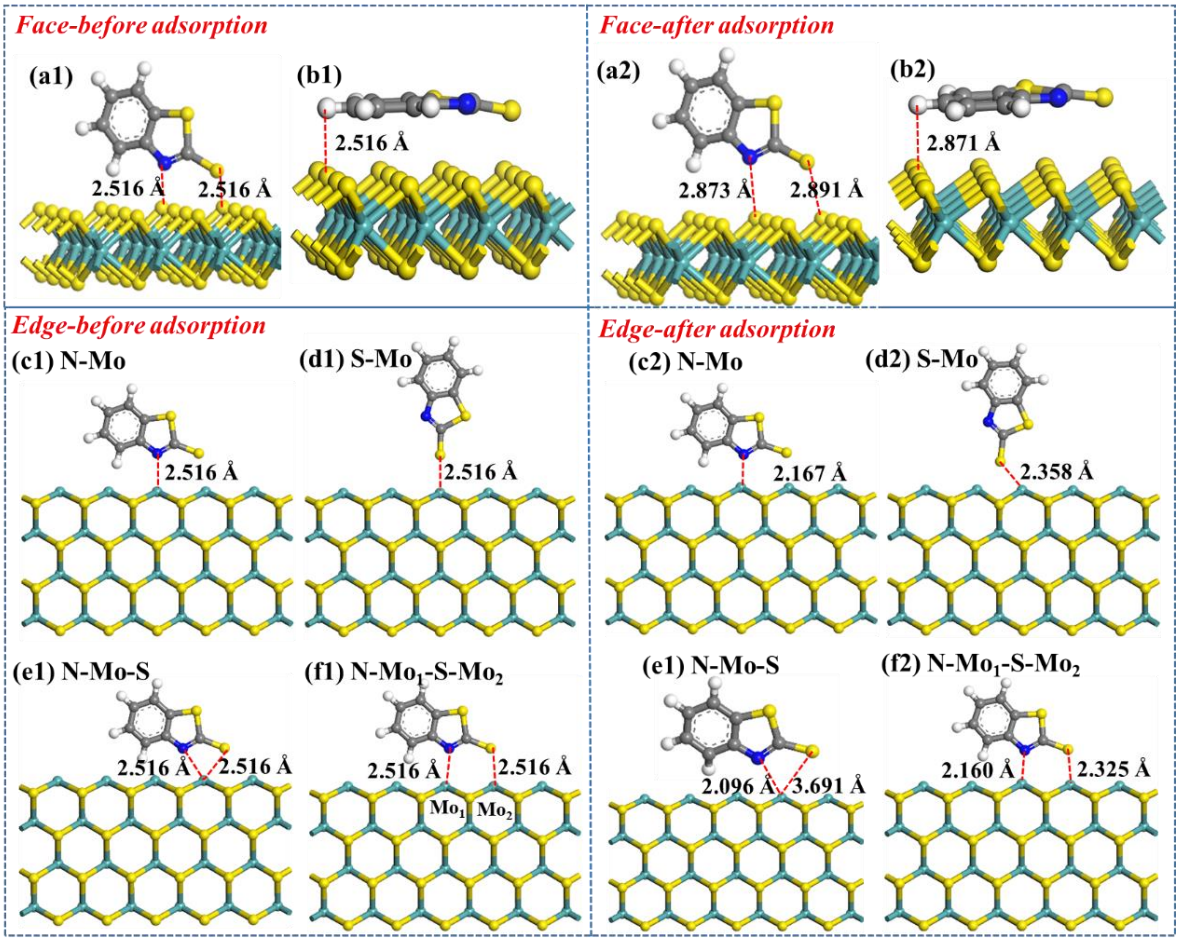

Fig. 6.10 The adsorption configurations of MBT on faces(a-b) and edges (c-f) before (1) and after (2) adsorption.

Table 6.1 Adsorption energies of MBT on faces and edges

Surface	Adsorption configuration	E_{ads} (kJ/mol)
Faces	a	–32.85
	b	–40.09
Edges	c	–222.34
	d	–243.96
	e	–232.92
	f	–268.87

6.3.7.2 Electron density and electron density difference

The electron density of MBT on edges and faces is shown in Fig. 6.11. It was clear that an apparent overlap of electron distributions was detected between N and S atoms in MBT

and two Mo atoms on edges, demonstrating that N and S atoms interacted with Mo atoms. Whereas, MBT did not overlap with faces, suggesting that the interaction of MBT on faces was very weak. These results elucidated that the interaction between MBT and edges was much stronger than faces.

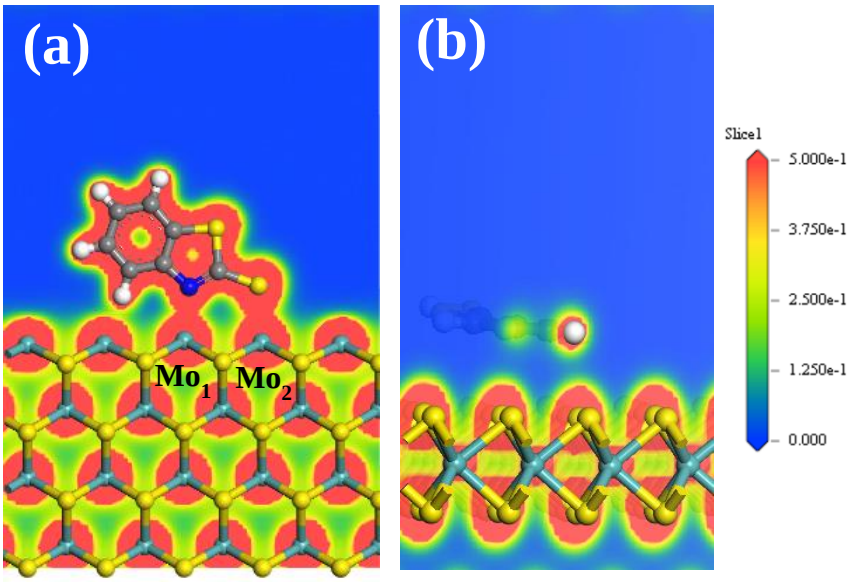

Fig. 6.11 Electron density of MBT on edges (a) and faces (b).

The electron density difference of MBT on edges and faces is presented in Fig. 6.12. In Fig. 6.12 (a), the regions near two Mo atoms were blue, while the areas around N and S atoms of MBT were red, suggesting a decline in electron density of Mo atoms on edges and an increase in electron density of MBT [29]. The connection of the red and blue regions between N, S and Mo atoms indicated that new chemical bonds were generated during the interaction. Conversely, no apparent connection of the blue and red regions was observed between MBT and the faces. Combined with the result of electron density, it was reasonable to deduce that no chemical bond was formed between MBT and molybdenite faces. Therefore, MBT might be physically adsorbed on molybdenite faces.

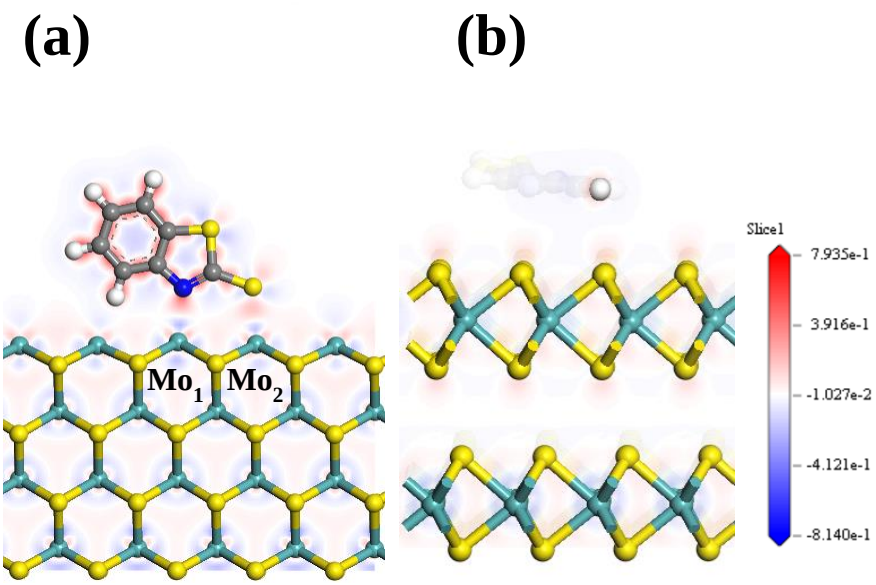

Fig. 6.12 Electron density difference of MBT on edges (a) and faces (b).

6.3.7.3 Mulliken populations and partial density of states (PDOS)

Mulliken bond population values of N–Mo_1 and S–Mo_2 are presented in Table 6.2. After the adsorption of MBT on edges, the lengths of N–Mo_1 and S–Mo_2 bonds were 2.16 and 2.325 Å, both of which were smaller than the sum of radius of N and Mo atoms (2.2 Å), S and Mo atoms (2.46 Å), suggesting the formation of N–Mo_1 and S–Mo_2 bonds. Moreover, the bond population values of N–Mo_1 and S–Mo_2 bonds were 0.26 and 0.59, respectively, manifesting that the covalence character of the S–Mo_2 bond was stronger than the N–Mo_1 bond.

Table 6.2 Mulliken bond population of N–Mo_1 and S–Mo_2

Bond	Population	Bond length (Å)
N–Mo_1	0.26	2.16
S–Mo_2	0.59	2.325

Table 6.3 displays the Mulliken charge of N, S and Mo atoms with and without MBT adsorption on edges. The charge variations indicated the N and S atoms of MBT gained electrons, with the N 2p and S 3p orbitals mainly receiving electrons of 0.05 and 0.12 e, respectively. On the other side, Mo atoms on edges lost electrons, with Mo_1 4d and Mo_2 4d orbital losing 0.14 and 0.16 e. The results confirmed that Mo atoms on edges took part in the bonding with N and S atoms within MBT.

Table 6.3 Mulliken atomic population of N, S and Mo atoms

Atom	Adsorption state	s	p	d	Total	Change (e)
N	Before	1.56	3.84	0	5.39	0.05
	After	1.55	3.9	0	5.44	
S	Before	1.82	4.19	0	6	0.12
	After	1.79	4.33	0	6.12	
Mo_1	Before	2.47	6.27	5.11	13.85	–0.14
	After	2.46	6.29	4.96	13.71	
Mo_2	Before	2.47	6.27	5.11	13.85	–0.16
	After	2.45	6.28	4.93	13.69	

Fig. 6.13 displays PDOS of S and N atoms within MBT and Mo atoms on edges before and after adsorption. After adsorption, both N 2p and S 3p orbitals moved to the valence band, and their peaks near the Fermi level decreased, suggesting that N 2p and S 3p orbitals might receive electrons and participate in the bonding reaction. Meanwhile, Mo_1 4d and Mo_2 4d orbitals shifted to the conduction band and the peak close to the Fermi level improved, indicating that Mo_1 4d and Mo_2 4d orbitals could lose electrons and take part in the bonding reaction [30]. Furthermore, the N 2p orbital overlapped with the Mo_1 4d orbital in the range of –9.5 to –6.2 eV and –2.9 to 3.2 eV, and the S 3p orbital overlapped with the Mo_2 4d orbital in the range of –9.2 to –7.3 eV, –5.6 to –2.8 eV, and 0.4 to 3.3 eV. These orbital hybridization confirmed that a strong bonding reaction occurred between N and Mo_1 atoms, S and Mo_2 atoms.

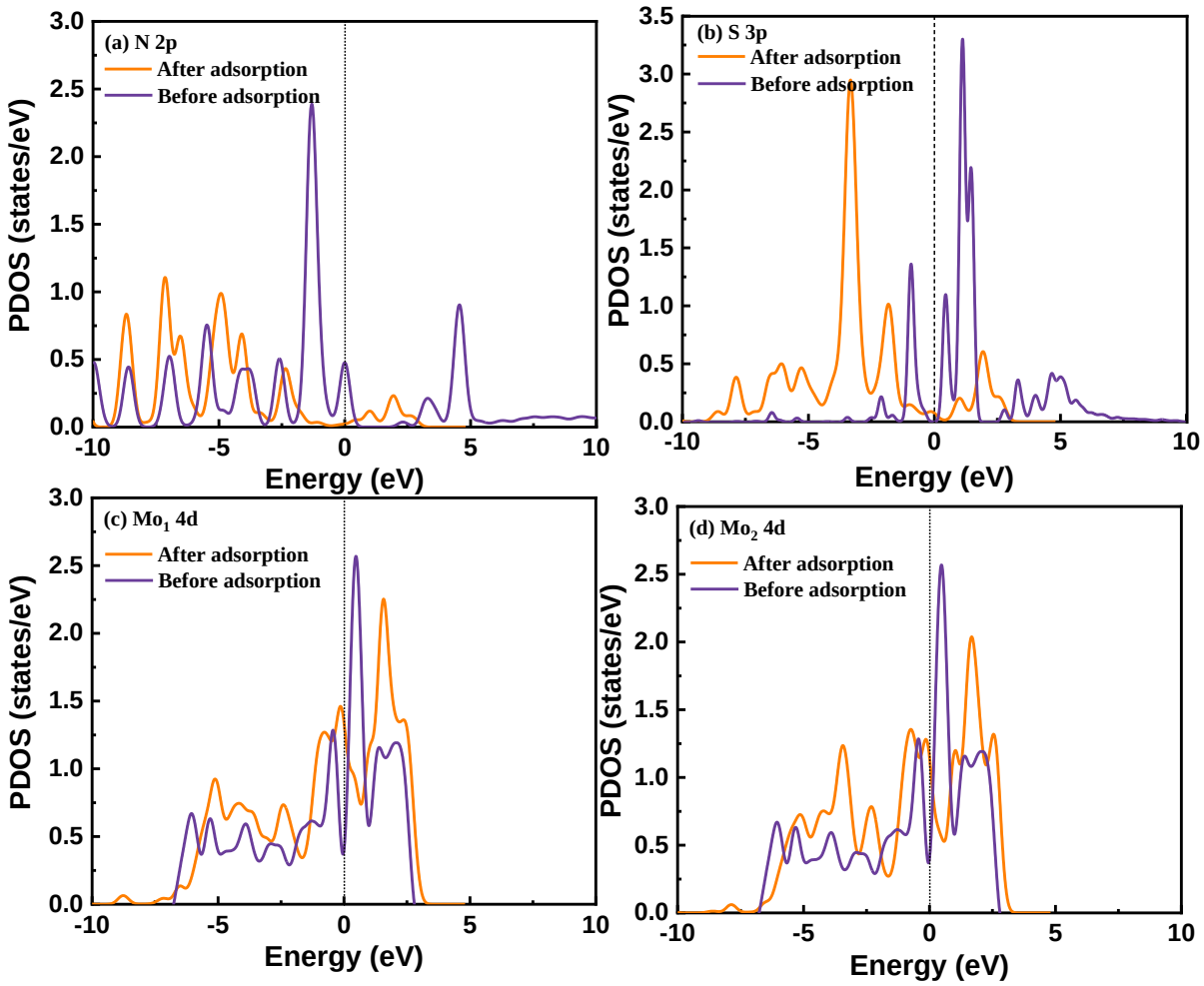

Fig. 6.13 PDOS of N 2p (a), S 3p (b), Mo1 4d (c) and Mo2 4d (d) before and after adsorption.

6.3.8 Adsorption model

In conclusion, an adsorption model is proposed according to the results of contact angle, SEM-EDS, adsorption capacity, zeta potential, XPS and DFT calculations. MBT was weakly adsorbed on molybdenite faces through physical adsorption. On the other hand, MBT strongly interacted with edges via hybridization of N 2p and S 3p orbitals of MBT with Mo 4d orbital on edges. As illustrated in Fig. 6.14, the interaction of MBT with faces and edges greatly enhanced the hydrophobicity of molybdenite.

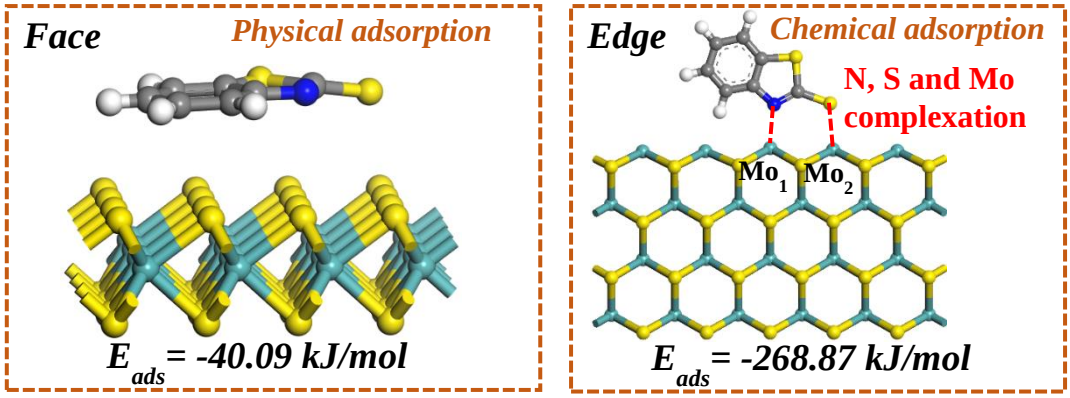

Fig. 6.14 The proposed adsorption configuration of MBT on faces and edges.

6.4 Conclusions

In this work, MBT is developed as an effective collector in the flotation of molybdenite fines, and its adsorption mechanisms were uncovered through various characterizations. The flotation tests indicated that MBT outpermormed kerosene in the flotation of molybdenite fines. Contact angle, adsorption capacity, SEM-EDS and Zeta potential results illustrated that MBT interacted more strongly with edges than faces, hence improving their hydrophobicity. XPS results and DFT calculations further elucidated that MBT was physically adsorbed on faces while chemisorbed with edges via hybridizing N 2p and S 3p of MBT with Mo 4d to generate a bidentate model.

Reference

[1] Q. Zhang, X. Li, M. Li, C. Yuan, Study on flotation separation experiment of molybdenite using new type collector, Adv. Mater. Res. 753–755 (2013) 81–84.

[2] G. Yi, E. Macha, J. Van Dyke, R.E. Macha, T. McKay, M.L. Free, Recent progress on research of molybdenite flotation: A review, Adv. Colloid Interface Sci. 295 (2021).

[3] L. Sun, Y. Cao, L. Li, Q. Zeng, Adsorption characteristics and mechanism of calcium ions on different molybdenite surfaces via experiments and DFT simulations, Separations. 8 (2021).

[4] S. Li, X. Ma, J. Wang, Y. Xing, X. Gui, Y. Cao, Effect of polyethylene oxide on flotation of molybdenite fines, Miner. Eng. 146 (2020) 106146.

[5] S. Castro, A. Lopez-valdivieso, J.S. Laskowski, Review of the fl otation of molybdenite . Part I : Surface properties and fl oatability, Int. J. Miner. Process. 148 (2016) 48–58.

[6] T. He, H. Li, J. Jin, Y. Peng, Y. Wang, H. Wan, Improving fine molybdenite flotation using a combination of aliphatic hydrocarbon oil and polycyclic aromatic hydrocarbon, Results Phys. 12 (2019) 1050–1055.
[7] J. Fu, K. Chen, H. Wang, C. Guo, W. Liang, Recovering molybdenite from ultrafine waste tailings by oil agglomerate flotation, Miner. Eng. 39 (2012) 133–139.
[8] S. Song, X. Zhang, B. Yang, A. Lopez-Mendoza, Flotation of molybdenite fines as hydrophobic agglomerates, Sep. Purif. Technol. 98 (2012) 451–455.
[9] H. Wan, Y. An, J. Qu, C. Zhang, J. Xue, S. Wang, X. Bu, Research on optimization method of flotation kinetic model based on molybdenite particle size effect, Physicochem. Probl. Miner. Process. 59 (2023) 163004.
[10] I.S. Kim, V.K. Sangwan, D. Jariwala, J.D. Wood, S. Park, K.-S. Chen, F. Shi, F. Ruiz-Zepeda, A. Ponce, M. Jose-Yacaman, Influence of stoichiometry on the optical and electrical properties of chemical vapor deposition derived MoS2, ACS Nano. 8 (2014) 10551–10558.
[11] Y. Numata, K. Takahashi, R. Liang, T. Wakamatsu, Adsorption of 2-mercaptobenzothiazole onto pyrite, Int. J. Miner. Process. 53 (1998) 75–86.
[12] Y. Feng, S. Chen, H. Zhang, P. Li, L. Wu, W. Guo, Characterization of iron surface modified by 2-mercaptobenzothiazole self-assembled monolayers, Appl. Surf. Sci. 253 (2006) 2812–2819.
[13] G. Liu, H. Zeng, Q. Lu, H. Zhong, P. Choi, Z. Xu, Adsorption of mercaptobenzoheterocyclic compounds on sulfide mineral surfaces: A density functional theory study of structure-reactivity relations, Colloids Surfaces A Physicochem. Eng. Asp. 409 (2012) 1–9.
[14] G. Noirant, M. Benzaazoua, M. Kongolo, B. Bussière, K. Frenette, Alternatives to xanthate collectors for the desulphurization of ores and tailings: Pyrite surface chemistry, Colloids Surfaces A Physicochem. Eng. Asp. 577 (2019) 333–346.
[15] J. Wang, L. Xie, Q. Lu, X. Wang, J. Wang, H. Zeng, Electrochemical investigation of the interactions of organic and inorganic depressants on basal and edge planes of molybdenite, J. Colloid Interface Sci. 570 (2020) 350–361.
[16] Z. Wei, Y. Li, L. Huang, New insight into the anisotropic property and wettability of molybdenite: A DFT study, Miner. Eng. 170 (2021) 107058.
[17] G.S. Maier, X. Qiu, B. Dobias, New collectors in the flotation of sulphide minerals: a study of the electrokinetic, calorimetric and flotation properties of sphalerite, galena and chalcocite, Colloids Surfaces A Physicochem. Eng. Asp. 122 (1997) 207–225.
[18] S.Chander, W.Fuerstenau, On the natural floatability of molybdenite, Trans. SME/AIME. 252 (1972) 62–69.
[19] D. Yuan, K. Cadien, Q. Liu, H. Zeng, Adsorption characteristics and mechanisms of O-Carboxymethyl chitosan on chalcopyrite and molybdenite, J. Colloid Interface Sci. 552 (2019) 659–670.
[20] B. Yang, P. Huang, Q. An, An efficient chalcopyrite depressant for Cu-Mo separation and its interaction mechanism: Adsorption configuration and DFT calculations, J. Mol. Liq. 345 (2022) 118171.
[21] B. Yang, H. Yan, M. Zeng, P. Huang, F. Jia, A. Teng, A novel copper depressant for selective flotation of chalcopyrite and molybdenite, Miner. Eng. 151 (2020) 106309.

[22] Y. Chen, X. Chen, Y. Peng, The effect of sodium hydrosulfide on molybdenite flotation as a depressant of copper sulfides, Miner. Eng. 148 (2020).
[23] F. Jia, C. Liu, B. Yang, S. Song, Microscale control of edge defect and oxidation on molybdenum disulfide through thermal treatment in air and nitrogen atmospheres, Appl. Surf. Sci. 462 (2018) 471–479.
[24] A.N. Buckley, G.A. Hope, G.K. Parker, E.A. Petrovic, R. Woods, Mercaptobenzothiazole collector adsorption on Cu sulfide ore minerals, Int. J. Miner. Process. 153 (2016) 95–108.
[25] C. Wang, R. Liu, M. Wu, Z. Xu, M. Tian, Z. Yin, W. Sun, C. Zhang, Flotation separation of molybdenite from chalcopyrite using rhodanine-3-acetic acid as a novel and effective depressant, Miner. Eng. 162 (2021) 106747.
[26] J. Wei, P. Hing, Z.Q. Mo, TEM, XPS and FTIR characterization of sputtered carbon nitride films, Surf. Interface Anal. 28 (1999) 208–211.
[27] Y. Cai, H. Yang, J. Zhou, Z. Luo, G. Fang, S. Liu, A. Pan, S. Liang, Nitrogen doped hollow MoS2/C nanospheres as anode for long-life sodium-ion batteries, Chem. Eng. J. 327 (2017) 522–529.
[28] N. Masatoshi, T. Jumpei, O. Shinzo, XPS study of nitrided molybdena/titania catalyst for the hydrodesulfurization of dibenzothiophene, J. Phys. Chem. B. 103 (1999) 10180–10188.
[29] H. Zhu, B. Yang, J. Feng, F. Jia, Evaluation of 1-hydroxyethylidene-1 , 1-diphosphonic acid as an efficient and low-toxic sphalerite depressant in the selective flotation of galena from sphalerite, J. Clean. Prod. 329 (2021) 129612.
[30] X. Long, Y. Chen, J. Chen, Z. Xu, Q. Liu, Z. Du, The effect of water molecules on the thiol collector interaction on the galena (PbS) and sphalerite (ZnS) surfaces: A DFT study, Appl. Surf. Sci. 389 (2016) 103–111.

The main content of this chapter was published in *Colloids and Surfaces A: Physicochemical and Engineering Aspects*.

Chapter VII. Improving the Flotation of Unoxidized and Oxidized Molybdenite Fines Using Dodecylamine as a Collector: Flotation Tests and Interaction Mechanism

7.1 Introduction

Molybdenum (Mo) is a rare and strategic metal, which has been broadly used in metallurgy, machinery, chemical and aerospace industries owing to its high strength and excellent corrosion resistance [1, 2]. Up to now, 95% molybdenum production originates from molybdenite. With the gradual reduction of high-grade molybdenite ores, exploiting low-grade and fine-disseminated molybdenite deposits is essential to satisfy increasing consumption demand. Nevertheless, these refractory ores are required to be finely ground to liberate them from other gangue minerals. As a laminar mineral with distinct anisotropic properties, molybdenite possesses polar edges and non-polar faces [3]. The hydrophilic edge originates from the cleavage of S-Mo covalent bonds, while the hydrophobic face is derived from the break of van der Waals force between S–Mo–S layers [4]. Notably, molybdenite hydrophobicity depends on the edge/face ratio. As particle size decreases, the hydrophilic edge gradually dominates, leading to a significant decline in the floatability of molybdenite fines [5].

In addition, oxidation is another important factor affecting the flotation of molybdenite ores. Molybdenite ores are prone to be oxidized in the presence of oxygen, moisture, microbial activity, and acidic substances [6], leading to diminishing hydrophobicity. [7]. Yi et al. reported that the oxidation reaction made molybdenite surface less hydrophobic [8]. Wei et al. further revealed that both faces and edges exhibited hydrophilic properties after oxidation [9]. Because covalent bonds are ruptured to produce edges, they are known to be considerably more reactive than faces. As a result, the oxidation reaction occurs primarily on edges, and on the defect sites in faces [10]. Notably, molybdenite fines are more readily to be oxidized due to the dominant edges, and then the hydrophobicity significantly decreases, resulting in a poor flotation performance of oxidized molybdenite fines.

Kerosene is a commonly used collector in the flotation of molybdenite that preferentially adsorbs on molybdenite faces rather than edges via van der Waals forces and hydrophobic interactions [11]. However, kerosene cannot efficiently collect molybdenite fines owing to its poor affinity toward hydrophilic edges. After oxidation, since the hydrophobicity of faces decreases, the affinity between kerosene and faces becomes weaker, leading to worse floatability. Consequently, exploring novel collectors to improve the flotation of oxidized and unoxidized molybdenite fines is essential.

Dodecylamine (DDA) is a common cationic collector, which can be used to collect silicate and oxidized minerals. In its molecular structure, DDA contains a long carbon chain and an amine group. The amine group has a lone-pair electron that can complex with metal sites. Meanwhile, the long carbon chain renders the mineral surface hydrophobic. In this work, DDA was first tested as a collector of molybdenite fines. The flotation performances and interaction mechanisms were probed via flotation, contact angle, Zeta potential, SEM-EDS, and XPS measurements. The objective was to verify if it was suitable for promoting the flotation of molybdenite fines and to shed some light on its interaction mechanism.

7.2 Experimental

7.2.1. Materials

Molybdenite samples were purchased from Guangxi province, China. These samples were selected, ground, and screened to obtain −20 μm size fractions for flotation tests and measurements. The XRD (D8 Advance, Bruker, Billerica, MA, USA) pattern of molybdenite is illustrated in Fig. 7.1, and there was no apparent impurity peak. The results of XRD and the chemical assay showed that the molybdenite samples were of high purity (97%).

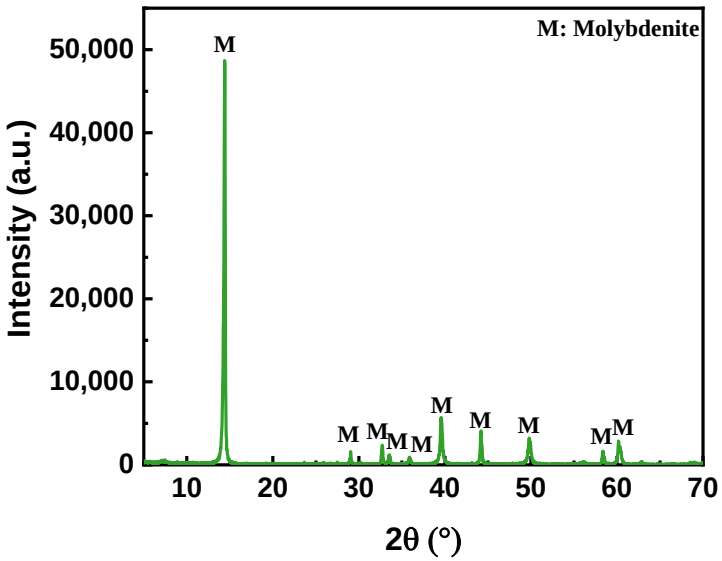

Fig. 7.1 XRD pattern of raw mineral samples.

Reagents utilized in this work include the collectors DDA and kerosene, pH modifiers NaOH and HCl, the frother methyl isobutyl carbinol (MIBC), and oxidant hydrogen peroxide (H_2O_2), which were all obtained from Aladin, China. Ultrapure water was used.

7.2.2 Oxidation Treatment and Flotation Tests

Molybdenite powders (2 g) were added to 1 M H_2O_2 (30% *v*/*v*) solution, and the suspension was stirred at 300 rpm for 24 h. Then, the pulp was transferred to a flotation cell. After pH adjustment, DDA or kerosene was introduced and conditioned for 5 min. When kerosene was employed as the collector, MIBC was introduced to the pulp and conditioned for 1 min before flotation. When DDA was used as a collector, MIBC was not needed. The flotation was performed for 3 min.

7.2.3 Characterizations

The contact angles of molybdenite faces and edges were measured using a contact angle goniometer (Dataphysics OCA20, Filderstadt, Germany) via the sessile drop method. During the measurements, ultrapure water droplets were dispensed through a needle with a diameter of 0.5 mm, producing droplets with a diameter of approximately 4 mm. Bulk molybdenite with good crystallinity was used to prepare both face and edge samples. Fresh face samples (0.5 × 0.5 cm^2) were obtained by mechanically exfoliating the top layers of molybdenite using Scotch tape. To prepare edge samples, a molybdenite block approximately 0.5 cm thick was cut into pieces with dimensions of 0.4 × 0.3 cm^2. The edge surfaces were sequentially polished using wet silicon carbide papers with grit sizes of 240, 400, 800, 1200, 3000, and 7000, followed by further polishing with alumina suspensions of 1 μm and 0.3 μm particle size. To obtain oxidized surfaces, the freshly prepared face and edge samples were immersed in an H_2O_2 solution for 24 h. For DDA-treated samples, both fresh and oxidized face and edge samples were immersed in a 100 mg/L dodecylamine (DDA) solution (pH = 7) for 5 min, followed by drying with nitrogen gas prior to measurement. The zeta potential was determined using a Zetasizer Nano analyzer (Malvern, UK). Briefly, 0.1 g of oxidized or unoxidized molybdenite samples was dispersed in a DDA solution (100 mg/L) containing 10^{-3} M NaCl as the background electrolyte and conditioned under stirring for 5 min. After adjusting the pH to the desired value, 1 mL of the suspension was withdrawn for zeta potential measurement. The morphology of the molybdenite face and edge samples was examined using scanning electron microscopy (SEM, JEM-2100F, JEOL, Tokyo, Japan). The elemental distribution was analyzed using an energy-dispersive X-ray spectrometer (EDS, EDAX Elite, Pleasanton, CA, USA) coupled with the SEM system. Raman spectra were collected using an InVia Raman microscope (Renishaw, Gloucestershire, UK) equipped with a 532 nm Ar laser. Face and edge samples with and without oxidation were prepared according to the procedure described in Section 7.2.3. In addition, the residual H_2O_2 solution obtained after the oxidation treatment of the face and edge samples was also analyzed. For Raman measurements involving DDA

treatment, 2 g of both unoxidized and oxidized molybdenite samples were conditioned in a 100 mg/L DDA solution (pH = 7) for 5 min, after which the samples were collected and dried prior to analysis. X-ray photoelectron spectroscopy (XPS) was performed using a Thermo Scientific K-Alpha spectrometer (Thermo Scientific, Waltham, MA, USA). The spectra were recorded using an Al Kα radiation source operated at 12 kV with a pass energy of 50 eV. Spectral fitting was carried out using Avantage software (version 5.9922). The binding energy scale was calibrated using the standard C 1s peak at 284.80 eV.

7.3 Results and Discussion

7.3.1 Flotation Tests

Fig. 7.2 (a) presents the floatability of molybdenite fines as a function of pH. It was clear that molybdenite floatability decreased gradually as pH increased, which might be attributed to the generation of hydrophilic molybdate ions [12]. After the addition of DDA, the floatability of molybdenite fines increased to 97% at a pH 5, whereas a high dosage of kerosene achieved a floatability of 88.82%. Compared with kerosene, a lower dosage of DDA could achieve higher floatability, indicating that DDA was more efficient in the flotation of molybdenite fines at a broad pH range.

Fig. 7.2 (b) shows the impact of collector dosage on the floatability of molybdenite fines. Notably, molybdenite floatability improved remarkably as the collector dosage increased. At a DDA dosage of 50 mg/L, the floatability reached 94.96%, which was much higher than that (88.56%) obtained at a kerosene dosage of 400 mg/L. These results indicated that DDA exhibited much stronger collecting ability for molybdenite fines, which had the potential to replace kerosene.

Fig. 7.2 (c) illustrates molybdenite floatability after oxidation as a function of pH. When kerosene was used as a collector, the floatability of oxidized molybdenite fines decreased slightly as pH increased. On the contrary, the floatability improved substantially after the introduction of DDA at a pH 5–7. It was clear that a low dosage of DDA achieved a floatability of 74.52%, while a high dosage of kerosene only obtained a floatability of 33.62% at a pH 7. The large difference in floatability meant that less reagent was needed when DDA was used. These results indicated that DDA also significantly improved the flotation of oxidized molybdenite fines.

The influence of collector dosage on the flotation of oxidized molybdenite fines is presented in Fig. 7.2 (d). It was obvious that oxidized molybdenite exhibited very poor floatability (8.69%). After the addition of kerosene, the floatability reached 33.62% at 400 mg/L of kerosene. Notably, the floatability surged dramatically to nearly 90% when 100 mg/L

of DDA was introduced. These results indicated that DDA was more effective than kerosene in collecting oxidized molybdenite fines.

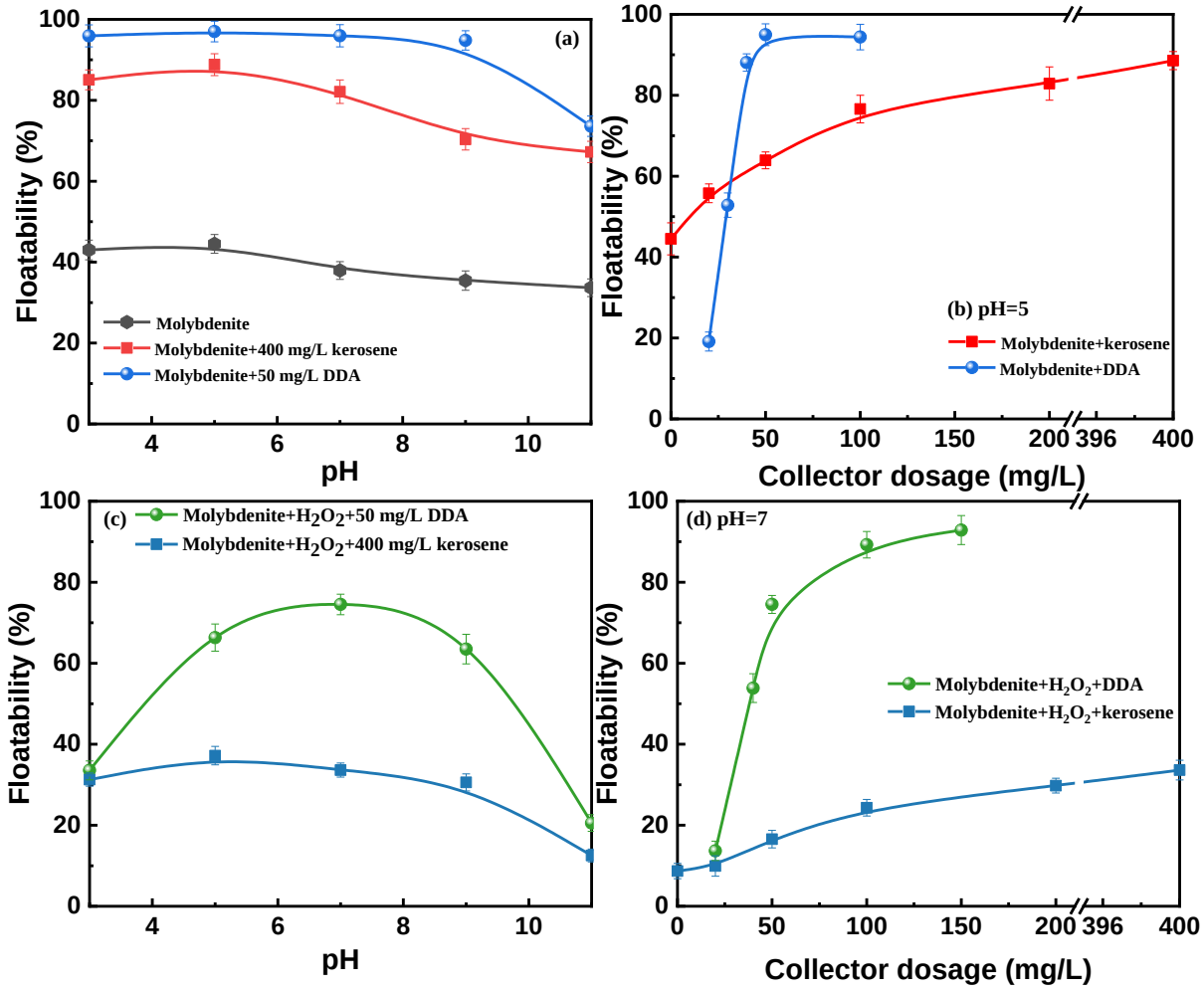

Fig. 7.2 The influence of pH and collector dosage on the floatability of unoxidized (a, b) or oxidized (c, d) molybdenite fines.

7.3.2. Contact Angle

Fig. 7.3 depicts contact angles of treated and untreated faces and edges under various conditions. The contact angle of fresh molybdenite faces and edges were 76.5 ° and 42.5 °, respectively. After adding DDA, the contact angle of the faces and edges increased to 89 ° and 86 °, suggesting that DDA improved the hydrophobicity of fresh faces and edges. After oxidation, the contact angle of both the faces and edges decreased to 38.5 ° and 20 °, which explained the poor flotation of oxidized molybdenite fines. For oxidized molybdenite fines treated with DDA, the contact angle of the faces and edges reached 88 ° and 80 °, respectively,

which indicated that DDA could also remarkably enhance the hydrophobicity of both oxidized faces and edges. These results revealed that DDA could improve the hydrophobicity of the faces and edges before and after oxidation, which corresponded well with the flotation results.

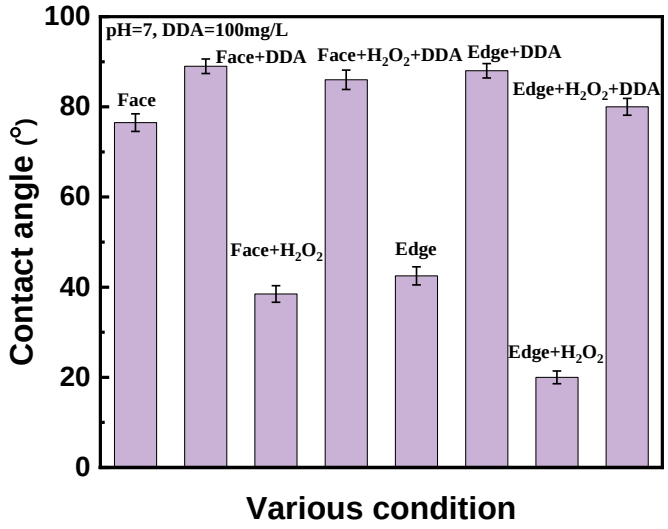

Fig. 7.3 Contact angles of the molybdenite faces and edges under various conditions.

7.3.3. Zeta Potential

The effect of pH on the zeta potential of oxidized and unoxidized molybdenite fines with and without DDA is displayed in Fig. 7.4 (a). For molybdenite, the zeta potential was negative throughout the pH range. After oxidation, it shifted to more negative values over the pH range, which might be ascribed to the formation of more negatively charged molybdate ions ($HMoO_4^-/MoO_4^{2-}$) [7]. After the introduction of DDA, the zeta potential of both oxidized and unoxidized molybdenite fines became positive at a pH ≈ 2 – 10, and their isoelectric point (IEP) moved to an approximate pH of 10.54 and 10.70, respectively. Based on the DDA species distribution diagram (Fig. 7.4 (b)), the cationic species RNH_3^+ dominated, where a few neutral species of RNH_2(aq) were also present in the pH range of 0–9.54. Consequently, it was easy to understand that these DDA species were adsorbed on unoxidized and oxidized molybdenite surfaces and reversed their Zeta potential from negative to positive [13].

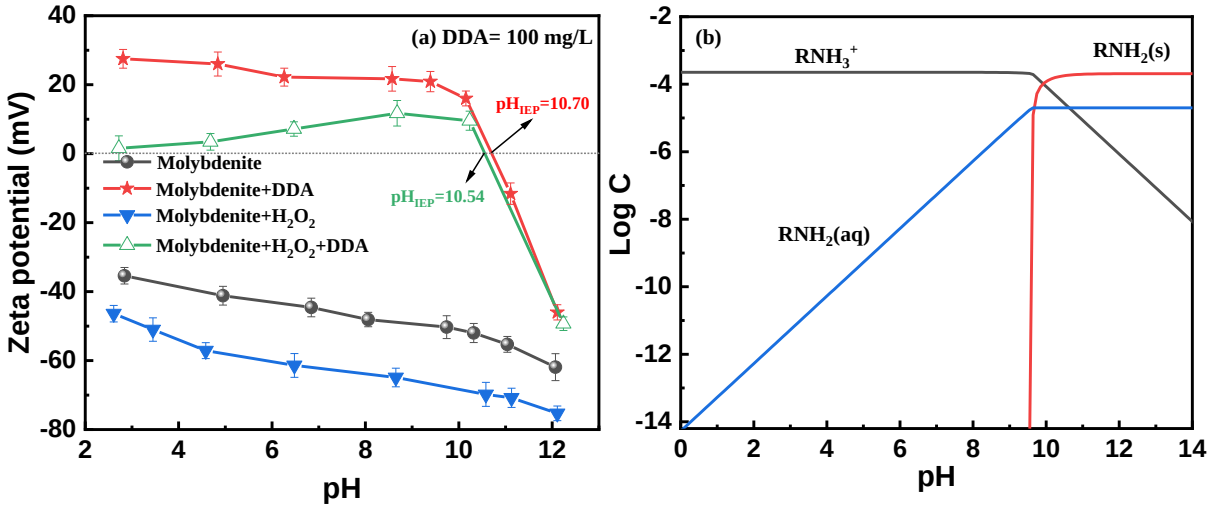

Fig. 7.4 Zeta potential of treated and untreated molybdenite fines (a), DDA species distribution (b) as a function of pH.

7.3.4. Raman and SEM-EDS Analysis

The species of molybdenite faces and edges were examined using Raman spectroscopy. Fig. 7.5 (a) depicts Raman spectra of faces and edges before and after oxidation. The distinct peaks at 380 and 405 cm^{-1} represented the in-plane E^1_{2g} and out-of-plane A_{1g} vibration modes of Mo–S bonds [14], which were detected on both unoxidized faces and edges. For oxidized edges, a new peak at 285 cm^{-1} appeared, which was ascribed to MoO_3, indicating that the oxidation degree of the edges increased. For oxidized faces, the A_{1g} peak was broadened, suggesting the softening of the Mo–S phonon mode, which might be attributed to the decrease in Mo–S bonds [15]. Furthermore, both faces and edges exhibited red shifts of E^1_{2g} and A_{1g} peaks after oxidation, which might be attributed to the generation of sulfur vacancies during oxidation [16].

Raman spectra of molybdenite species in oxidation leach liquor are displayed in Fig. 7.5(b). For the edge liquor, the peaks at 899 and 1054 cm^{-1} represented Mo=O in MoO_4^{2-} and HSO_4^-. For the face liquor, the same two peaks were also detected, and another peak at 979 cm^{-1} of the faces was ascribed to SO_4^{2-} [17]. The appearance of HSO_4^- and SO_4^{2-} indicated the oxidation of sulfur in molybdenite. Compared with the edge liquor, the intensity of MoO_4^{2-} reduced while HSO_4^- increased in the face liquor, and the new peak of SO_4^{2-} appeared, indicating that more sulfur and fewer molybdenum oxidized products dissolved from faces than edges. Furthermore, ICP results illustrated that the sulfur and molybdenum elemental contents were 1016.84 mg/L and 330.03 mg/L in the liquor, suggesting the oxidized products of sulfur were more soluble than those of molybdenum.

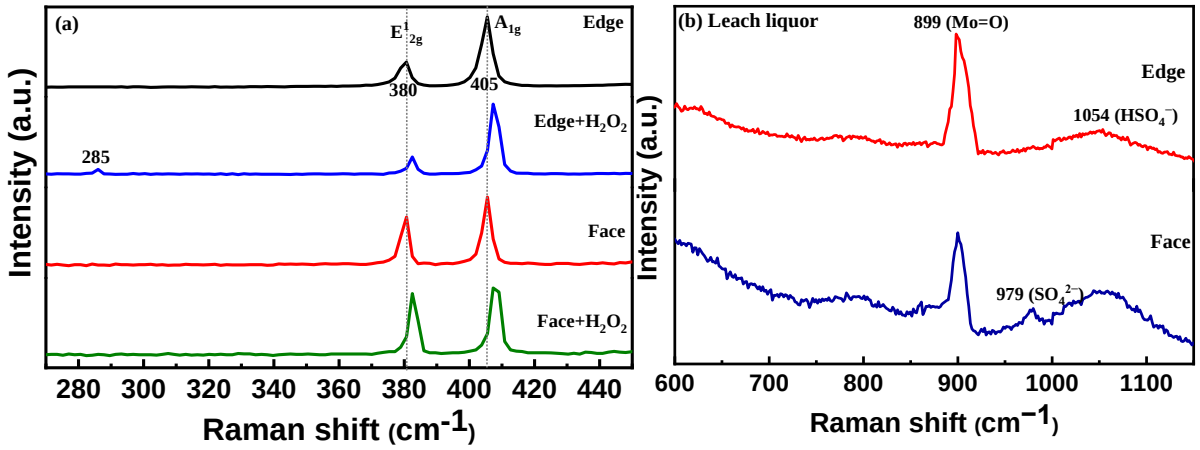

Fig. 7.5 The Raman spectra of molybdenite faces and edges with and without H_2O_2 treatment (a), oxidation leach liquor (b).

Fig. 7.6 and Table 7.1 present the SEM images and elemental atomic concentration of fresh and oxidized molybdenite faces and edges. The fresh faces and edges surfaces were smooth and O content was relatively low. After oxidation, many hexagonal defects formed on faces. Meanwhile, the EDS results showed that the S and Mo content decreased slightly while the O content increased around these defects. Therefore, it was reasonable to deduce that the oxidation mainly caused the generation of defects on faces. For oxidized edges, large white oxides were observed. EDS analysis indicated that these oxides were primarily molybdenum oxide. Combined with Raman results, the broadened A_{1g} peak and red shift further demonstrated that these defects on oxidized faces might be sulfur vacancies, and the deposited molybdenum oxide on oxidized edges could be ascribed to MoO_3.

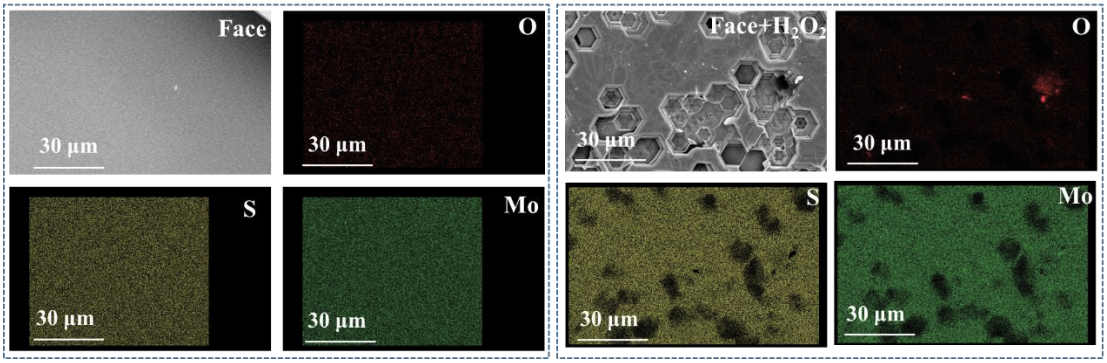

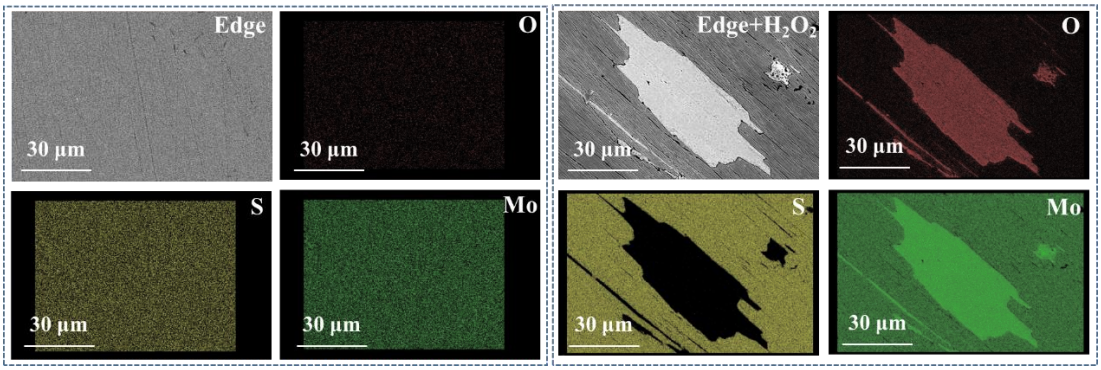

Fig. 7.6 SEM-EDS images of molybdenite face and edge before and after oxidation.

Table 7.1 Elemental atomic concentration of the face and edge with and without oxidation.

Surface	Oxidation State	Element Atomic Conc. (%)		
		S	Mo	O
Face	Before	59.417	37.121	2.462
	After	57.568	36.937	5.495
Edge	Before	59.278	37.258	3.464
	After	31.736	50.530	17.734

The effect of DDA on oxidized and unoxidized faces and edges was also investigated by SEM-EDS. The photographs and element atomic concentration are displayed in Fig. 7.7 and Table 7.2. Notably, a lot of the N element was detected on both fresh and oxidized faces and edges, suggesting DDA species adsorbed onto fresh and oxidized faces and edges, which was consistent with the contact angle results. Furthermore, the N atom concentration on oxidized faces and edges was higher than fresh faces and edges, which implied that DDA species were more readily adsorbed on the oxidized face and edge. Therefore, DDA species enhanced the hydrophobicity of the fresh and oxidized faces and edges, thus improving the floatability of unoxidized and oxidized molybdenite fines, which was in line with the contact angle result.

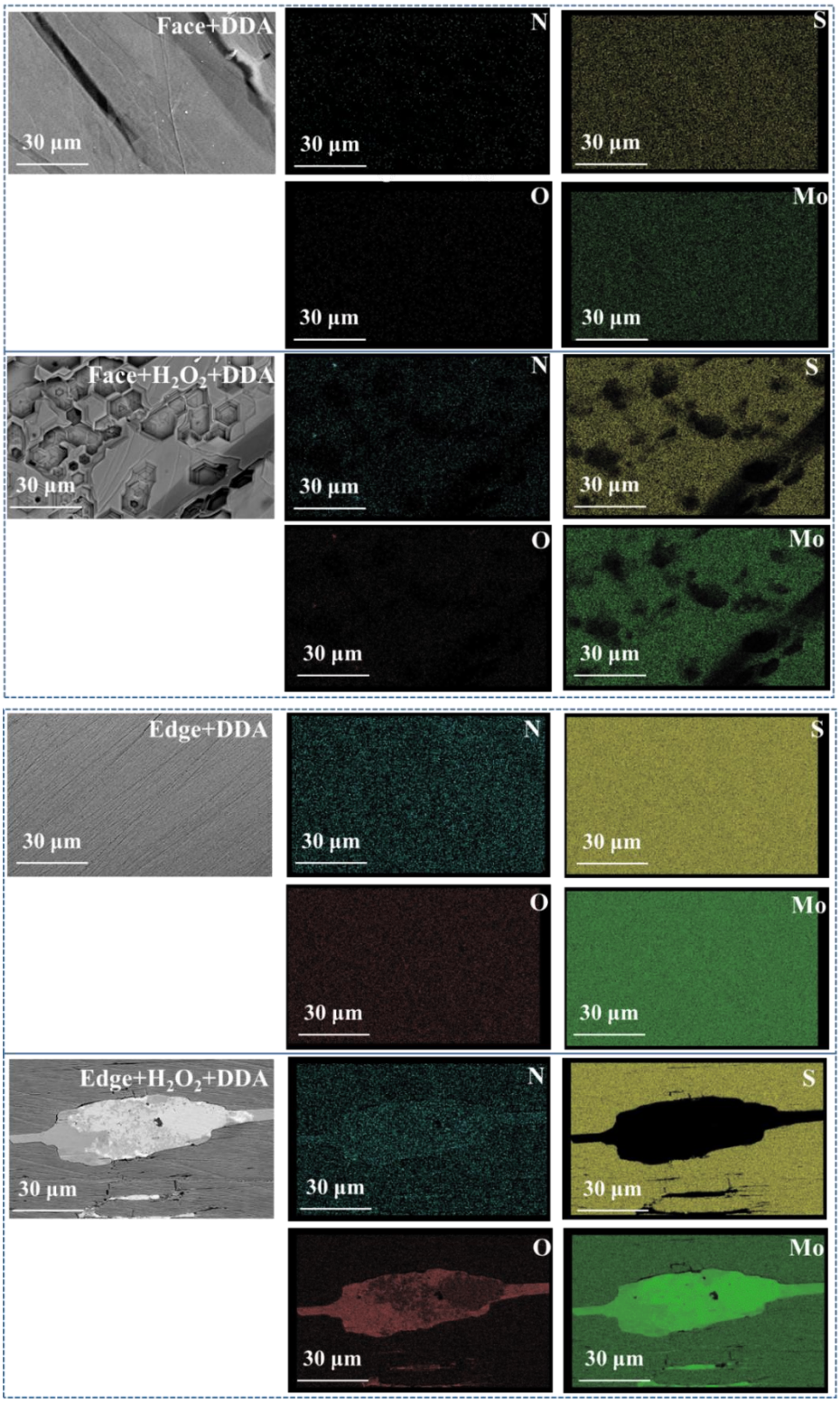

Fig. 7.7 SEM-EDS images of fresh and oxidized molybdenite faces and edges in the absence and presence of DDA.

Table 7.2 Elemental atomic concentration of oxidized and unoxidized molybdenite faces and edges with and without DDA treatment.

Surface	Oxidation State	Element Atomic Conc. (%)			
		S	Mo	O	N
Face	Before	59.417	37.121	2.462	0.798
	After	57.568	36.937	5.495	1.173
Edge	Before	61.212	37.895	0.344	0.549
	After	26.880	61.514	9.125	2.481

7.3.5. XPS Analysis

The XPS spectra of Mo 3d, S 2p, N 1s, and O 1s are shown in Fig. 7.8. The peak binding energy and atomic concentration are listed in Table 7.3. In Fig. 7.8 (a), the peak at 226.72 eV represented S 2s. The peaks at 229.37, 230.22, and 231.88 eV were assigned to the Mo $3d_{5/2}$ of MoS_2, MoO_2, and MoO_3. The peaks at 232.52, 233.57, and 235.17 eV were assigned to the Mo $3d_{3/2}$ of MoS_2, MoO_2, and MoO_3, respectively [14]. After adding DDA, the peak of MoS_2 moved by approximately 0.33 eV, indicating that DDA species might be adsorbed on the Mo sites of molybdenite. After oxidation, it was clear that the MoO_3 concentration greatly increased from 7.672% to 21.7% and the MoO_2 concentration slightly increased from 4.79% to 8.04%. For oxidized molybdenite treated with DDA, the movement of MoS_2 was 0.24 eV, while the movements of MoO_2 (0.09 eV) and MoO_3 (0.05 eV) were insignificant, implying that DDA species might be chemisorbed on MoS_2 but physisorbed on MoO_3 and MoO_2.

In S 2p spectra (Fig. 7.8 (b)), for untreated molybdenite, the peaks centered at 162.30 and 163.50 eV, which denoted S $2p_{3/2}$ and S $2p_{1/2}$ of MoS_2 [18]. For the oxidized molybdenite, the S $2p_{3/2}$ and S $2p_{1/2}$ of MoS_2 shifted to 162.53 and 163.74 eV. After the addition of DDA, the peaks of both unoxidized and oxidized molybdenite moved slightly to a lower binding energy. It has been reported that the sulfur atom was prone to form H bonds with RNH_2 and RNH_3^+ species [19, 20]. Thus, it could be inferred that the decrease in binding energy might be attributed to hydrogen bonding.

In Fig. 7.8 (c), the peak at 401.35 eV represented RNH_3^+ of DDA [19]. For molybdenite treated with DDA, the peaks at 395.64, 397.63, 399.22, and 401.42 eV denoted Mo 3p of MoS_2 [4], Mo–N [21], RNH_2 [22], and RNH_3^+. The same peaks were also detected on the oxidized molybdenite treated with DDA, which centered at 395.60, 397.79, 399.19, and 401.45 eV, respectively. The appearance of RNH_2 and RNH_3^+ indicated that DDA species were adsorbed on both unoxidized and oxidized molybdenite surfaces [23]. Meanwhile, the appearance of the Mo–N bond might imply the formation of a molybdenum-amine complex ion, in which the RNH_2 bonded with the Mo sites [19]. In addition, the higher RNH_2 and RNH_3^+ concentrations

on oxidized molybdenite compared to unoxidized molybdenite suggested that RNH_2 and RNH_3^+ were more readily adsorbed on oxidized molybdenite surfaces, which was in accordance with SEM-EDS results.

In Fig. 7.8 (d), for pure molybdenite, the peaks at 530.68, 531.85, and 533.20 eV correspond to MoO_2, MoO_3, and O_2/MoS_2 [24]. After oxidation, the three peaks moved to 530.94, 532.06, and 533.55 eV. Meanwhile, the atomic concentration of MoO_3 increased significantly, confirming that the surface oxidation degree increased. After the treatment with DDA, three peaks of unoxidized and oxidized molybdenite also shifted to lower binding energies, which was similar to the S 2p. Since the electronegativity of the O atoms was higher than the S atoms, RNH_2 and RNH_3^+ might be adsorbed on the O atoms of unoxidized and oxidized molybdenite surfaces via hydrogen bonding.

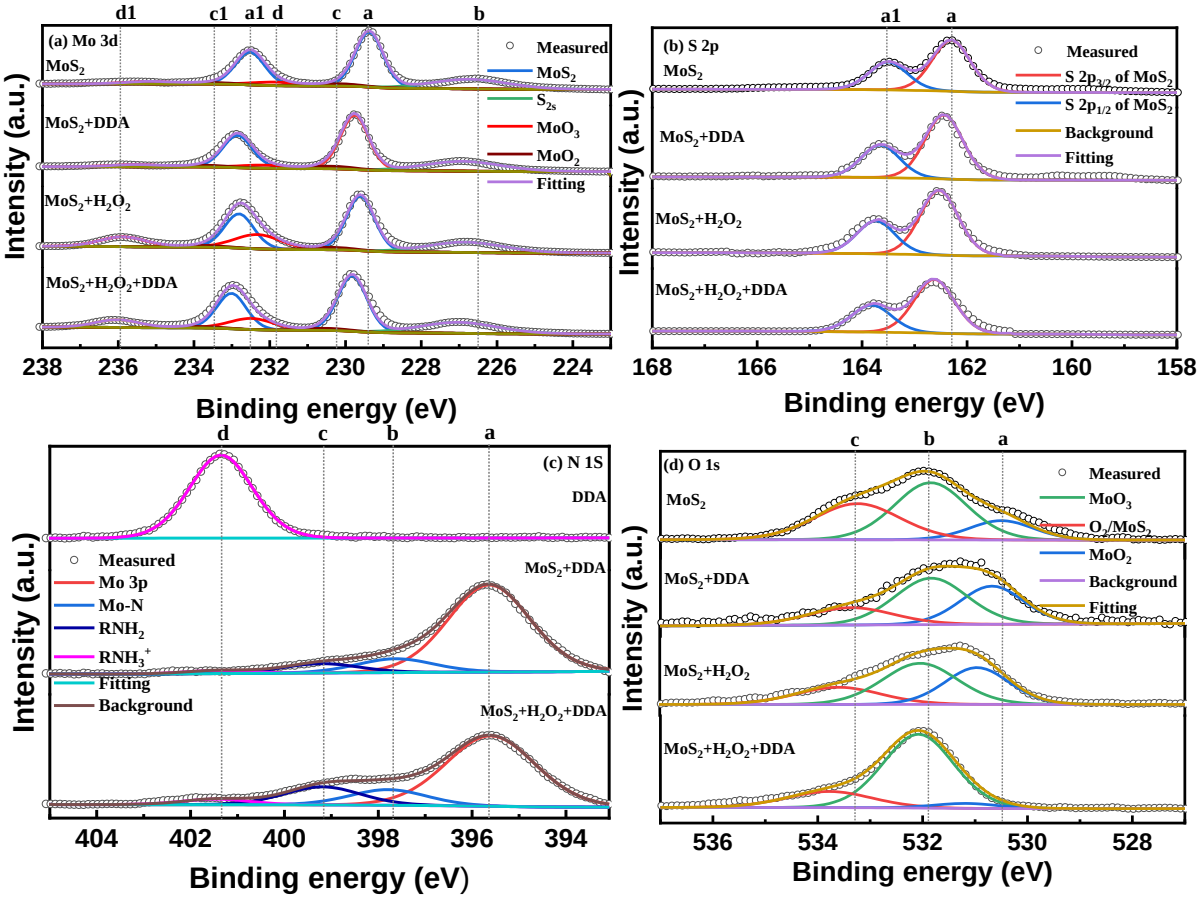

Fig. 7.8 XPS spectra of Mo 3d (a), S 2p (b), N 1s (c), and O 1s (d) for treated and untreated molybdenite fines.

Table 7.3 Fitting parameters of XPS spectra.

Orbital	Species	Untreated		+DDA		$+H_2O_2$		$+H_2O_2$+DDA	
		BE	AC	BE	AC	BE	AC	BE	AC
Mo 3d	a (MoS_2)	229.37	40.58	229.70	41.64	229.61	32.71	229.85	33.89
	a1(MoS_2)	232.52	28.07	232.85	26.13	232.81	21.81	233.05	23.4
	b (S_{2s})	226.72	19.31	226.90	20.33	226.83	15.75	277.01	18.39
	c(MoO_2)	230.22	2.83	230.43	2.97	230.40	4.82	230.49	4.69
	c1(MoO_2)	233.57	1.96	233.74	2.05	233.75	3.22	233.86	3.24
	d(MoO_3)	231.88	4.29	232.19	4.06	232.32	13.02	232.47	9.68
	d1(MoO_3)	235.17	2.97	233.54	2.81	235.88	8.68	236.03	6.7
S 2p	a(S $2p_{3/2}$)	162.30	64.53	162.24	66.19	162.53	66.19	162.42	66.61
	a1(S $2p_{1/2}$)	163.50	35.37	163.45	33.81	163.74	33.81	163.63	33.39
N 1s	a(Mo_{3p})	-	-	395.64	75.98	-	-	395.60	68.05
	b(Mo-N)	-	-	397.63	13.74	-	-	397.79	14.62
	c(RNH_2)	-	-	399.22	8.25	-	-	399.19	12.71
	d(RNH_3^+)	401.35	100	401.42	2.02	-	-	401.45	4.63
O 1s	a(MoO_2)	530.68	19.47	530.59	19.94	530.94	1.88	530.87	2.18
	b(MoO_3)	531.85	55.69	531.70	57.65	532.06	76.61	531.86	73.63
	c(O_2/MoS_2)	533.20	24.84	533.15	22.41	533.55	21.51	533.40	24.18

BE—bind energy (eV), AC—atomic concentration (%), "-" denotes none.

7.3.6. Interaction Mechanism

Based on the analysis of zeta potential, contact angle, SEM-EDS, and XPS, the adsorption mechanism of DDA species on fresh and oxidized faces and edges is proposed. As illustrated in Fig. 7.9, for fresh faces, RNH_3^+ and RNH_2 interacted with S atoms by hydrogen bonding. For

fresh edges, RNH_2 and RNH_3^+ were adsorbed on the negatively charged edges via chemical bonding and electrostatic force. On the other hand, for oxidized faces, RNH_2 and RNH_3^+ were adsorbed on newly exposed S atoms by hydrogen bonding and interacted with oxidized micro-edges through hydrogen bonding and electrostatic forces. For oxidized edges, RNH_2 and RNH_3^+ were adsorbed on deposited MoO_3 by hydrogen bonding and electrostatic force.

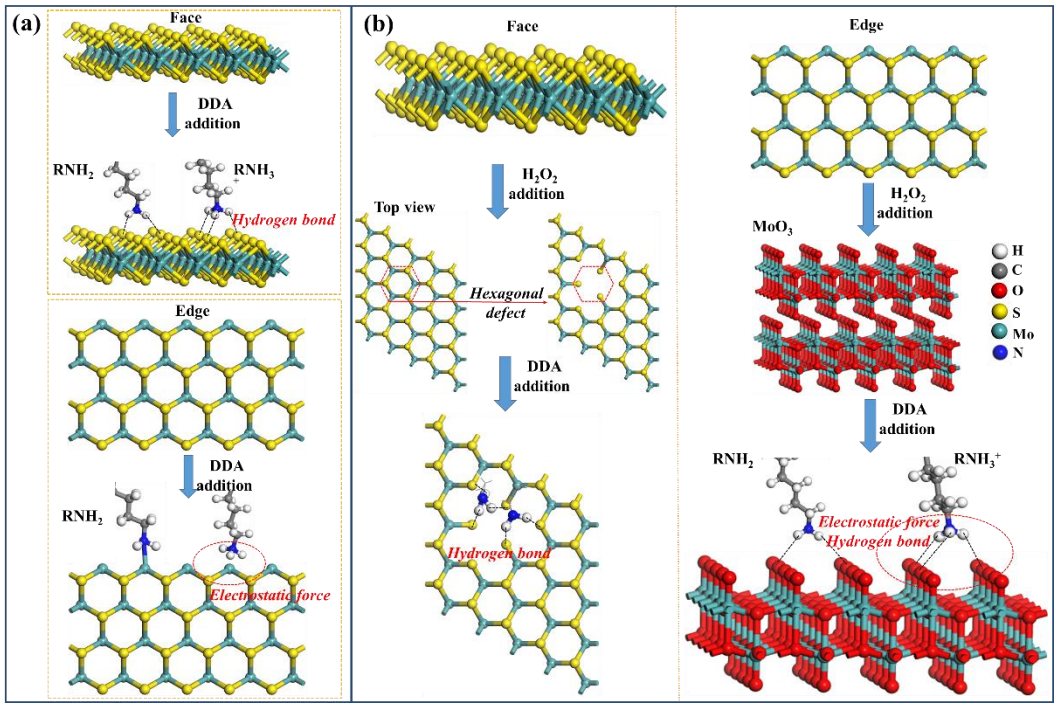

Fig. 7.9. The possible interaction mechanism of DDA on molybdenite faces and edges before (a) and after (b) oxidation.

7.4. Conclusions

(1) DDA is more efficient than kerosene in the flotation of unoxidized and oxidized molybdenite fines. For unoxidized molybdenite fines, a low dosage of DDA (50 mg/L) achieved a much higher floatability (94.96%) than that (88.56%) obtained at kerosene dosage of 400 mg/L. For oxidized molybdenite fines, the floatability was only 33.62% using 400 mg/L kerosene, while the floatability increased significantly to about 90% at DDA dosage of 100 mg/L. DDA could effectively improve the flotation of unoxidized or oxidized molybdenite fines because of the adsorption of DDA species on both faces and edges.

(2) RNH_2 and RNH_3^+ interacted with S atoms on fresh faces through hydrogen bonding while adsorbed on fresh edges by chemical bonding and electrostatic interaction.

(3) After oxidation, RNH_2 and RNH_3^+ were adsorbed on newly exposed S atoms by hydrogen bonding or interacted with MoO_3 on oxidized micro-edges by hydrogen bonding and

electrostatic forces. RNH_2 and RNH_3^+ interacted with deposited MoO_3 on oxidized edges via hydrogen bonding and electrostatic force interaction.

References

[1] H. Wan, P. Yi, X. Song, S. Luukkanen, J. Qu, W. Yang, H. Li, X. Bu, Role of improving molybdenite flotation by using aromatic hydrocarbon collector in high-calcium water: A multiscale investigation, Miner. Eng. 191 (2023).

[2] J. Li, W. Deng, Z. Liu, B. Pei, S. Ning, Z. Cai, R. Liu, Detrimental effect of dissolved natural organic matter on molybdenite flotation, Miner. Eng. 193 (2023).

[3] Z. Lu, Q. Liu, Z. Xu, H. Zeng, Probing Anisotropic Surface Properties of Molybdenite by Direct Force Measurements, Langmuir. 31 (2015) 11409–11418.

[4] J. Wu, B. Yang, S. Song, Q. Mildred, F. Jia, X. Tian, The efficient recovery of molybdenite fines using a novel collector: Flotation performances, adsorption mechanism and DFT calculation, Miner. Eng. 107848 (2022).

[5] J. Wu, J. Feng, B. Yang, R. Martin, S. Song, M. Quintana, F. Jia, X. Tian, The anisotropic adsorption of potassium cetyl phosphate on molybdenite surface and its implication for improving the flotation of molybdenite fines, J. Mol. Liq. 378 (2023) 121616.

[6] G.S. Plumlee, T.L. Ziegler, The medical geochemistry of dusts, soils and other earth materials, In Environmental Geochemistry, Treatise on Geochemistry, Elsevier Ltd, Oxford, UK, 2005.

[7] S.Chander, W.Fuerstenau, On the natural floatability of molybdenite, Trans. SME/AIME. 252 (1972) 62–69.

[8] G. Yi, E. Macha, J. Van Dyke, R.E. Macha, T. McKay, M.L. Free, Recent progress on research of molybdenite flotation: A review, Adv. Colloid Interface Sci. 295 (2021).

[9] Z. Wei, Y. Li, L. Huang, New insight into the anisotropic property and wettability of molybdenite: A DFT study, Miner. Eng. 170 (2021) 107058.

[10] P. Problems, Kinetics of Hydrophobic Agglomeration of, 51 (2015) 181–189.

[11] S. Song, X. Zhang, B. Yang, A. Lopez-Mendoza, Flotation of molybdenite fines as hydrophobic agglomerates, Sep. Purif. Technol. 98 (2012) 451–455.

[12] P.F.A. Braga, A.P. Chaves, A.B. Luz, S.C.A. Fran ça, The use of dextrin in purification by flotation of molybdenite concentrates, Int. J. Miner. Process. 127 (2014) 23–27.

[13] Z. Gao, W. Sun, Y. Hu, New insights into the dodecylamine adsorption on scheelite and calcite: An adsorption model, Miner. Eng. 79 (2015) 54–61.

[14] I.S. Kim, V.K. Sangwan, D. Jariwala, J.D. Wood, S. Park, K.-S. Chen, F. Shi, F. Ruiz-Zepeda, A. Ponce, M. Jose-Yacaman, Influence of stoichiometry on the optical and electrical properties of chemical vapor deposition derived MoS_2, ACS Nano. 8 (2014) 10551–10558.

[15] X. Wang, Y. Zhang, H. Si, Q. Zhang, J. Wu, L. Gao, X. Wei, Y. Sun, Q. Liao, Z. Zhang, K. Ammarah, L. Gu, Z. Kang, Y. Zhang, Single-Atom Vacancy Defect to Trigger High-Efficiency Hydrogen Evolution of MoS_2, J. Am. Chem. Soc. 142 (2020) 4298–4308.

[16] A. Mondal, A. Paul, D.N. Srivastava, A.B. Panda, Defect- and Phase-Induced Acceleration of Electrocatalytic Hydrogen Production by Ultrathin and Small MoS_2-Decorated rGO Sheets, ACS Appl. NANO Mater. 1 (2018) 4622–4632.

[17] Y. Fu, Q. Xiao, Y. Gao, P. Ning, H. Xu, Y. Zhang, Pressure aqueous oxidation of molybdenite concentrate with oxygen, Hydrometallurgy. 174 (2017) 131–139.

[18] Y. Chen, X. Chen, Y. Peng, The effect of sodium hydrosulfide on molybdenite flotation as a depressant of copper sulfides, Miner. Eng. 148 (2020).

[19] S. Xu, J. Kou, T. Sun, K. Jong, A study of adsorption mechanism of dodecylamine on sphalerite, Colloids Surf. A- Physicochem. Eng. Asp. 486 (2015) 145–152.

[20] L.J. Karas, C. Wu, R. Das, J.I. Wu, Hydrogen bond design principles, Wiley Interdiscip. Rev. Comput. Mol. Sci. 10 (2020) e1477.

[21] N. Masatoshi, T. Jumpei, O. Shinzo, XPS study of nitrided molybdena/titania catalyst for the hydrodesulfurization of dibenzothiophene, J. Phys. Chem. B. 103 (1999) 10180–10188.

[22] W. Liu, W. Liu, S. Dai, T. Yang, Z. Li, P. Fang, Enhancing the purity of magnesite ore powder using an ethanolamine-based collector: Insights from experiment and theory, J. Mol. Liq. 268 (2018) 215–222.

[23] R. Xu, J. Liu, W. Sun, L. Wang, Insights into the synergistic adsorption mechanism of mixed SDS/DDA collectors on biotite using quartz crystal microbalance with dissipation, Sep. Purif. Technol. 310 (2023).

[24] G.P.W. Suyantara, T. Hirajima, H. Miki, K. Sasaki, M. Yamane, E. Takida, S. Kuroiwa, Y. Imaizumi, Effect of Fenton-like oxidation reagent on hydrophobicity and floatability of chalcopyrite and molybdenite, Colloids Surfaces A-Physicochemical Eng. Asp. 554 (2018) 34–48.

The main content of this chapter was published in *Minerals*.

Chapter VIII. Conclusions

1. This work demonstrates that the flotation behavior of molybdenite fines is predominantly constrained by edges hydrophobicity rather than faces due to the high edge/face ratio. Therefore, targeted regulation of edge hydrophobicity is the key to improving the flotation efficiency of molybdenite fines.

2. SIBX significantly enhanced the flotation efficiency of molybdenite fines over a wide pH range. Xanthate species preferentially chemisorbed on molybdenite edges via covalent bonding formed by hybridization between the Mo 4d orbital and S 3p orbital, while dixanthogen formed on faces and physically adsorbed on faces. This anisotropic adsorption of xanthate species on edges and dixanthogen on faces simultaneously increased surface hydrophobicity and improved flotation performance.

3. NBPT exhibited strong collecting ability for molybdenite fines across a broad pH range. NBPT preferentially chemisorbed on edges through the hybridization of S 3p orbitals with Mo 4d orbitals, forming covalent bonds that significantly increased edge hydrophobicity.

4. PCP effectively promoted the flotation of molybdenite fines by selectively improving edge hydrophobicity. PCP strongly interacted with Mo sites at edges through phosphate complexation and chemisorbed via O 2p and Mo 4d hybridization, forming two high ionicity bonds.

5. MBT showed superior flotation performance compared with kerosene. MBT physically adsorbed on molybdenite faces while chemically bonding with edges through the hybridization of N 2p and S 3p orbitals with Mo 4d orbitals, forming a stable bidentate adsorption configuration that enhanced edge hydrophobicity.

6. DDA was more efficient than kerosene for the flotation of both unoxidized and oxidized molybdenite fines. For unoxidized molybdenite, RNH_2 and RNH_3^+ species adsorbed on faces through hydrogen bonding with surface S atoms and interacted with edges through chemical bonding and electrostatic interactions.

7. After surface oxidation, conventional collectors such as kerosene showed poor flotation performance. In contrast, DDA remained effective because RNH_2 and RNH_3^+ species could interact with newly exposed S atoms and oxidized MoO_3 species on edges through hydrogen bonding and electrostatic interactions, restoring surface hydrophobicity.

8. The anisotropic adsorption mechanisms of these novel collectors on molybdenite faces and edges were systematically revealed at both experimental and theoretical levels, clarifying that edge hydrophobicity is the dominant factor influencing the flotation of molybdenite fines.

9. A new collector design strategy for molybdenite fines flotation was proposed, emphasizing selective edge adsorption or synergistic adsorption on both faces and edges, which provides theoretical guidance for developing highly efficient collectors for fine molybdenite flotation.

Appendix I

1. Articles published in international journals during the Ph. D. study

1) **Jie Wu,** Bingqiao Yang, Rudolph Martin, Shaoxian Song, Mildred Quintana, Feifei Jia, Huihua. Luo, Fang Zhou, Xiang Tian, Anisotropic adsorption of xanthate species on molybdenite faces and edges and its implication on the flotation of molybdenite fines, *Minerals Engineering*. 207 (2024) 108571.
2) **Jie Wu,** Bingqiao Yang, Shaoxian Song, Mildred Quintana, Feifei Jia, Xiang Tian, The efficient recovery of molybdenite fines using a novel collector: Flotation performances, adsorption mechanism and DFT calculation, *Minerals Engineering*. 188 (2022) 107848.
3) **Jie Wu,** Jinchan Feng, Bingqiao Yang, Rudolph Martin, Shaoxian Song, Mildred Quintana, Feifei Jia, Xiang Tian, The anisotropic adsorption of potassium cetyl phosphate on molybdenite surface and its implication for improving the flotation of molybdenite fines, *Journal of Molecular Liquids*. 378 (2023) 121616.
4) Bingqiao Yang*, **Jie Wu****, Bing Deng, Hui Shao, Shaoxian Song, Mildred Quintana, Improving the flotation of unoxidized and oxidized molybdenite fines using dodecylamine as a collector: flotation tests and interaction mechanism, *Minerals*. 14 (2024), 468.
5) **Jie Wu,** Siyi Li, Bingqiao Yang, Hui Shao, Shaoxian Song, Mildred Quintana, Feifei Jia, Improving the flotation of molybdenite fines based on the targeted regulation of edges using a novel chelating collector, *Colloids and Surfaces A: Physicochemical and Engineering Aspects*. 703 (2024), 135354.
6) Guangfeng Dong, Peng Chen, **Jie Wu***, Hao Yi**, Tianxing Chen, Feifei Jia, Shaoxian Song, Efficient flotation separation of picromerite and halite by a novel collector of sodium dodecyl benzene sulfonate, *Minerals Engineering*. 202 (2023) 108278.
7) Xiang Tian, Z. Yang, **Jie Wu***, Xulong Lv, H. Liu, S. Hu, C. Gao, T. Jiang, L. Wang, Strength enhancement and resistance to chloride ions penetration mechanisms of metakaolin/Fe-rich tailings hybrid geopolymers with equivalent flowability in accelerated marine environments, *Construction and Building Materials*. 493 (2025): 143273.
8) Xiang Tian, Jia Shuai, **Jie Wu***, Jun Luo, Yan Zhou, Compressive strength and gel structure improvement in the high-volume calcium carbide residue activated-blast furnace slag system combined with sodium carbonate and silica fume, *Construction and Building Materials.* 441 (2024): 137500.
9) Xiang Tian, Zhifang Cheng, **Jie Wu***, Chang Gao, Yong Chen, Tianyong Jiang, Lei Wang**, Plasma surface modification of silica-rich tailings in alkali-activated blast

furnace slag binders: Hydroxylation-driven interfacial transition zone (ITZ) reinforcement, *Construction and Building Materials*. 491 (2025): 142815.

10) **Jie Wu**, Hanyu Zhang, Bingqiao Yang, Xiang Tian, Mildred Quintana, Qi Liu, Enhancing flotation recovery of fine cerium phosphate using dodecyl hydroxamic acid: Flotation performance and adsorption mechanism, *Journal of Rare Earth*. Accepted.

(*indicates corresponding author.)

2. Patents approved during the Ph. D. study

1) Bingqiao Yang, **Jie Wu,** Jinchan Feng, Dongshen He, Hanquan Zhang, Feifei Jia, Shaoxian Song. An application of N-(N-butyl) thiophosphoric triamide and a flotation method for molybdenite fines. Chinese Patent, CN114618686A.
2) Bingqiao Yang, **Jie Wu,** Hui Shao, Siyi Li, Yifan Zhang, Huihua Luo, Huanyu Zhu, Shaoxian Song, Feifei Jia. A combined collector and its application in the flotation of molybdenite fines, Chinese Patent, CN119056588A.

Appendix II

Experimental datas

Table II. 1 Effect of SIBX concentration on molybdenite flotation at pH of 9.

SIBX concentration ($\times10^{-3}$ mol/L)	0	0.581	1.16	2.32	3.48	4.65	5.81
Floatability (%)	39.5	54.9	65.4	73.49	80.59	86.17	88.09

Table II. 2 Effect of pH on molybdenite flotation with or without 3.48 $\times10^{-3}$ mol/L SIBX.

pH		3	5	7	9	11
Floatability (%)	0 SIBX	45.4	43.76	41.11	39.15	31.82
	3.48 $\times10^{-3}$ mol/L SIBX	85.99	87.7	74.25	75.59	69.17

Table II. 3 Effect of NBPT concentration on the floatability of molybdenite fines at pH of 4.

NBPT concentration (ppm)	0	100	200	400	600	800	1000
Floatability (%)	43.14	61.91	76.54	82.46	88.89	90.36	94.54

Table II. 4 Effect of pH on molybdenite flotation with or without 600 ppm of NBPT.

pH		2	4	6	8	10	12
Floatability (%)	0 NBPT	47.57	43.14	48.58	46.46	44.5	43.14
	600 ppm of NBPT	87.29	88.74	83.1	76.93	73.32	69.69

Table II. 5 Effect of kerosene concentration on the floatability of molybdenite fines with or without 200 ppm of NBPT at pH of 4.

Kerosene concentration (ppm)		0	10	20	40	60	80	100	400	1000
Floatability (%)	0 NBPT	43.15	45.08	47.37	50.97	51.34	52.89	53.71	57.6	64.89
	200 ppm of NBPT	76.54	76.16	75.31	77.09	76.62	78.05	78.12	78.76	82.06

Table II. 6 The impact of collector dosage on the floatability of molybdenite fines at pH of 10.

Collector dosage (ppm)		0	200	400	500	600	800	1000
Floatability (%)	PCP	27.82	50.07	70.61	83.77	86.52	89.46	91.39
	Kerosene	27.82	33.17	37.2	40.94	/	/	44.78

Table II. 7 The impact of pH on the floatability of molybdenite fines with or without 500 ppm of PCP.

pH		2	4	6	8	10	12
Floatability (%)	0 PCP	44.5	42.67	39.11	28.61	27.82	27.01
	500 ppm of PCP	51.08	61.33	72.52	79.77	83.77	83.84

Table II. 8 The effect of pH on the floatability of molybdenite fines with or without collector.

pH		2	4	6	8	10	12
Floatability (%)	Without collector	37.48	32.05	30.07	23.28	22.12	21.68
	100 mg/L of MBT	95.54	95.53	92.64	91.25	90.05	50.17
	500 mg/L of kerosene	71.03	68.47	66.94	64.72	56.43	36.99

Table II. 9 The effect of collector dosage on the floatability of molybdenite fines at pH of 4 or 10.

Collector	pH	Dosage (mg/L)	Floatability (%)
MBT	4	0	32.05
		10	47.31
		25	73
		50	90.67
		100	95.53
	10	0	22.12
		25	41.61
		50	60.08
		75	73.94
		100	90.05
Kerosene	4	0	32.05
		50	46.43
		100	54.57
		200	57.31

		400	62.46
		500	68.47

Table II. 10 The influence of pH on the floatability of unoxidized molybdenite fines.

pH		3	5	7	9	11
Floatability (%)	Without collector	43.01	44.51	37.94	35.44	33.66
	50 mg/L of DDA	95.92	97	95.95	94.81	73.6
	400 mg/L of kerosene	85.06	88.82	82.13	70.35	67.24

Table II. 11 The influence of collector dosage on the floatability of unoxidized molybdenite fines at pH of 5.

Collector dosage (mg/L)		0	20	30	40	50	100	200	400
Floatability (%)	DDA	/	19.13	52.84	88.09	94.96	94.93	/	/
	Kerosene	44.51	55.77	/	/	63.91	76.59	82.89	88.56

Table II. 12 The influence of pH on the floatability of oxidized molybdenite fines.

pH		3	5	7	9	11
Floatability (%)	50 mg/L of DDA	33.55	66.34	74.52	63.51	20.55
	400 mg/L of kerosene	31.28	37.19	33.62	30.58	12.53

Table II. 13 The influence of collector dosage on the floatability of oxidized molybdenite fines at pH of 7.

Collector dosage (mg/L)		0	20	40	50	100	150	200	400
Floatability (%)	DDA	/	13.68	53.85	74.52	89.27	92.88	/	/
	Kerosene	8.69	9.92	/	16.56	24.32	/	29.78	33.62